Doctoral Dissertation

PARAMETERIZATION OF MIXING IN THE OCEAN;

DOUBLE DIFFUSION, TURBULENT EDDIES, AND DISSIPATION RATIO

March 2016

Graduate School of Marine Science and Technology

Tokyo University of Marine Science and Technology

Doctoral Course of Applied Marine Environmental Studies

Haruka Nakano

Doctoral Dissertation

PARAMETERIZATION OF MIXING IN THE OCEAN;

DOUBLE DIFFUSION, TURBULENT EDDIES, AND DISSIPATION RATIO

March 2016

Graduate School of Marine Science and Technology

Tokyo University of Marine Science and Technology

Doctoral Course of Applied Marine Environmental Studies

Haruka Nakano

Preface

Micro-scale mixing such as turbulence and the double diffusive convection is one of the curious physical processes in the ocean. Where, why, and how much does it occur? How are their effects? A better understanding of how micro-scale mixing behaves contributes to not only understanding of large scale ocean structures but also that of atmospheric ones. That's why micro-scale mixing has been investigated by theoretical examinations, fields' observations, laboratory experiments and even numerical models.

The fields where such knowledge of micro-scale mixing contributes include climate modeling, understandings of modification processes of water masses, distribution of nutrients, and so on; however the knowledge supplied by observations is not enough all over the world because of the limitation on microstructure measurements due to ridiculously expensive instruments, difficulties in handling microstructure data, and limited ship time. Particularly, micro structure data is few to resolve physical processes in nearshore region and upper ocean because fisheries activities prevent us from investigating by observations and their spatio-temporal scales are smaller than those detected by observation. To elucidate effects of micro-scale mixing in the upper ocean and nearshore region, we would like to estimate eddy diffusivities which could determine the amount of mixing in those regions.

For the first step of it, I focused on estimating methods of eddy diffusivities in

the upper ocean in my Ph.D. thesis. Estimation methods of micro-scale mixing activities, eddy diffusivities or energy dissipation rates, have been developed with hydrographic data collected by CTD, LADCP, and other common oceanic instruments. This is so-called the "***PARAMETERIZATION***". Better parameterizations of turbulent mixing in natural flows enable us to predict mixing effects precisely.

However, parameterizations are not completely developed. For example, Most of all methods are constructed with limited observational data. Parameterizations due to the double diffusive convection were consisted by laboratory experiments and direct numerical simulations. A parameterization called as fine scale parameterization is not applied in the upper ocean and nearshore region, since it has a restriction of the vertical resolution, while data processing.

In my Ph.D. thesis, I tried to solve the uncertainty of previous parameterizations. This Ph.D. thesis has seven chapters with some appendices. Chapter 1 is dedicated to general introduction to mixing processes in the ocean. Chapter 2 shows observation sites and observation instruments. Chapter 3 shows parameterization of eddy diffusivities due to the double diffusive convection. In Chapter 4, eddy scales such as the Thorpe scale, which is the vertical displacement scale of density, and the Ozmidov scale, which is the scale calculated from turbulent energy are considered. Chapter 5 describes the mixing efficiency in the North Pacific Ocean. In chapter 6, summary and conclusion are

described. Finally, in chapter 7, some perspectives for future works are presented.

List of contents

Chapter 1 Introduction ~invitation to ocean mixing~

1.1. Ocean mixing

Mixing in the ocean, combination processes of sea water has many forms (Fig. 1.1), such as lateral intrusions, Langmuir circulations, internal waves, surface waves, shear instabilities, turbulence, and the Double Diffusive Convection (hereafter abbreviated as DDC). These processes are distinguished by their scales; medium-scale (*O* (~10m), *e.g.*, horizontal currents), fine-scale (*O* (~1m), *e.g.*, overturning), and micro-scale (*O* (0.1m), *e.g.*, turbulence, and DDC). Mixing takes place two directions both vertical and horizontal.

Note that these processes interact with each other. For example, internal waves which break around abrupt topography regions generate strong turbulence [*e.g.* Polzin *et al.* 1997]. Intrusions off *Sanriku* coast, Japan are induced by DDC [*e.g.* Nagata 1970; Nagasaka *et al.* 1999]. Taken together, studies on micro-scale mixing are highly correlated with large scale mixing studies.

Mixing activities, such as eddy diffusivities $K_\rho = \Gamma \frac{\varepsilon}{N^2}$ (where Γ is the mixing efficiency for turbulence, ε is the kinematic energy dissipation rates, and N is the buoyancy frequency) are strong near the boundary (upper ocean: surface mixing layers, deep ocean: bottom mixing layers), while one is weak in the ocean interior.

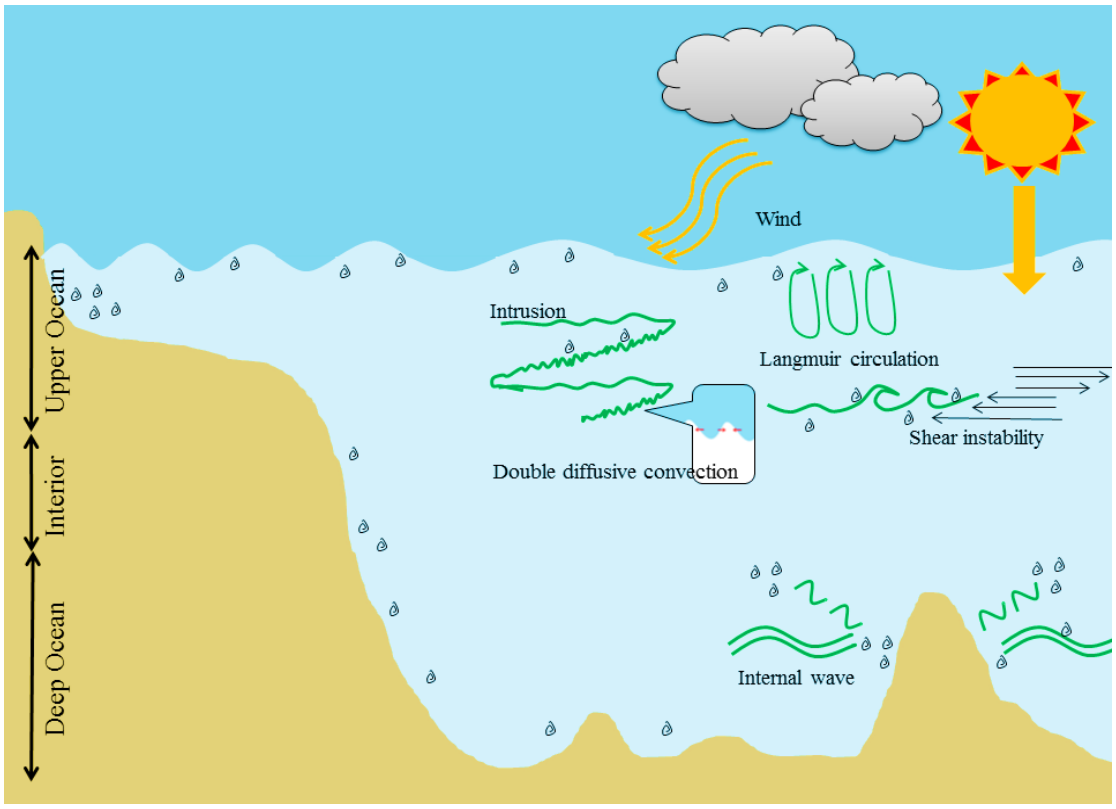

Fig 1.1 Schematic of ocean mixing.
The Sun, heating the sea surface, and winds (disturbance in the atmosphere) input energies directly into the ocean interior. Also, the tidal effects from the Sun, the Moon and so on⋯, input one and generate barotropic tides, which are converted into baroclinic internal tides around abrupt topography regions. Horizontal density gradients are the energy source for lateral intrusions. Vertical shear generates instabilities of the water column such as the Kelvin - Helmholtz instability. Winds generate the Langmuir circulation. The DDC and turbulence are typical microscale mixings.

1.2. Importance of diapycnal mixing

Except in and near the boundary layers, almost oceans are stably stratified. Thus, studies on diapycnal mixing have a long history associated with the thermohaline circulation. Munk [1966] introduced the equation which describes the balance between the transportation of density via the vertical advection (left hand of Eq. 1.1), and the density flux via the vertical diffusion which are generated by the diapycnal mixing (right hand of Eq. 1.1).

$$w\frac{\partial \rho}{\partial z} = K_\rho \frac{\partial^2 \rho}{\partial z^2}, \qquad (1.1)$$

where w is the vertical velocity of advection (upwelling velocity), $\partial\rho/\partial z$ is the vertical density gradient, K_ρ is the vertical eddy diffusivity of density, $\partial^2\rho/\partial z^2$ is the second derivative of the density gradient, and z is the vertical coordinate positive upward. K_ρ represents activities of the diapycnal mixing. The upwelling velocity is estimated using the production rate of abyssal water in the whole ocean, and is about 1cm/day ($\sim 1.15\times10^{-7}$m/s). The ratio of the vertical density gradient to its second derivative represents the typical thermocline vertical scale H ($H = [\partial\rho/\partial z]/[\partial^2\rho/\partial z^2]$) which is estimated to be O (10^3m). Taken together, estimated K_ρ in the global ocean is about 10^{-4}m^2/s.

Consequently, the studies on MOC (Meridional Overturning Circulation) have been conducted with various types of eddy diffusivities. Bryan [1987] first investigated

the effects of eddy diffusivities on MOC with the general ocean circulation model. He used both eddy diffusivities of heat K_T and that of momentum K_v, and described the dependence of stratification on K_T and K_v as Fig. 1.2 (when eddy diffusivities were large, thermocline deepened and MOC strengthened).

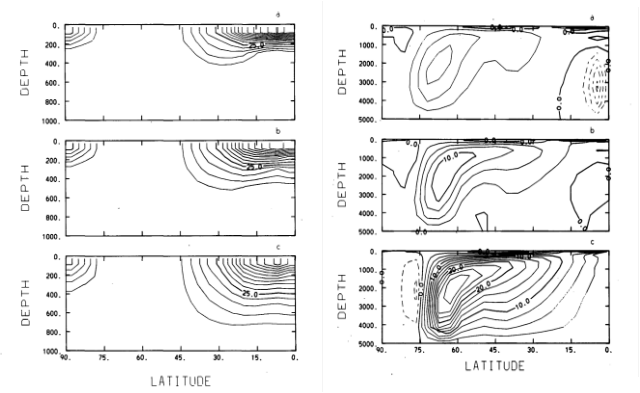

Fig. 1.2
Structures of potential density (left) and stream function (right) obtained by Bryan [1987] .Categorized by K_T (Upper: 0.1cm^2/s, middle: 0.5 cm^2/s, bottom: 2.5 cm^2/s).

Also Gargett and Holloway [1992] conducted the ocean circulation model considering different diffusivities of salinity K_S and K_T due to DDC (Fig. 1.3). In their model, when K_S was larger than K_T ($D = K_S / K_T = 2.0$), MOC weakened. Additionally the salinity minimum appeared near 1000m depth in the subpolar gyre (Fig. 1.4). In contrast, when K_S was smaller than K_T ($D = 0.5$), MOC strengthened, and salinity in the deep layers is homogeneous.

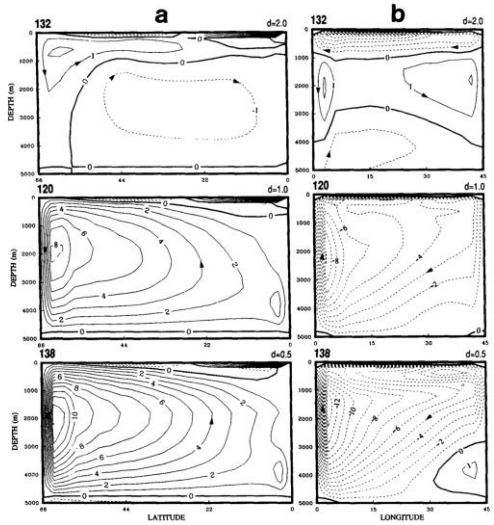

Fig. 1.3
Stream functions of meridional (left) and zonal (right) obtained by Gargett and Holloway [1992]. Categorized by $D(=K_S/K_T)$ (Upper: 2.0, middle: 1.0, bottom: 0.5).

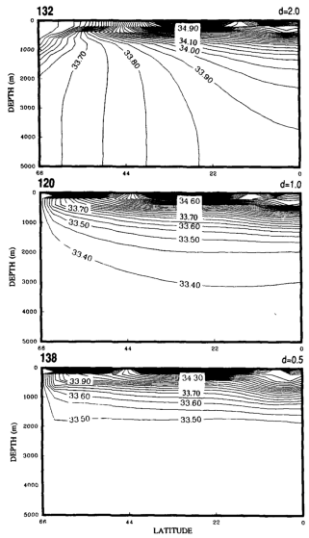

Fig. 1.4
Salinity structures obtained by Gargett and Holloway [1992].
Categorized by $D(=K_S/K_T)$ (Upper: 2, middle: 1, bottom: 0.5). In case of $D>1$, salinity minimum appeared near 1000m in the subpolar gyre.

Likewise, diapycnal mixing affects local processes such as nutrient distributions and modification processes of water masses. Karl [1999] suggested that the nutrients in the STPG (SubTropical Pacific Gyre) were supplied from lower layer to surface mixed layer through some physical processes such as diapycnal mixing (Fig. 1.5). Talley and Yun [2001] indicated that cabbeling[1] and DDC modified water and generated water masses having salinity minimum called NPIW (North Pacific Intermediate Water) in the perturbed region.

[1] Cabbeling is one of the non-linear effects of mixing processes. It increases the density of water masses.

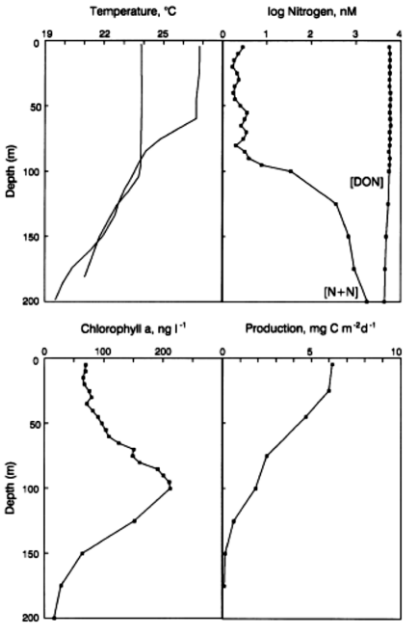

Fig. 1.5
Typical patterns of vertical profiles of temperature (upper left), nutrients (upper right), chlorophyll-*a* (bottom left) and production (bottom right) described by Karl [1999]. Amount of nutrients in upper layers is less than that in lower layers, while production in upper layers is larger than that in lower layers.

In nearshore region, mixing have been investigated associated with transportation of nutrients (Fig. 1.6). Eddy diffusivities are used for calculating the flux of nutrients.

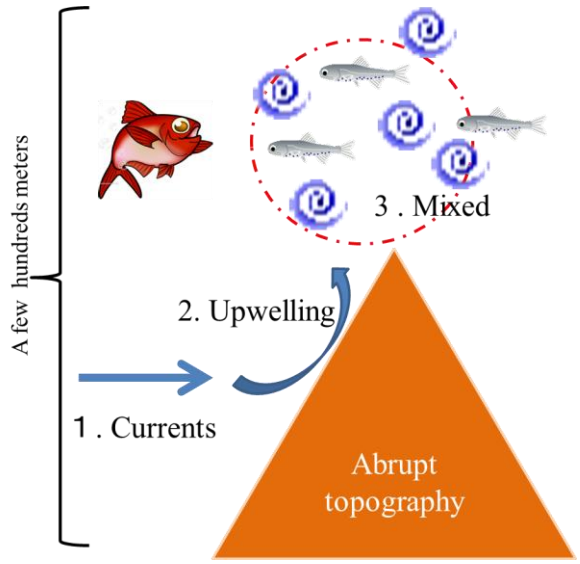

Fig. 1.6
Schematic sketch of a fish spot near the abrupt topography region. Upwelling occurs with coming of strong currents around abrupt topography regions. Abundant nutrients are transported with upwelling.

These are why; a lot of researchers have been investigating eddy diffusivities in the ocean; however knowledges on the true contribution of diapycnal mixing are not enough because of insufficient observations on microstructure. Particularly, micro structure data is so few to resolve physical processes in near shore region and Upper

Ocean because fisheries activities prevent us from investigating by observation and their spatiotemporal scales are smaller than those detected by observation (Fig. 1.7).

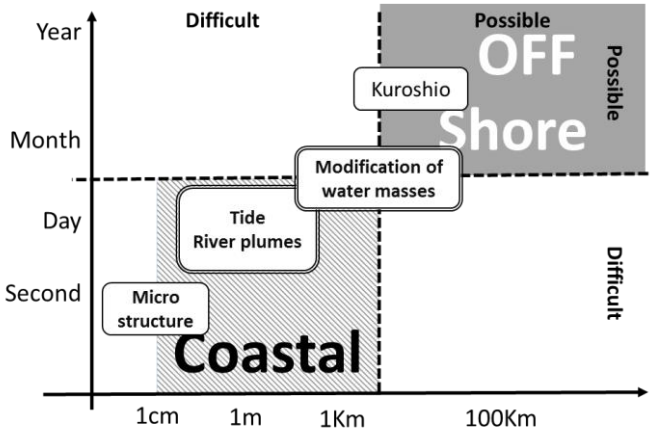

Fig. 1.7
Physical processes with spatio-temporal frame. Those in coastal (near shore region) are short term and narrow range processes. In contrast, those in off shore changed slowly and their scales are large.

1.3. Eddy diffusivities

1.3.1. Turbulence

Turbulent Kinematic Energy (TKE) dissipation rates ε are obtained by the turbulent energy Equation [Osborn 1980, Appendix A *Energy equation of turbulence*], defined as

$$\varepsilon = \frac{15}{2}\nu\overline{\left(\frac{\partial u'}{\partial z}\right)^2} \quad , \tag{1.2}$$

where ν is the kinematic viscosity (10^{-6}m^2/s), and u' is the fluctuation of horizontal velocity ($u' = u - \overline{U}$, $\overline{U}$ is the mean velocity). Over bar shows the ensemble average. When the ocean is in fully turbulent condition, all eddy diffusivities of heat K_T, salt K_S, density K_ρ, and momentum K_ν are equal to each other,

$$K_T = K_S = K_\nu = K_\rho . \tag{1.3}$$

Under the assumption above and using ε, eddy diffusivities due to the turbulence is written as

$$K_\rho = \frac{Rf}{1-Rf}\frac{\varepsilon}{N^2} = \Gamma\frac{\varepsilon}{N^2} , \tag{1.4}$$

where Rf is the flux Richardson number, and N is the buoyancy frequency. Rf is defined by the ratio between the energy production by buoyancy and shear (See Eq. A.10 on the 1st and 2nd terms), and is

$$Rf = \frac{g\overline{\rho' w'}}{-\rho\overline{u'w'}\left(\frac{\partial\overline{U}}{\partial z}\right)} . \tag{1.5}$$

w' is the fluctuation of vertical velocity ($w' = w - \bar{w}, \bar{w}$ is the mean velocity), ρ' is the density fluctuation, and $\frac{\partial \overline{U}}{\partial z}$ is the vertical gradient of mean velocity. $Rf/(1-Rf)$ is traditionally called as mixing efficiency Γ. When we assume that Rf has a value between 0.17 and 0.25, Γ gets 0.2 and 0.33 [*e.g.*, Oakey 1982]. This means that the only 17 ~ 25% of turbulent energy gets converted into the potential energy to mix the water column. Recently, Γ is a function of the gradient Richardson number R_i ($= N^2/S_h^{\,2}$), and not constant [*e.g.* Kantha and Carniel 2009]. Hence, the assumption which eddy diffusivities equals to each other, could not be adapted in ocean flows. Thus, a better parameterization on Γ is needed.

1.3.2. Double diffusive convection

As was shown in section 1.2, we know however different diffusivities affected the general circulation of the ocean [*e.g.*, Garget and Holloway 1984]. Are these eddy diffusivities same every time and everywhere?

DDC occurs when both heat and salt are increasing or decreasing with depth, and then their eddy diffusivities are not equal, as

$$K_T \neq K_S \neq K_v \neq K_\rho . \tag{1.6}$$

Here, K_S and K_T are obtained by the theory of DDC [Appendix B *The beginning of studies on double diffusive convection*]. Active salt finger (SF) convection exists when the density ratio $R_\rho = \dfrac{\alpha T_z}{\beta S_z}$ (where α is the thermal expansion and β is the haline contraction coefficients, respectively. T_z and S_z are the mean vertical gradients of temperature and salinity, respectively) is between 1 and 2, and the buoyancy Reynolds Number $R_{eb} = \varepsilon / \nu N^2$ is below 20 [*e.g.*, Inoue *et al*. 2007]. K_S and K_T due to SF are described as

$$K_S^{\mathrm{SF}} = \left(\frac{R_\rho - 1}{1 - \gamma^{\mathrm{SF}}} \right) \frac{\varepsilon}{N^2}, \tag{1.7}$$

$$K_T^{\mathrm{SF}} = \left(\frac{\gamma^{\mathrm{SF}}}{R_\rho} \right) K_S^{\mathrm{SF}}, \tag{1.8}$$

where γ^{SF} is the vertical density flux ratio of SF. Also, active diffusive convection (DC) exists when R_ρ is between 0.5 and 1, and when R_{eb} is below 20. K_S and K_T due to

DC are described as

$$K_S^{\mathrm{DC}} = \gamma^{\mathrm{DC}} R_\rho K_T^{DC} = \frac{\gamma^{\mathrm{DC}}\left(1-R_\rho\right)}{1-\gamma^{\mathrm{DC}}}\frac{\varepsilon}{N^2}, \tag{1.9}$$

$$K_T^{\mathrm{DC}} = \frac{1}{1-\gamma^{\mathrm{DC}}}\frac{1-R_\rho}{R_\rho}\frac{\varepsilon}{N^2} \quad , \tag{1.10}$$

where γ^{DC} is the vertical density flux ratio of DC [*e.g.* Kelley 1984]. From theses equations, we can obtain a negative value of K_ρ^{DDC} [Appendix B *The beginning of studies on double diffusive convection*]. We do not permit ignoring it in the upper ocean.

Focusing the effect of DDC layers, St. Laurent and Schmitt [1999] surveyed distributions of Γ with R_ρ and R_i, and found that Γ got large values due to the DDC compared with that due to the turbulent mixing. Γ is not a constant. That's why, Γ means the dissipation ratio between ε and the dissipation rate of temperature variance χ_θ [*e.g.* Moum 1996].

1.4. A brief history of observation and instrument of microstructure

The first microstructure observation was deployed by Grant *et al*. [1962]. After a decade, temperature Micro Structure Recorder (MSR) observation was conducted by Gregg and Cox [1971] in the San Diego Trough. The MSR has 2mm solutions. After that, Osborn [1974] first used the shear probe in the microstructure profiler called as Camel. Gregg *et al.* [1982] used the Advanced Microstructure Profiler, (AMP) down to 300db. AMP has a shear probe and temperature and conductivity sensors. Caldwell *et al*. [1985] used the Rapid Sampling Vertical Profiler (RSVP). Dewey *et al*. [1987] used the Fast Light Yo-yo (FLY 2), and observed bottom boundary layer by the shear probe and CTD. Oakey [1988a] conducted micro structure observation down to 2000db by the Epsilon Sonde (EPSONDE). Schmitt *et al*. [1995] also observed to the deep bottom of ocean by the High Resolution Profiler (HRP). In these days, some researchers (containing our group) used the Turbulence Ocean Microstructure Acquisition Profiler (TurboMAP).

Shear probe can obtain the time derivative of fluctuating part in the horizontal velocity. From the definition called as the Frozen Turbulent Theory [Taylor 1938] we can obtain the vertical derivative of u' from the time series measurement of u' and its derivative

$$\frac{\partial u'}{\partial t} = -W \frac{\partial u'}{\partial z}. \qquad (1.11)$$

Here, W is the descending speed of the instrument. Using Eq. (1.11) to convert time derivation of u' into that of vertical shear, we can estimate ε.

Recently, microstructures are estimated by fine structures data detected by CTD (Conductivity Temperature and Depth) and XCTD (eXpendable CTD). This is so-called the "***PARAMETERIZATION***". Frants *et al*. [2013] evaluated eddy diffusivities obtained by the density overturning and the fine scale parameterizations (details on these parameterizations are described in subsection 1.6.3). Are these instruments suitable for estimating eddy diffusivities? This point is needed to be solved.

1.5. Eddy diffusivities observed in the ocean

Eddy diffusivities have been investigated by various ways such as tracer release experiments, direct microstructure observations. For example, Ledwell *et al*. [1991] conducted tracer dispersion experiment (NATRE: North Atlantic Tracer Release Experiment), and showed that K_ρ in the interior ocean is smaller than the value estimated by Munk [1966, 10^{-4}m^2/s (section 1.2)], and the value is about 10^{-5}m^2/s.

The observed eddy diffusivities are smaller than the theoretical value by one order of magnitude. It is not enough to maintain the thermocline. The discrepancy between the theoretical eddy diffusivities and observed eddy diffusivities is now called as "missing mixing". Some scientists such as Garrett [2003] and Kunze and Smith [2004] proposed that eddy diffusivities due to localized mixing hot spots occurred in the surface, shelf boundaries, ocean bottom (ridge) and interior should be summed up to achieve the theoretical value as 10^{-4}m^2/s.

Where is the hot spot of mixing? A lot of researchers have been searching the area where enhanced diapycnal mixing occurred by the direct micro-scale measurements (Fig. 1.8, Table 1.1).

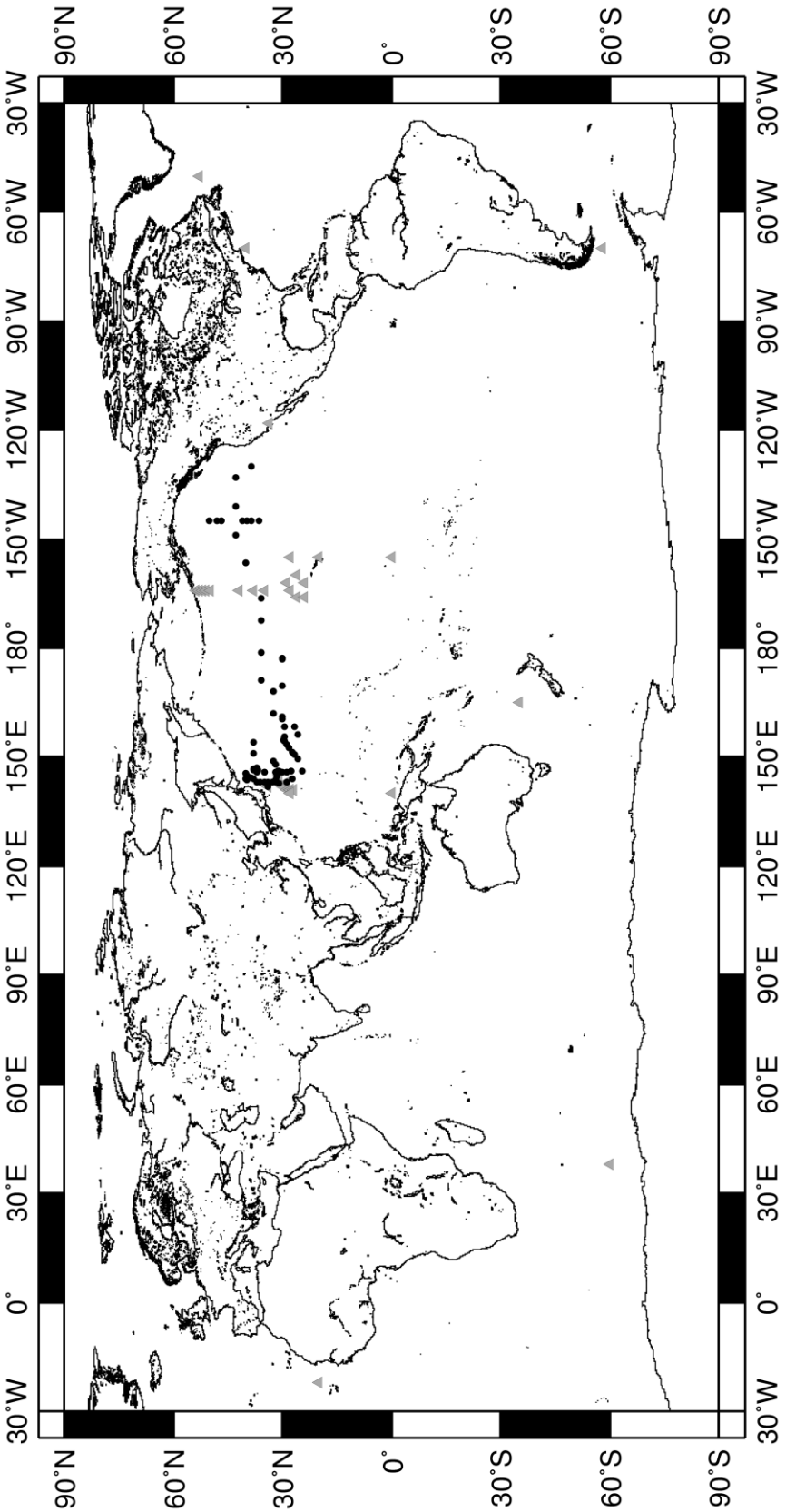

Fig. 1.8 Map of previous microstructure observations (dots: in this study, triangles: other studies in table 1.1). The area which already observed is few. Thus, more microstructure observations are needed.

Table 1.1 Examples of microstructure observation in the world.

published	place
Gregg *et al.* [1973]	Center of subtropical gyre of NPO
Gregg [1976a]	Central North Pacific , near the edge of the trade wind
Gregg [1976b]	Equator region in the Pacific
Ledwell *et al*. [1991]	Santa Monica basin
Kitade *et al.* [2003a in Japanese]	Tasmanian Sea
Inoue *et al.* [2007]	Perturbed region
Inoue *et al.* [2010a,b]	the Gulf stream
Inoue *et al.* [2012]	Equatorial region in the Pacific
Mori *et al.* [2008]	in the STMW
Robertson *et al.* [1995]	Weddle Sea
Polzin *et al.* [1995]	Brazil Basin
Rehmann and Duda [2000]	New England Shelf
Lozovatsky *et al.* [2006]	North Atlantic
Hibiya's group	North Pacific Ocean

Accordding to Garrett [2003], turbulence highly correlates to strong shear regions assosiated with internal waves. In order to investigate the relationship between turbulence and internal waves, Hibiya and Nagasawa [2004] focused on K_ρ produced by the interacting processes of internal waves with topography through the mechanism so called Parametric Sub-harmonic Instability (PSI). After that, Nagasawa *et al*. [2007] observed ε to estimate K_ρ from XCP (eXpendable Current Profiler) data collected from the surface down to maximum depth to about 2000 m near the Aleutian Ridge, the Hawaiian Ridge, and the Izu-Ogasawara Ridge, and indicated that K_ρ was the largest at

the Izu-Ogasawara Ridge. They concluded that K_ρ is large around Izu-Ogasawara Ridge because of PSI.

In contrast, some researchers have been focusing K_ρ in typical water masses. Mori *et al*. [2008] described that difference of K_ρ in the STMW (Subtropical Mode Water) between summer and winter. K_ρ in the winter was larger than that in the summer in the STMW; however, K_ρ was small O (10^{-5}) in even winter. Inoue *et al*. [2007] conducted microstructure observation in the perturbed region, and focused on effects of DDC on NPIW. They described the way to distinguish DDC from turbulence with R_{eb}. Inoue *et al*. [2010a, b] also investigated the formulation of the EDW (Eighteen Degree Water) in the Atlantic Ocean.

1.6. Parameterization of eddy diffusivities

Of course, more microstructure observations are needed for understanding of the MOC, modification processes of water mass, and distribution of nutrients, and so on; however microstructure observations are not commonly because of the high price of microstructure profilers and the limitation of ship time. Thus, the parameterization of ε has been conducted using fine scale structure data measured by CTD and LADCP (Fig. 1.9)

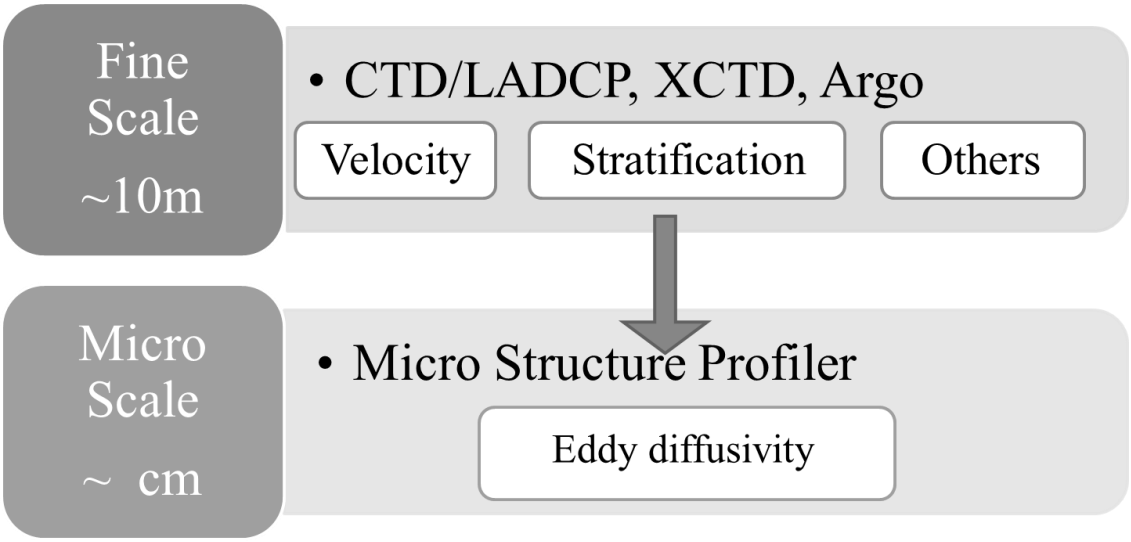

Fig. 1.9 Schematic of parameterization.

Many types of parameterizations have been proposed (Fig. 1.10). Parameterizations are constructed by focusing the energy source of mixing. Also, better parameterizations of mixing parameters lead us to better understanding of mixing effects. Following subsection, some parameterizations are introduced.

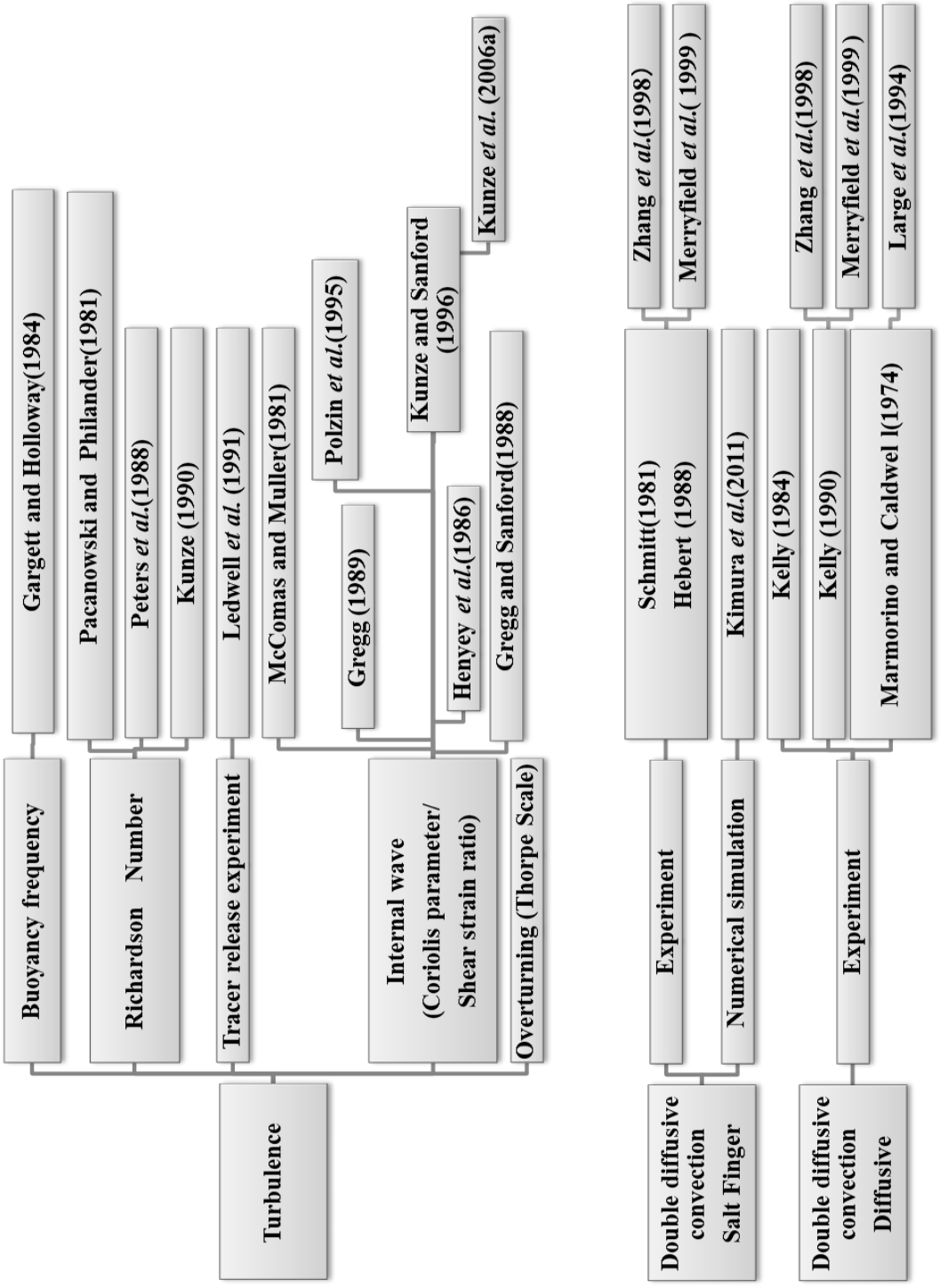

Fig. 1.10 Parameterizations of eddy diffusivities.

1.6.1. Buoyancy frequency

Gargett and Holloway [1984] found the relationships between the buoyancy frequency N and ε or K_ρ . N is described as

$$N = \left(-\frac{g}{\rho_0} \frac{d\rho}{dz} \right)^{1/2}, \tag{1.12}$$

where ρ_o is the reference density, $d\rho/dz$ is the vertical gradient of density, g is gravitational acceleration. N implies the buoyancy effect (large N describes strong stratification). They described K_ρ as

$$K_\rho^{GH} = \alpha_{GH} N^{-\beta_{GH}}, \tag{1.13}$$

where α_{GH} is a coefficient, β_{GH} is between -1.00 and -0.5. This parameterization means that turbulence in a weak stratification layer is strong.

1.6.2. Richardson number

Some researchers have been focusing on velocity shear using the Richardson number R_i indicating the stability of ocean fields

$$R_i = N^2 / S_h{}^2 , \tag{1.14}$$

where $S_h{}^2$ is square of the vertical velocity shear, as

$$S_h{}^2 = \left(\frac{\partial u}{\partial z} \right)^2 + \left(\frac{\partial v}{\partial z} \right)^2 , \tag{1.15}$$

where $\frac{\partial u}{\partial z}$ and $\frac{\partial v}{\partial z}$ is the vertical gradient of velocities. When R_i is under 0.25, turbulence should prevail [*e.g.*, Thorpe 2005].

Pacanowski and Philander [1981] and Peters *et al*. [1988] used R_i in order to estimate K_ν and K_T in the equator region. Especially, Pacanowski and Philander [1981] first simulated the response of the upper equatorial ocean to wind forcing, they described K_ν and K_T as

$$K_\nu^{\mathrm{P81}} = \frac{K_{\nu_0}}{\left(1+5R_i\right)^{n^{81}}} + K_{\nu_b} , \tag{1.16a}$$

$$K_T^{\mathrm{P81}} = \frac{K_\nu^{\mathrm{P81}}}{(1+5R_i)} + K_{T_b} , \tag{1.16b}$$

where K_{ν_0} is O (50~150cm/s), K_{ν_b} is $10^{-3}\mathrm{m}^2/\mathrm{s}$, and K_{T_b} is $10^{-4}\mathrm{m}^2/\mathrm{s}$, and n^{81} is 2. Peters *et al*. [1988] conducted microstructure observetions in the eqator region, and they parameterizes K_ν and K_T when $0.2 < R_i < 0.4$ as

$$K_\nu^{\mathrm{P88}} = 5.6\times10^{-8} R_i^{-8.2} , \tag{1.17a}$$

$$K_T^{\mathrm{P88}} = 3.0\times10^{-9} R_i^{-9.6}. \qquad (1.17b)$$

Kunze [1990] also used R_i to estimate K_v by the data obtained in the offshore region of Los Angeles. In these parameterizations, turbulence is strengthened by a strong shear ($R_i \to 0$).

1.6.3. Fine scale parameterization

Some researchers focused on the turbulence caused by internal waves. Hence, the term of the existence of internal waves is important for the parameterization, and is

$$f < \omega < N , \tag{1.18}$$

where f is the Coriolis parameter, ω is the frequency of internal waves. Recently, the Fine Scale Parameterization (FSP) is commonly used, and is considered as the most brilliant parameterization.

Garrett and Munk [1972, 1975] introduced the universal equilibrium the energy spectrum of internal waves E_{GM} [Appendix D *The GM spectrum*, Fig. 1.11].

$$E_{GM} \propto \omega^{-2} . \tag{1.19}$$

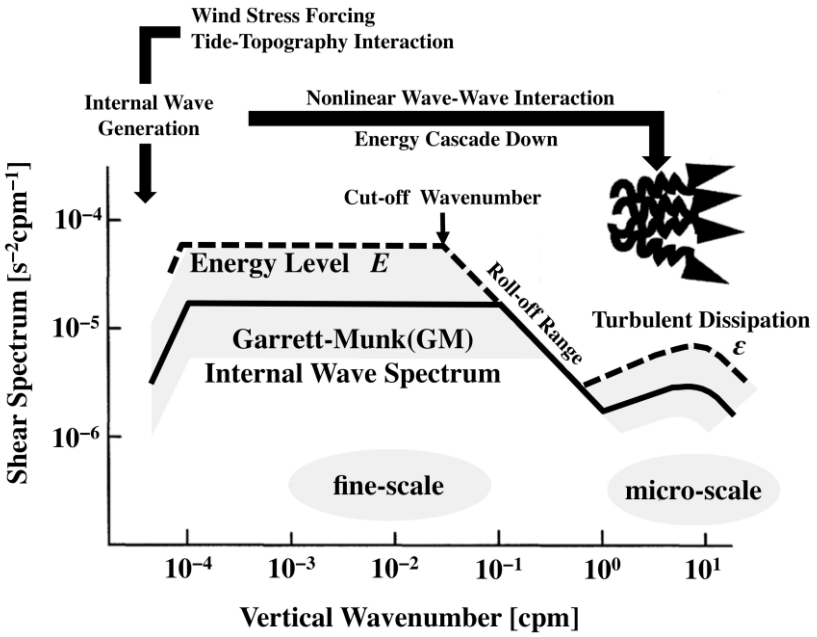

Fig. 1.11 Schematic of GM spectrum from Ijichi [2013]. Broken line shows an energy spectrum of a certain internal wave. The Thorpe scale (see chapter 4) exists in the roll-off range. Also the Ozmidov scale exists in micro-scale O (10^0).

Based on this, Henyey *et al*. [1986] approached the theory of mixing due to internal

waves and first showed that the latitudinal dependence of energy dissipation rates [see Appendix C *Latitudinal dependence of mixing due to internal waves*]. ε is described as

$$\varepsilon \propto fN^2 \cos^{-1}\left(N/f\right) \times E_{GM}^2 \quad . \tag{1.20}$$

Gregg [1989] also focused on turbulence due to the breaking of internal waves, and considered the ratio between shear spectrum and the GM spectrum. Polzin *et al*. [1995] defined the shear - strain ratio R_ω which indicates the variance of the fieald caused by internal waves [Appendix *E The shear and the strain ratio*], and it is written as

$$R_\omega = \frac{\left\langle S_h^{\,2} \right\rangle}{N^2 \left\langle \xi_z^{\,2} \right\rangle} = \frac{\omega^2 + f^2}{N^2} \cdot \frac{N^2 - \omega^2}{\omega^2 - f^2}, \tag{1.21}$$

where ξ_z is strain, $\left\langle S_h^{\,2} \right\rangle$ is variance of S_h, and $\left\langle \xi_z^{\,2} \right\rangle$ is variance of ξ_z. If we consider the energy balance of internal waves, Eq. (1.21) should be the ratio of kinetic energy to potential energy.

Kunze and Sanford [1996] combined these parameterizations [Henyey *et al*. 1986; Gregg 1989; Polzin *et al*. 1995], and made a new parameterization. It is now called as “GHP parameterization”. Kunze *et al*. [2006a] refined the GHP parameterization, and described K_ν using the shear or the strain.

① Strain based parameterization

$$K_\nu^{K06\xi} = K_0 \cdot \frac{\left\langle \xi_z^2 \right\rangle^2}{{}_{GM}\left\langle \xi_z^2 \right\rangle^2} h_2\left(R_\omega\right) j\left(\frac{N}{f}\right), \tag{1.22}$$

$$h_2\left(R_\omega\right)=\frac{1}{6\sqrt{2}}\frac{R_\omega\left(R_\omega+1\right)}{\sqrt{R_\omega-1}},\ j\left(\frac{N}{f}\right)=\frac{f\cosh^{-1}\left(\frac{N}{f}\right)}{f\cosh^{-1}\left(\frac{N_0}{f_{30}}\right)}\ , \tag{1.23}$$

② Shear based parameterization

$$K_v^{K06V}=K_0\cdot\frac{\left\langle V_z^2\right\rangle^2}{\underset{GM}{\left\langle V_z^2\right\rangle^2}}h_1\left(R_\omega\right)j\left(\frac{N}{f}\right), \tag{1.24}$$

$$h_2\left(R_\omega\right)=\frac{1}{2\sqrt{2}R_\omega}\frac{3\left(R_\omega+1\right)}{\sqrt{R_\omega-1}},\ j\left(\frac{N}{f}\right)=\frac{f\cosh^{-1}\left(\frac{N}{f}\right)}{f\cosh^{-1}\left(\frac{N_0}{f_{30}}\right)}, \tag{1.25}$$

where $f_{30}=f\left(30^\circ\mathrm{N}\right),\ N_0=5.2\times10^{-3}\mathrm{rad/s},\ K_0=0.05\times10^{-4}\mathrm{m^2/s}$.

1.6.4. Turbulent eddies' scale

Ozmidov [1965] first introduced the length scale L_O, which is determined by ε and N.

$$L_O = \sqrt{\varepsilon / N^3} . \tag{1.26}$$

In contrast, Thorpe [1977] proposed a scale associated it with overturning events L_T.

$$L_T = \sqrt{\frac{\sum_1^n d^2}{n}} , \tag{1.27}$$

where d is the density displacement scale (Thorpe displacement scale, see Chapter 4). If we compare these scales, we can obtain ε easily in the upper ocean.

The proportionality constant $R_{OT} = L_O / L_T$ (in the $L_O - L_T$ relationship $L_O = R_{OT} L_T$) is not a universal constant and appears to depend on both location and hydrographic conditions. However, L_O has been considered as 0.8 L_T in most of previous studies [*e.g.* Dillon 1982]. Thus, estimating methods for R_{OT} is needed to use this parameterization.

1.6.5. Considering the double diffusive convection

Large *et al*. [1994] simulated the MOC containing the DDC effects. When SF occurred, They used the constant value of 0.7 for density flux ratio γ^{SF} presented by Schmitt [1981]. They described K_S^{SF} $(1<R_\rho<1.9)$ and K_T^{SF} as

$$K_S^{\mathrm{Large,SF}}=\left[1-\left(\frac{R_\rho-1}{0.9}\right)^2\right]^3\times10^{-3}, \qquad (1.28a)$$

$$K_T^{\mathrm{Large,SF}}=\gamma^{\mathrm{SF}}\left[1-\left(\frac{R_\rho-1}{0.9}\right)^2\right]^3\times10^{-3}. \qquad (1.28b)$$

When DC occurred, they used γ^{DC} presented by Marmorino and Caldwell [1976] and Kelley [1986, 1990]. They described K_S^{DC} and K_T^{DC} as

$$0.5<R_\rho<1 \qquad K_S^{\mathrm{Large,DC}}=(1.85-0.85R_\rho^{-1})R_\rho K_T^{\mathrm{Large,DC}}, \qquad (1.29a)$$

$$R_\rho<0.5 \qquad K_S^{\mathrm{Large,DC}}=0.15R_\rho K_T^{\mathrm{Large,DC}}, \qquad (1.29b)$$

$$K_T^{\mathrm{Large,DC}}=0.909\times1.5\times10^{-6}\exp\left[4.6\exp\left(-0.54\left(R_\rho^{-1}-1\right)\right)\right], \qquad (1.29c)$$

$$\text{or} \qquad 8.7\times10^{-6}R_\rho^{1.1}. \qquad (1.29d)$$

Zhang *et al*. [1998] and Merryfield *et al*. [1999] also simulated MOC using other parameterized K_S and K_T in the active DDC layers. When SF occurred, they also used the constant value of 0.7 for γ^{SF} presented by Schmitt [1981] . They described K_S^{SF} and K_T^{SF} as

$$K_S^{\mathrm{Zhang,SF}}=\frac{1\times10^{-4}}{1+\left(\frac{R_\rho}{1.6}\right)^6}+3\times10^{-5}. \qquad (1.30a)$$

$$K_T^{\text{Zhang,SF}} = 1\times10^{-4}\times\left(\frac{\gamma^{\text{SF}}}{R_\rho}\right)\Bigg/\left(1+\left(\frac{R_\rho}{1.6}\right)^6\right)+3\times10^{-5}. \qquad (1.30b)$$

When DC occurred, they used γ^{DC} presented by Kelley [1990], and described K_S^{DC} and K_T^{DC} as

$$K_S^{\text{Zhang,DC}} = R_\rho\gamma^{\text{DC}}(K_T^{\text{Zhang,DC}}-3\times10^{-5})+3\times10^{-5}. \qquad (1.31a)$$

$$K_T^{\text{Zhang,DC}} = 0.0032e^{4.8R_\rho^{0.72}}\times(0.25\times10^9/R_\rho^{1.1})^{1/3}\times1.4\times10^{-7}+3\times10^{-5}. \qquad (1.31b)$$

Kimura *et al*. [2011] also parameterized K_S and K_T when SF is active ($1<R_\rho<2$).

$$K_T^{\text{SF,DNS}}(R_\rho,R_i) = 4.38\times10^{-5}R_\rho^{-2.7}R_i^{0.17}, \qquad (1.32a)$$

$$K_T^{\text{SF,DNS}}(R_\rho,R_i) = 3.07\times10^{-5}R_\rho^{-4.0}R_i^{0.17}. \qquad (1.32b)$$

Theses parameterizations mean that K_S and K_T increase/decrease toward R_ρ as unity.

1.7. Tasks from ocean mixing

Effects of DDC have been ignored hitherto because DDC is only distinguished from turbulence with using R_{eb} obtained by microstructure profiler. Other scientists majoring in the modification processes of water masses, and climate change, should include the contribution of DDC. Therefore the methods using hydrographic data which can distinguish DDC from turbulence are needed to be established.

In these days, the FSP considering vertical strain is usually used for estimating ε, because it is closely related to the energy of internal waves [*e.g.*, Polzin *et al*. 1995; Gregg 1989]. Kunze *et al*. [2006a], and also refined the parameterization considering internal wave fields using LADCP and CTD. Whalen *et al*. [2012] revealed the distribution of ε in the global ocean with Argo data following Kunze *et al*. [2006a]; however their result is problematic because the FSP cannot be applied in the Upper Ocean and nearshore region. Therefore, the other type of parameterization should be needed for estimating ε.

R_{OT} is not a universal constant. R_{OT} is needed to parameterize by hydrographic data to estimate K_ρ accuracy. If we know the way to estimate, mixing information in the upper ocean would increase.

The value of Γ is not a constant, but this point is not resolved yet [*e.g.,* Oakey 1982; Oakey 1985; Rohr and Vanatta 1987; Ivey and Imberger 1991; Moum 1996;

Lozovatsky and Fernando 2012; Mater and Vanayaganoorthy 2014]. Smyth *et al.* [2001] described that Γ changed with the progress stages of eddies in their simulations. Also, Γ in DDC layers is only the dissipation ratio. Mixing efficiency and dissipation ratio wait for being revealed.

Chapter 2 Observation and Instruments

2.1. Western North Pacific Ocean

Observations were conducted by the R/V Hakuho-Maru of the Japan Agency for Marine-Earth Science and Technology (JAMSTEC) during three periods, Nov. 2005 (KH05-4 cruise), May 2007 (KH07-1 cruise) and Oct. 2008 (KH08-3 cruise), in the North Pacific Ocean (NPO) (Fig. 2.1).

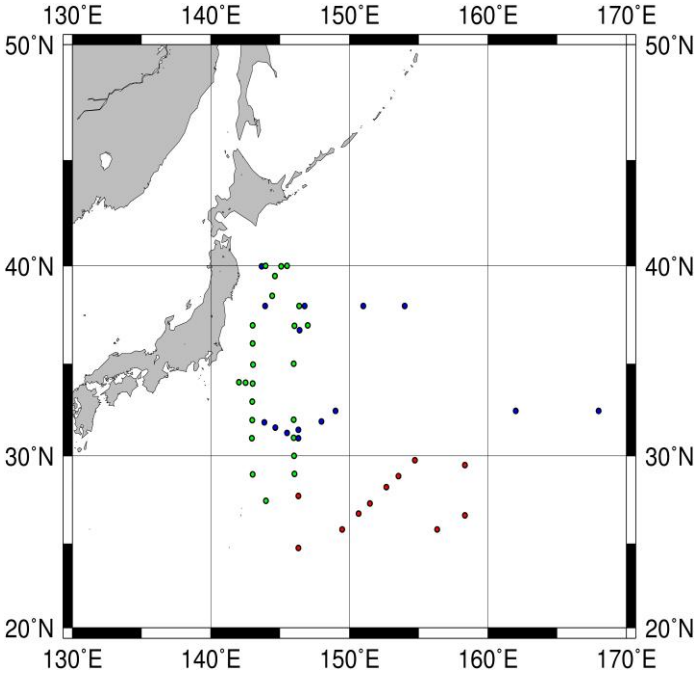

Fig. 2.1 Map of TM stations. Red(KH05), blue(KH07), green(KH08).

I obtained ε to estimate eddy diffusivities using a microstructure profiler called TurboMAP (hereafter, abbreviated as TM), and 49 casts were conducted. CTDO (SBE) equipped with LADCP, and XCTD observations were also conducted simultaneously at each TM station (Tables 2.1 and 2.2).

Table 2.1 Number of casts in NPO.

Period	Cruise	CTD/LADCP	XCTD	TurboMAP
Nov. 2005	**KH05-4**	**51**	**34**	**11**
May 2007	**KH07-1**	**58**	**101**	**15**
Oct. 2008	**KH08-3**	**89**	**112**	**24**

Table 2.2 Station information for TM in NPO.

Station name		observed depth	shear1	shear2	Slow temperature	Fast temperature	conductivity
Cruise	Station	(db)			(℃)	(℃)	
KH05	TM01	350	○	-	○	○	○
	TM02	450	○	-	○	○	○
	TM03	363	○	-	○	○	○
	TM04	440	○	-	○	○	○
	TM05	430	○	-	○	○	○
	TM06	403	○	-	○	○	○
	TM07	440	○	-	○	○	○
	TM08	414	○	-	○	○	○
	TM09	380	○	-	○	○	○
	TM10	440	○	-	○	○	○
	TM11	330	○	-	○	○	○
KH07	TM01	417	○	○	○	○	○
	TM02	445	○	○	○	○	○
	TM03	454	○	○	○	○	○
	TM04	533	○	○	○	○	○
	TM05	520	○	○	○	○	○
	TM06	364	○	○	○	○	○
	TM09	481	○	○	○	○	○
	TM10	592	○	○	○	○	○
	TM11	426	○	○	○	○	○
	TM12	471	○	○	○	○	○
	TM13	455	○	○	○	○	○
	TM14	376	○	○	○	○	○
	TM15	464	○	○	○	○	○
KH08	TM01	409	-	-	○	○	○
	TM02	525	○	-	○	○	○
	TM03	435	○	-	○	○	○
	TM04	620	○	-	○	○	○
	TM05	627	○	-	○	○	○
	TM06	546	○	-	○	○	○
	TM07	549	○	-	○	○	○

KH08	TM08	691	○	-	○	○	○
	TM09	582	○	-	○	○	○
	TM10	490	○	-	○	○	○
	TM11	550	○	-	○	○	○
	TM12	615	○	-	○	○	○
	TM13	446	○	-	○	○	○
	TM14	666	○	-	○	○	○
	TM15	576	○	-	○	○	○
	TM16	567	○	-	○	○	○
	TM17	630	○	-	○	○	○
	TM18	490	○	-	○	○	○
	TM19	486	○	-	○	○	○
	TM20	535	○	-	○	○	○
	TM21	560	○	-	○	○	○
	TM22	536	○	-	○	○	○
	TM23	521	○	-	○	○	○
	TM24	566	○	-	○	○	○

Note that, theses cruises were planned by late Prof. Masaki Kawabe of University of Tokyo in order to estimate the path of deep ocean circulation. He deployed some moorings in the NPO. Also, XCTD observations were mainly conducted by Prof. Toshio Suga of Tohoku University.

2.2. Seamount offshore of Miyake Island

Beryx splendens inhabits in the south of Ibaraki in Japan. Particularly, longline fishings have been conducted in Sagami-nada and around the Izu-islands. Akimoto and Takahashi [2008, in Japanese] conducted the observation of CTD over the knoll near the Miyake Island offshore in order to reveal the connections between the fishery spot and oceanic conditions. As a result, the distance between the knoll and the Kuroshio is an important factor of hauls of *Beryx splendens*; however the physical processes which dominate nutrients transportation to maintain the primary production were not determined in this area (Fig. 2.2).

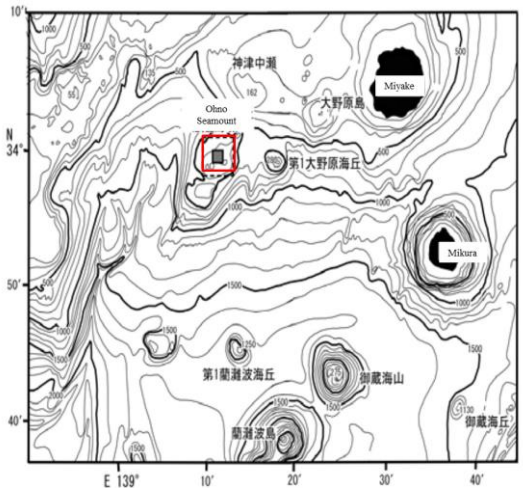

Fig. 2.2 Location of the Second Ohnohara knoll in the offshore of Miyake Island.

Consequently, the surveys in habitat area of *Beryx splendens* were planned by Dr. Yugo Shimizu. The observations were deployed near the second Ohno Seamount offshore of Miyake Island in the south of Tokyo by the Soyo-maru belonging to FRA in Aug. 2014,

and Oct. 2014 (Fig. 2.2). During these cruises, TM, XCTD, CTD and plankton net were conducted in each station (Tables 2.3 and 2.4). The velocity data were also collected by the shipboard ADCP made by RDI company. The measurements were deployed 12 times in one cruise. Unfortunately, the TM belonging to FRA was defective in Aug. 2014, and fortunately it could be repaired by Oct. 2014.

Table 2.3 Number of casts around the knoll offshore of Miyake Island.

Period	Cruise	CTD	XCTD	TurboMAP	Ship board ADCP
Aug. 2014	SY05	12	12	—	○
Oct. 2014	SY06	24	23	26	○

Table 2.4 Station information for TM around the knoll offshore of Miyake Island.[2]

Station name		observed depth	shear1	shear2	Slow temperature	Fast temperature	conductivity
Cruise	Station	(db)			(℃)	(℃)	
SY05	ALL Station	—[3]					
SY06	Y3-09	395	○	○	○	—	○
	Y3-10	201	○	○	○	—	○
	Y3-11	276	○	○	○	—	○
	Y3-12	300	○	○	○	—	○
	Y3-13	350	○	○	○	—	○
	Y3-14	370	○	○	○	—	○
	T3-57	342	○	○	○	—	○
	T3-58	339	○	○	○	—	○
	T3-59	227	○	○	○	—	○
	T3-60	271	○	○	○	—	○
	T3-61	350	○	○	○	—	○
	T3-62	355	○	○	○	—	○
	Y4-09	318	○	○	○	—	○
	Y4-10	234	○	○	○	—	○
	Y4-11	269	○	○	○	—	○
	Y4-12	332	○	○	○	—	○
	Y4-13	343	○	○	○	—	○
	Y4-14	340	○	○	○	—	○
	T4-57	300	○	○	○	—	○
	T4-58	346	○	○	○	—	○
	T4-59	265	○	○	○	—	○
	T4-60	252	○	○	○	—	○
	T4-61	370	○	○	○	—	○
	T4-62	360	○	○	○	—	○

[2] The data is shown only for those obtained at the knoll around the offshore of Miyake island. Deep two casts conducted far from the knoll were not used in this paper because I would like to compare the fully turbulent condition with the condition in the open ocean.
[3] The data could not be collected because TM was broken.

2.3. TurboMAP

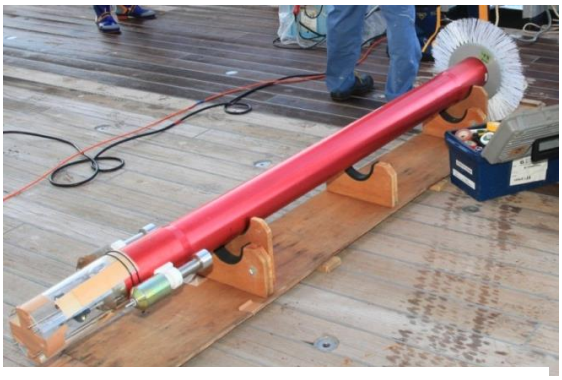

Fig. 2.3 TurboMAP.

Turbulence Microstructures Acquisition Profiler (TurboMAP) is manufactured by JFE Advantech Co. (Fig. 2.3). Our TurboMAP can get time series of the velocity fluctuation by two shear probes, and high speed temperature fluctuation by a high response thermistor FPO-7 at 512 Hz sampling rate, respectively. These fluctuation components are converted into time derivative ones by the derivative circuit within. In addition, we can get slow response temperature, conductivity, pressure, acceleration in *x*, *y*, *z* directions, chlorophyll *a* and turbidity (Fig 2.4). The list of sensors and some specs are summarized in Table 2.5.

Fig. 2.4 Sensors of TurboMAP.

Table 2.5 Sensors' and Resolutions

Item	Resolution	Item	Resolution
du/dt	$1\times10^{-6}S^{-1}$	**X- acceleration**	0.001G
T+dT/dt	0.001℃/m	**Y- acceleration**	0.001G
Temperature (T)	0.001℃	**Z- acceleration**	0.001G
Conductivity	0.001mS	**Chlorophyll**	0.005μg/L
Depth	0.01m	**Turbidity**	0.005ppm

Time series of time derivative of fluctuation velocity is converted into the vertical shear of the fluctuation velocity under the hypothesis of Frozen Turbulence Theory by Taylor [1938] (Eq. 1.11), therefore, TM must freely fall at a constant speed between 0.6m/s and 0.7m/s [Oakey 1982]. In this observation, the speed was controlled by some weights equipped inside of TM. Observations of TM are limited by the length of sea cable, and observation was terminated at about 600m depth.

Chapter 3 Parameterization of the eddy diffusivity due to double diffusive convection

Abstract

ε in the western NPO were observed using a microstructure profiler at 49 stations and the measured values were converted into diffusivities of heat K_T and salt K_S. I obtained a new relationship between R_i and R_{eb} in the ocean, which enables us to use R_i, instead of R_{eb}, as an indicator for distinguishing DDC from turbulence. I further obtained new relationships among K_S, K_T, R_i and R_ρ by improving the parameterization proposed by Kimura *et al*. [2011].

3.1. Introduction

A better knowledge on DDC effects on modification processes of water masses are contributed to a better understanding of distribution of nutrients in the NPO. Toyama and Suga [2012] found that DDC contributed to the formation and maintenance of Central Mode Water (CMW) generating in northern part of the NPO. They used R_ρ to discuss the effects of DDC. In the upper ocean, however, turbulence and DDC can co-exist. From the point of view of micro-scale mixing studies, their study was not completed because R_ρ only indicates the activity of DDC and cannot discriminate that from turbulence. Hence, inaccuracy of the mechanism for the formulation and maintenance of CMW have been remained.

R_{eb} is used to discriminate DDC from turbulence. Inoue *et al*. [2007] discussed this point in detail. They conducted microstructure observations focusing on K_S and K_T in the perturbed region where turbulence and DDC both contribute to mixing. They proposed a simple eddy diffusivities model to account properly for activity of turbulence and DDC. They also used the combination of R_{eb} and R_ρ which enables us to distinguish DDC from turbulence. When R_{eb} is below 20 and R_ρ is between 0.5 and 2.0, they suggested that DDC should prevail.

Thus, we need to use R_{eb}; however, it must be calculated from ε obtained by direct micro-structure measurements. If we have other indicators which can distinguish

DDC from turbulence, such indicators enable researchers to evaluate the effect of micro-scale mixing precisely. Thus, we need other parameters calculated from general hydrographic measurements to distinguish DDC from turbulence.

Lozovatsky and Fernando [2012] discussed the relationship between R_i and R_{eb} in the atmosphere in Salt Lake City, USA, and found the distribution of Γ on R_i - R_{eb} plane (Fig. 3.1). Smaller value of R_i means fluids are unstable with turbulent activity is strong (R_{eb} goes infinity). Following Lozovatsky and Fernando [2012], I evaluate R_i whether it could be used instead of R_{eb} in the ocean (when R_i is below 0.25, turbulence occurs [*e.g.*, Thorpe 2005]). If we can use R_i instead of R_{eb}, it becomes easier to distinguish DDC from turbulence.

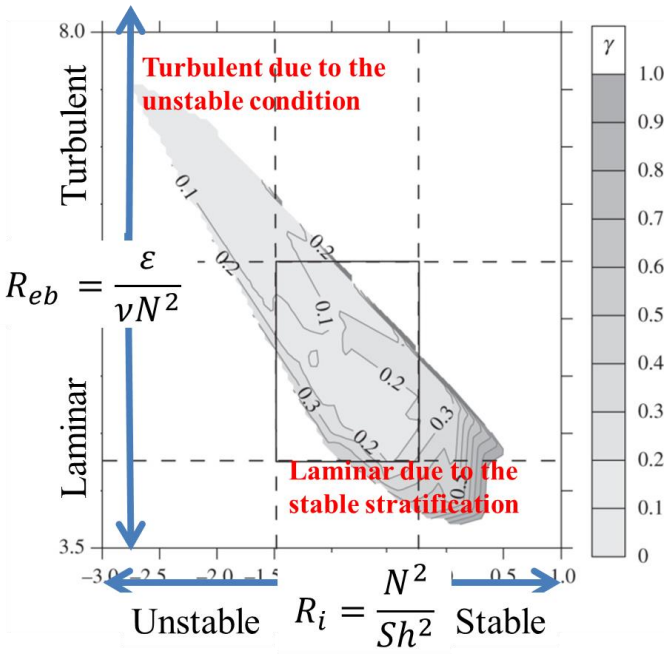

Fig. 3.1 Contour of Γ on R_i and R_{eb} plane rewritten of Lozovatsky and Fernando [2012].

Additionally, accurate estimation of K_ρ is needed to elucidate the variations of density. However, K_ρ is not evaluated by observational data. K_S and K_T have been parameterized by laboratory experiments and direct numerical simulations (DNS) due to the DDC (Tables 3.1, and 3.2). That's why, an evaluation of the

estimation methods are needed.

Table 3.1 Parameterization for SF.

	K_S	K_T
Large *et al*. [1994]	$\left[1-\left(\frac{R_\rho -1}{0.9}\right)^2\right]^3 \times 10^{-3}$	$\gamma^{\mathrm{SF}}\left[1-\left(\frac{R_\rho -1}{0.9}\right)^2\right]^3 \times 10^{-3}$
Zhang *et al*. [1998]	$1\times10^{-4}\Big/\left(1+\left(\frac{R_\rho}{1.6}\right)^6\right)+3\times10^{-5}$	$\left(10^{-4}\times\frac{\gamma^{\mathrm{SF}}}{R_\rho}\right)\Big/\left(1+\left(\frac{R_\rho}{1.6}\right)^6\right)+3\times10^{-5}$
Kimura *et al*. [2011]	$4.38\times10^{-5}R_\rho^{-2.7}R_i^{0.17}$	$3.07\times10^{-5}R_\rho^{-4.0}R_i^{0.17}$

Table 3.2 Parameterization for DC.

	K_S	K_T
Large *et al*. [1994]	$0.5 < R_\rho < 1$ $K_S^{\mathrm{Large,DC}} = (1.85-0.85R_\rho^{-1})R_\rho K_T^{\mathrm{Large,DC}}$ $R_\rho < 0.5$ $K_S^{\mathrm{Large,DC}} = 0.15R_\rho K_T^{\mathrm{Large,DC}}$	$0.909\exp\left[4.6\exp\left(-0.54(R_\rho^{-1}-1)\right)\right]\times10^{-6}$ or $8.7\times10^{-6}R_\rho^{1.1}$
Zhang *et al*. [1998]	$\frac{1/R_\rho+1.4(1/R_\rho-1)^{3/2}}{1+14(1/R_\rho-1)^{3/2}}\times$ $R_\rho(K_T-0.3\times10^{-4})+0.3\times10^{-4}$	$0.0032e^{4.8R_\rho^{0.72}}\times(0.25\times10^9/R_\rho^{1.1})^{1/3}$ $\times1.5\times10^{-7}$
Kimura *et al*. [2011]	—	—

In this study, I focus on the parameterization proposed by Kimura *et al.* [2011] who proposed eddy diffusivity parameterizations with R_i and R_ρ by the DNS (Fig. 3.2). They directly simulated SF in fine grids by changing R_ρ and R_i. They obtained relationships among K_S, K_T, R_i and R_ρ; however the parameterizations were not evaluated by observational data. So, I evaluate the parameterization proposed by Kimura *et al.* [2011] in this chapter.

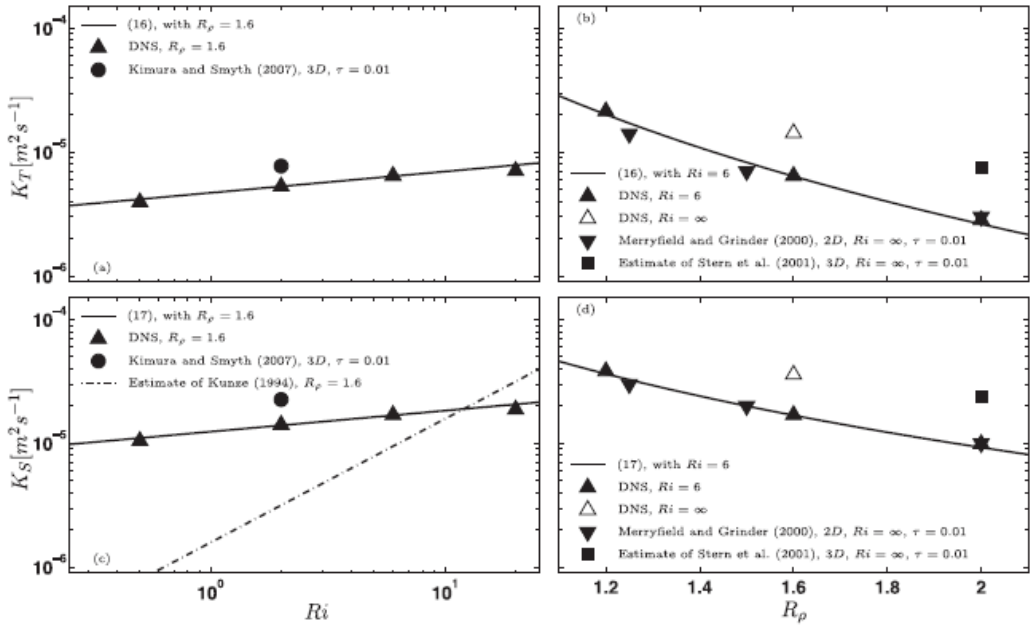

Fig. 3.2. Functional dependence of the eddy diffusivity on R_i and R_ρ proposed by Kimura et al. [2011].

3.2. Data processing

3.2.1. Identification of the double diffusive convection

I calculated R_ρ, and the Turner angle T_u. First, R_ρ is defined in subsection 1.3.2 as

$$R_\rho = \alpha \frac{\partial \theta}{\partial z} \Big/ \beta \frac{\partial S}{\partial z}, \tag{3.1}$$

where α is the thermal expansion and β is the haline contraction coefficients, respectively. $\partial\theta/\partial z$ and $\partial S/\partial z$ are the mean vertical gradients of potential temperature and salinity, respectively. Then, T_u is defined by R_ρ as

$$T_u = \tan^{-1} \frac{R_\rho + 1}{R_\rho - 1}. \tag{3.2}$$

SF is active when $1 < R_\rho < 2$ ($72^o < T_u < 90^o$). DC is also active when $0.5 < R_\rho < 1$ ($-90^o < T_u < -72^o$). Kantha *et al*. [2016 personal communication] proposed to use 'Circle diagram' together with T_u. Using this diagram, we can easily judge whether DDC is active or not. I will use this diagram in the following section.

3.2.2. Energy dissipation rate

I obtained ε, following the relation obtained by Osborn [1980],

$$\varepsilon = \frac{15}{2}\nu\overline{\left(\frac{\partial u'}{\partial z}\right)^2}, \qquad (3.3)$$

where ν is the molecular viscosity ($\sim 10^{-6}$m^2/s), $\partial u'/\partial z$ is the vertical shear of the horizontal velocity fluctuations with the over bar denoting the ensemble average. After the FFT (Fast Fourier Transform) of shear data, the shear data was fitted to the Nesmith universal spectrum. In this analysis, the data was fitted each 10m scale.

3.2.3. Eddy diffusivities

I estimated eddy diffusivities when DDC was active. Following Inoue *et al.* [2007], in order to distinguish DDC from turbulence, we used R_{eb} defined by

$$R_{eb} = \frac{\varepsilon}{\nu N^2}. \tag{3.4}$$

When R_{eb} is below 20, DDC is effective to enhance mixing [*e.g.*, Padman and Dillon 1987; Gregg, 1989; Inoue *et al*. 2007; Kantha *et al*. 2013 personal communication]. In the present study, when R_ρ is between 1 and 2, and R_{eb} is below 20, K_S^{SF} and K_T^{SF} are estimated by

$$K_S^{\mathrm{SF}} = \left(\frac{R_\rho - 1}{1-\gamma^{\mathrm{SF}}}\right)\frac{\varepsilon}{N^2}, \tag{3.5}$$

$$K_T^{\mathrm{SF}} = \left(\frac{\gamma^{\mathrm{SF}}}{R_\rho}\right)K_S^{\mathrm{SF}}, \tag{3.6}$$

[*e.g.*, Kelley 1986]; when R_ρ is between 0.5 and 1, and R_{eb} is below 20, and K_S^{DC} and K_T^{DC} are estimated by,

$$K_S^{\mathrm{DC}} = \gamma^{\mathrm{DC}} R_\rho K_T^{\mathrm{DC}} = \frac{\gamma^{\mathrm{DC}}\left(1-R_\rho\right)}{1-\gamma^{\mathrm{DC}}}\frac{\varepsilon}{N^2}, \tag{3.7}$$

$$K_T^{\mathrm{DC}} = \frac{1}{1-\gamma^{\mathrm{DC}}}\frac{1-R_\rho}{R_\rho}\frac{\varepsilon}{N^2}, \tag{3.8}$$

[*e.g.*, Kelley 1984], where SF stands for Salt Finger convection, DC stands for Diffusive Convection, γ is the density flux ratio due to DDC defined by

$$\gamma = \frac{\alpha F_T}{\beta F_S}, \tag{3.9}$$

with αF_T and βF_S the vertical density fluxes due to heat and salt, respectively, and related to R_ρ such that

$$\gamma^{\mathrm{SF}} = \sqrt{R_\rho}\left(\sqrt{R_\rho} - \sqrt{R_\rho - 1}\right) \text{ , Kunze [1987],} \tag{3.10}$$

$$\gamma^{\mathrm{DC}} = \frac{1/R_\rho + 1.4\left(1/R_\rho - 1\right)^{3/2}}{1 + 14\left(1/R_\rho - 1\right)^{3/2}} \text{ , Kelley [1990].} \tag{3.11}$$

By the definition [Osborn 1980], I obtained eddy diffusivities due to turbulence as

$$K_\rho^{\mathrm{Turb}} = K_T^{\mathrm{Turb}} = K_S^{\mathrm{Turb}} = \frac{Rf}{1 - Rf} \cdot \frac{\varepsilon}{N^2} = \Gamma \cdot \frac{\varepsilon}{N^2}. \tag{3.12}$$

Here, Rf is assumed to be 0.17, then the mixing efficiency Γ becomes 0.2 for isotropic turbulence [*e.g.*, Schmitt *et al*. 2005]. Turb stands for Turbulence. Hereafter, I use K_T^{Obs} as representation of K_T^{Turb}, K_T^{SF} or K_T^{DC}. K_S^{Obs} also of K_S^{Turb} and K_S^{SF} or K_S^{DC}. *Obs* stands for the observation value (Fig. 3.3).

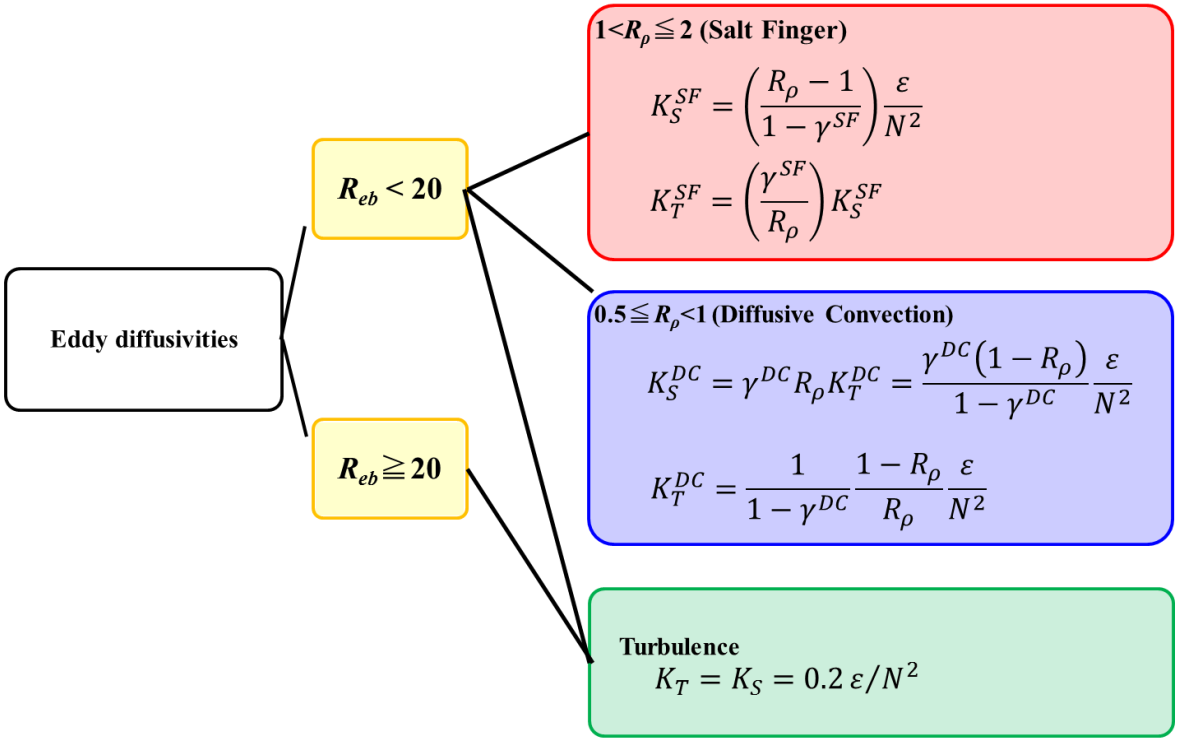

Fig. 3.3 Eddy diffusivities categorized by R_{eb}.

3.2.4. Richardson number

After removal obvious error of pitching and rolling angle for LADCP, the velocity data was arranged in order of depth. After removal the noise of velocity, the Richardson number R_i was calculated using the buoyancy frequency N and the vertical shear of horizontal velocity S_h, both defined at 10m vertical scale, such that

$$R_i = \frac{N^2}{S_h^{\,2}} = \frac{N^2}{\left(\frac{\partial u}{\partial z}\right)^2 + \left(\frac{\partial v}{\partial z}\right)^2}, \tag{3.13}$$

where *u* and *v* are horizontal velocities, respectively.

3.3. Results and discussion

3.3.1. Activity of the double diffusive convection

The circle diagram plot shows that DDC was not so active in observation area (Fig. 3.4). The percentage of active DDC layer was about 10%. A large amount of data clustered in the weak SF ($2 < R_\rho$) and weak DC ($R_\rho < 0.5$) areas.

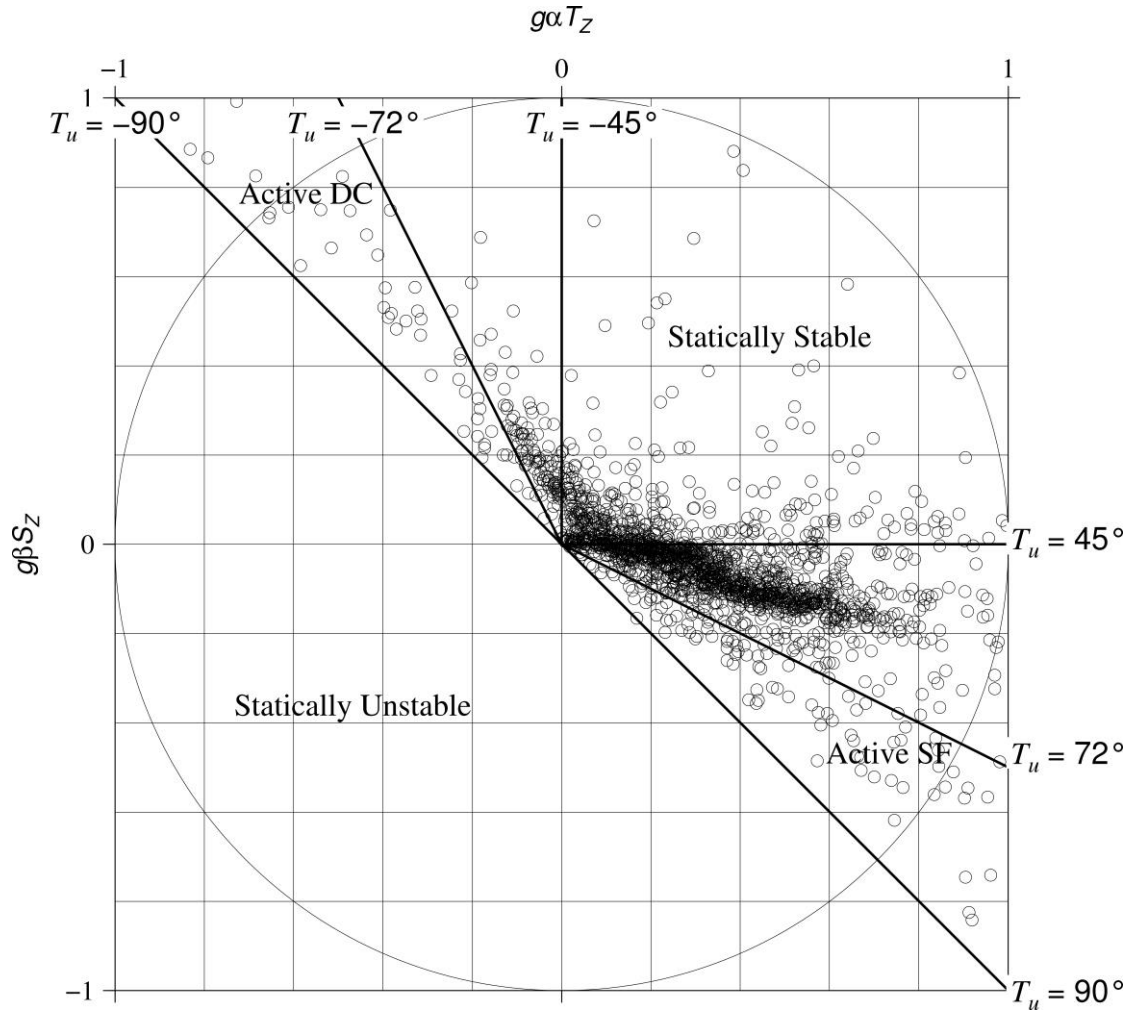

Fig. 3.4 Circle diagram.

Values were normalized by using 1×10^{-4} (this value is the almost maximum value of $g\alpha T_z$ and $g\beta S_z$.

3.3.2. Comparison of the Richardson number and the buoyancy Reynolds number

By the histograms of R_i and R_{eb}, modes of R_i and R_{eb} take 0.25 and 80, respectively (Fig. 3.5)

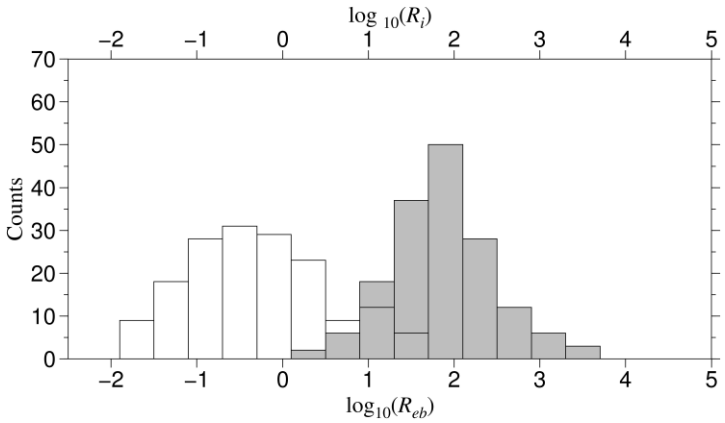

Fig. 3.5 Histograms of R_i and R_{eb}.
Gray histogram is distribution of R_{eb}, and white one is that of R_i.

The relationship between R_i and R_{eb} was obtained by EOF analysis. When DDC is active ($0.5 < R_\rho < 2$), the relationship between R_{eb} and R_i (Fig. 3.6) is

$$R_{eb} = 19.5 R_i^{-1.03}. \qquad (3.14)$$

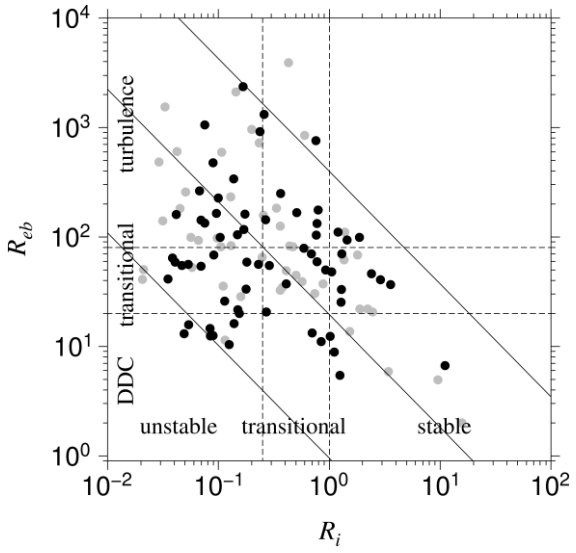

Fig. 3.6 Scatter plot of DDC layers on R_i and R_{eb} plane
Gray points indicate DC, black points indicate SF, and middle line shows the EOF 1st mode.

Eq. (3.14) means that ocean fields are unstable with smaller value of R_i along with turbulence activity being strong (R_{eb} takes large value). From the Eq. (3.14), for example, R_{eb} changed with R_i:

$(R_{eb},\ R_i) = (20, 0.25), (80, 1)\ldots$

Values of $R_i = 1.0$ means the stability criterion of water column, and if $R_i < 0.25$, water column become turbulent as was shown in subsection 1.6.2. Therefore, values of $R_{eb} = 20$, and 80 corresponding to R_i indicated the same criterion of water column.

DDC layers might be distributed when R_{eb} is below 10^3 (Fig. 3.6). However, Shih *et al*. [2005] found the importance of molecular processes in a certain range of:

$R_{eb} < 7$ *D* (diffusive regime),

$7 < R_{eb} < 100$ *I* (intermediate regime),

$100 < R_{eb}$ *E* (energetic regime).

Smyth *et al*. [2005] simulated turbulent mixings and obtained different values of K_S and K_T with various values of R_{eb} and R_ρ. D (the ratio between K_S and K_T) gets small when R_{eb} goes 0, and gets unity when R_{eb} goes 100. These means DDC should be effective when R_{eb} is below 100.

In contrast, DDC layers might be distributed when R_i is above 0.01. In laboratory experiments, Taylor [1991] showed that turbulence and DDC might co-exist since SF convection appears rapidly after it is destroyed by turbulence. Hence, DDC should appear in the range between 0.25 and 1 for R_i.

Taken together, the ranges, such as $R_{eb} < 80$ and $R_i > 0.25$ are suitable for new criterion of DDC. Thus $R_i > 0.25$ is applied in the next section using R_i instead of R_{eb}.

3.3.3. Parameterization proposed by Kimura *et al.* [2011]

I compared K_S^{Obs} and K_T^{Obs} calculated in this study with those obtained by Kimura *et al*. [2011] (hereafter, we call this as DNS parameterization). DNS parameterizations are conducted in limited situations; therefore it cannot be directly applied to observational results. However, I adapted their functional form to observation and tried to compare with microstructure data.

When 1 < R_ρ < 2, DNS parameterizations for K_S and K_T are expressed as

$$K_S^{\mathrm{SF,DNS}}\left(R_{\rho,}R_i\right) = 4.38\times10^{-5}R_\rho^{-2.7}R_i^{0.17}, \qquad (3.15a)$$

$$K_T^{\mathrm{SF,DNS}}\left(R_{\rho,}R_i\right) = 3.07\times10^{-5}R_\rho^{-4.0}R_i^{0.17}. \qquad (3.15b)$$

When R_ρ becomes large, $K_S^{\mathrm{SF,DNS}}$ and $K_T^{\mathrm{SF,DNS}}$ become small. When R_i becomes large, $K_S^{\mathrm{SF,DNS}}$ and $K_T^{\mathrm{SF,DNS}}$ become large. When I put observed R_i and R_ρ into DNS equations $K_S^{\mathrm{SF,DNS}}$ and $K_T^{\mathrm{SF,DNS}}$ (Fig. 3.7 small black points) are found to be smaller than K_S^{Obs} and K_T^{Obs} (large squares with error bars). Particularly, if I applied DNS parameterization when R_ρ is under 5, $K_T^{\mathrm{SF,DNS}}$ is obviously underestimated because it becomes smaller rapidly due to the functional dependence of R_ρ. However, dependences on R_ρ of $K_S^{\mathrm{SF,DNS}}$ and $K_T^{\mathrm{SF,DNS}}$ are similar to K_S^{Obs} and K_T^{Obs} (Fig. 3.7 a, b).

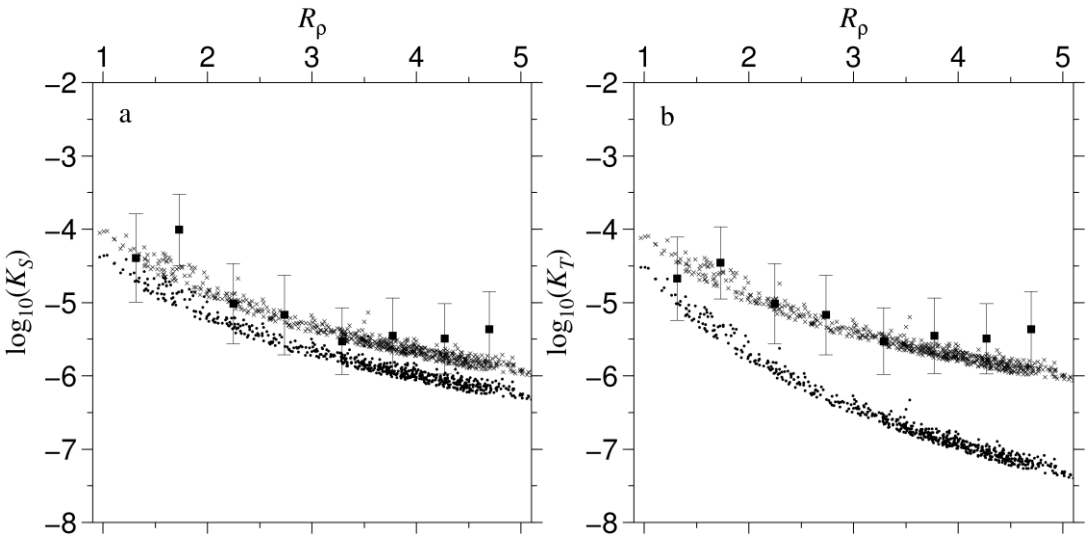

Fig. 3.7 Eddy diffusivities due to DDC (black squares: mean values of observational data, black points: DNS parameterization, crosses: improved, a: eddy diffusivity for salinity, b: eddy diffusivity for temperature).

The average value of the eddy diffusivity in the upper 1000m is about (2-4) $\times 10^{-5}\mathrm{m}^2/\mathrm{s}$ [Waterhouse *et al*. 2014]. If we use ordinary functional form of $K_T^{\mathrm{SF,DNS}}$, it becomes lower than the average value. This means that DNS parameterizations are not applied to oceanic data directly. Thus, I changed the functional form of $K_T^{\mathrm{SF,DNS}}$ to the same form as that of $K_S^{\mathrm{SF,DNS}}$ because the functional form of $K_S^{\mathrm{SF,DNS}}$ was a good performer when I use DNS parameterization with R_ρ under 5 (Fig. 3.7 a, b).

Then I calculated coefficients in order to fit to the observed values by following equations.

$$K_S^{Obs} = C^S R_\rho^{-2.7} R_i^{0.17}, \tag{3.16a}$$

$$K_T^{Obs} = C^T R_\rho^{-2.7} R_i^{0.17}, \tag{3.16b}$$

where C^S and C^T are the coefficients of each layer, and

$$K_s^{\mathrm{Obs}} = AR_\rho^{-2.7} R_i^{0.17}, \tag{3.17a}$$

$$K_T^{\mathrm{Obs}} = BR_\rho^{-2.7} R_i^{0.17}. \tag{3.17b}$$

Here,

$$A = \frac{\sum_{i=1}^{n} C_i^S}{n}, \tag{3.18a}$$

$$B = \frac{\sum_{i=1}^{n} C_i^T}{n}, \tag{3.18b}$$

where n is a number of layers. Then, I can finally obtain the new relationships

$$K_S^{\mathrm{Imp}}\left(R_\rho^{\mathrm{Obs}}, R_i^{\mathrm{Obs}}\right) = 9.35\times10^{-5} R_\rho^{-2.7} R_i^{0.17}, \tag{3.19a}$$

$$K_T^{\mathrm{Imp}}\left(R_\rho^{\mathrm{Obs}}, R_i^{\mathrm{Obs}}\right) = 7.61\times10^{-5} R_\rho^{-2.7} R_i^{0.17}. \tag{3.19b}$$

We can confirm that improved DNS parameterizations agree fairly well with the observed results (Fig. 3.7, crosses).

3.4. Summary and conclusion

A new indicator for DDC was proposed instead of R_{eb}. If R_i is larger than 0.25, we need to estimate eddy diffusivities due to the DDC when R_ρ is between 0.5 and 2. Also, refined functions of K_S or K_T focusing R_ρ and R_i were obtained by observational data by improving the DNS parameterization proposed by Kimura *et al*. [2011].

Chapter 4 Activities of mixing eddies inferred by the Richardson number

Abstract

A new relationship between the Thorpe scale L_T and the Ozmidov scale L_O ($L_O = R_{OT} L_T$, R_{OT} is the ratio between L_T and L_O) found in the western North Pacific Ocean differs from those obtained by previous studies. I found that the proportionality coefficient R_{OT} is a function of the buoyancy Reynolds number R_{eb} and is indicative of the stage of eddy decay. The functional form was estimated by the EOF analysis. Note that the EOF 1st mode is the fundamental relationship between the potential of stability and the turbulent activities, and the 95% confidential interval implied decay stage of turbulent eddies. Eddy activity is likely to be suppressed by buoyancy forces. Thus, R_{OT} is varies from place to place.

4.1. Introduction

Vertical displacements of isopycnal surface by strong current shear, internal waves or a turbulent eddy constitute an important mechanism of diapycnal mixing in the upper ocean and the nearshore region. The turbulence length scale has been used to estimate the turbulent diffusivity. Ozmidov [1965] first introduced such length scale L_O called as the Ozmidov scale, which is determined by ε and the buoyancy frequency N (Eq. 1.26 in subsection 1.6.4). Thorpe [1977] proposed a scale associated it with overturning events. The Thorpe scale L_T is inferred from vertical displacements needed to restore stable stratification by sorting the density profile to restore monotonicity (Fig. 4.1). Root Mean Square (RMS) of displacements is the Thorpe scale L_T (Eq. 1.27 in subsection 1.6.4). Thorpe [1977] also proposed a relationship between L_O and L_T from which eddy diffusivity can be estimated. Dillon [1982] found that L_O and L_T are related by $L_O = (0.8 \pm 0.4)L_T$ in the seasonal thermocline in lakes and ocean. Itsweire [1986] however proposed $L_O = (0.65 \pm 0.1)L_T$ in a grid generated turbulence experiments in a salt stratified water tunnel. Crawford [1986] proposed

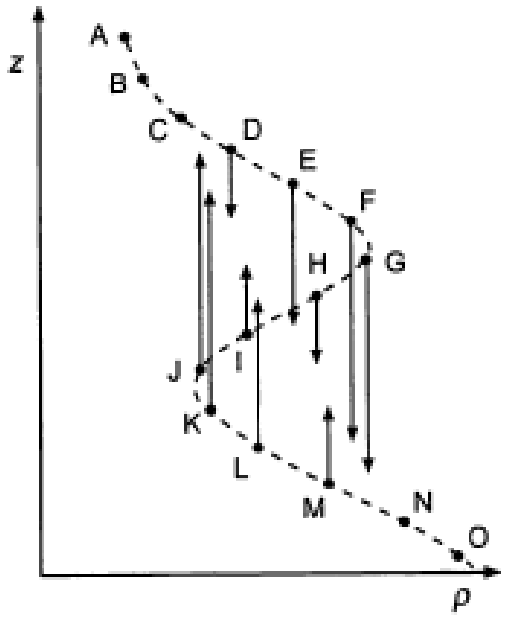

Fig. 4.1 Eddy in vertical density profile. Vectors show density inversion scales from Thorpe (2005).

$L_O = (0.66 \pm 0.27) L_T$ in the tropical Pacific Ocean. Wesson and Gregg [1988] found that L_O ranges between $0.25 L_T$ and $4 L_T$ from measurements at Camarinal Sill in the Strait of Gibraltar. Ferron *et al*. [1998] proposed $L_O = (0.95 \pm 0.6) L_T$ in the abyssal region near the Mid-Atlantic Ridge at the equator. Cheng and Kitade [2014] found that L_O is equal to $0.91 L_T$ in the equatorial Pacific. Thus, the proportionality constant R_{OT} in the $L_O - L_T$ relationship $L_O = R_{OT} L_T$ is not a universal constant and appears to depend on both location and hydrographic conditions. L_O is however considered as 0.8 L_T in most of previous studies [*e.g.* Stansfield *et al.* 2001(the Fuca Strait in between Canada and USA); Timmermans *et al*. 2003(the Canada Basin in the Arctic Ocean); Kitade *et al*. 2003b (Uchiura Bay in Japan); Thompson *et al.* 2007(Drake Passage); Jing and Wu 2010 (near the perturbed region in the North Pacific Ocean)]. Why does R_{OT} vary from place to place?

Smyth *et al*. [2001] showed that the mixing efficiency is a function of R_{OT} changes and with growth of eddies, and therefore R_{OT} is indicative of the stage of eddy decay. If R_{OT} implied the stage of eddy evolution, the mean value of R_{OT} should be same everywhere.

Recently, Mater *et al*. [2013] simulated the relationship between L_O and L_T using DNS. They obtained a relationship between R_{eb} $(= \varepsilon / \nu N^2)$ and turbulent time scale N_{TL}. They found that R_{OT} is a function of N_{TL} and thus a function of R_{eb}. As

for the role of R_{eb} in mixing events in the ocean, Nakano *et al*. [2014, chapter 3 in this thesis] introduced the relationship between R_{eb} and R_i obtained from CTD and LADCP data. Thus, R_{OT} can be considered to be a function of R_i.

R_{OT} is important for estimating eddy diffusivities using eddy scales; however the meaning of R_{OT} is unclear. In order to investigate this, I take following steps. First, the coefficient R_{OT} is estimated using both L_O and L_T. Second, the relationship between R_{eb} and R_{OT} is determined. Finally, I discuss the meaning of R_{OT}.

4.2. Data processing

After removing obvious errors in the vertical temperature and conductivity, I derived a 1-m running mean of the raw CTD data to remove the instrumental noise. [*e.g.* Kitade *et al.* 2003b]. Then the depth inversions are removed, and converted potential temperature θ and salinity S into potential density.

Using standard Thorpe technique, I reordered density profiles to restore stability. The difference between real depth Dep and reordered depth Dep' of a certain density is the Thorpe displacement scale d.

To detect overturning scale, I had to distinguish true overturning from density inversion obtained by CTD data. Thus, the water-mass test [Galbraith and Kelley 1996; hereafter GK96 filter] was conducted. I used GK96 filter as follows. First, the density inversion was detected. Next, a liner relationship between temperature (or salinity) and density within each density inversion was calculated using

$$\rho_\theta = a_\theta + b_\theta \theta , \tag{4.1a}$$

$$\rho_S = a_S + b_S S . \tag{4.1b}$$

RMS of density fluctuations between observed density ρ and liner fit density (ρ_S or ρ_θ) was calculated as

$$f1 = \left\{ \frac{1}{n} \sum_{i=1}^{n} (\rho_i - \rho_{\theta i})^2 \right\}^{\frac{1}{2}}, \tag{4.2a}$$

$$f2 = \left\{ \frac{1}{n} \sum_{i=1}^{n} (\rho_i - \rho_{Si})^2 \right\}^{\frac{1}{2}}, \qquad (4.2b)$$

where n is the number of data points in each overturn. These RMS values were normalized by density fluctuation $f3$ obtained by

$$f3 = \left\{ \frac{1}{n} \sum_{i=1}^{n} (\rho_i - \rho'_i)^2 \right\}^{\frac{1}{2}}, \qquad (4.3)$$

where ρ' is the Thorpe fluctuation density. Finally, if either of these normalized rms values ($f1/f3$ or $f2/f3$) were below 0.5, the inversion was regarded as real overturning.

L_T associated with the size of detected overturning was calculated by the following equation

$$L_T = \sqrt{\frac{\sum_{1}^{n} d^2}{n}}, \qquad (4.4)$$

where *d* is the Thorpe displacement [Thorpe 1977; Dillon 1982].

L_O is indicative of the upper bound on the size of the eddy, as proposed by Ozmidov [1965]

$$L_O = \sqrt{\varepsilon / N^3}, \qquad (4.5)$$

where ε is the turbulence kinetic energy (TKE) dissipation rate. I obtained $\varepsilon = \frac{15}{2} \nu \overline{\left(\frac{\partial u'}{\partial z} \right)^2}$ following the relation obtained by Osborn [1980]. The mean values of

$N = \sqrt{\frac{-g}{\rho_0}\frac{d\rho}{dz}}$ were also calculated from the back ground density gradients for each overturn. Using 0.2 as the value for the mixing efficiency Γ [Oakey 1982], $K_\rho = \Gamma \varepsilon / N^2$ can be estimated [*e.g.* Stansfields *et al.* 2001]. Note that, the vertical scales of ε, L_O and L_T were patch size of eddy.

4.3. Results and discussion

4.3.1. Relationship between the Thorpe scale and the Ozmidov scale

To illustrate the relationship between two scales, an example of eddies was provided. Overturning was observed to occur between 228db to 231db at station KH05TM07 during Hakuho - maru cruise, with a calculated L_T value of about 0.8m (Fig. 4.2). The corresponding L_O was estimated to be about 0.06m. The distributions of L_O and L_T in all the observed overturns were almost log – normal distribution (Fig. 4.3). The relationship between L_O and L_T obtained from least

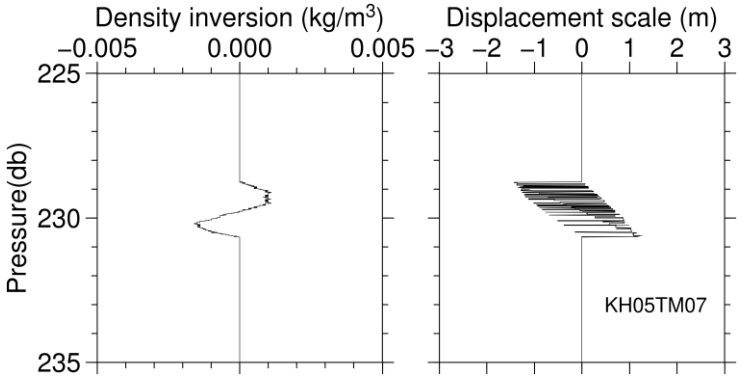

Fig. 4.2 Detected overturning (right: density inversion, left: displacement scales).

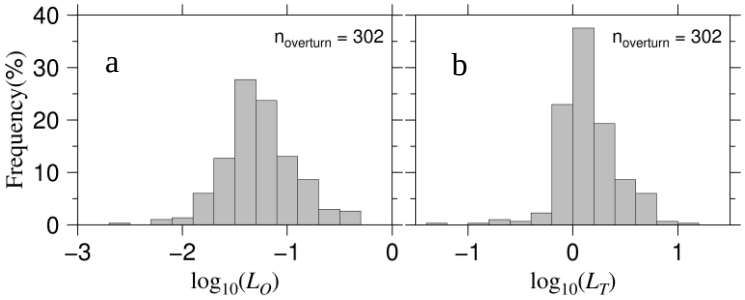

Fig. 4.3 Histograms of (a) L_O **and (b)** L_T**.**

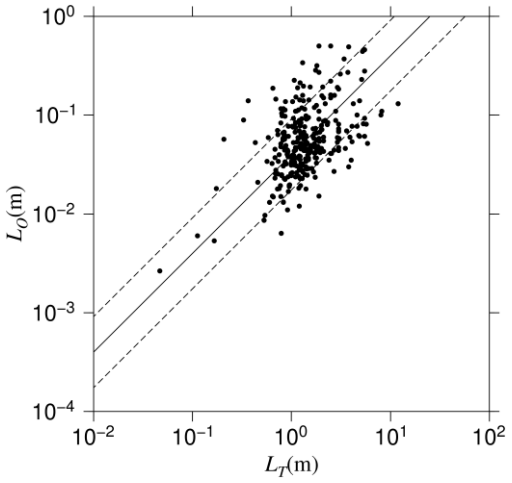

Fig. 4.4 Relationship between L_O **and** L_T**.** Black line shows best fitting line. Dashed lines are standard deviation ($\pm 1\sigma$).

square fitting (Fig. 4.4) is

$$L_O = 0.04 L_T . \qquad (4.6)$$

The correlation coefficient is about 0.5. Thus the value of R_{OT} is different from that proposed by Dillon [1982]. Wesson and Gregg [1994] obtained values ranging from 0.25 to 4 in high dissipation regions (values are about O (10^{-6}) ~ O (10^{-7})). In contrast, ε values in our data are lower by an order of magnitude (Table 4.1). This point will be further discussed in the following Section.

Table 4.1 Data from Hakuho-maru cruises[4].

Station	L_T 〔m〕	ε 〔W/kg〕	N 〔1/s〕	L_O 〔m〕
KH05TM02	1.89	1.19E-09	8.01E-03	1.52E-02
KH05TM06	1.10	4.24E-10	3.91E-03	8.41E-02
KH05TM10	0.87	2.82E-09	5.31E-03	1.37E-01
KH07TM02	0.80	2.50E-10	6.10E-03	1.00E-01
KH07TM04	3.80	1.60E-08	4.00E-03	4.90E-01
KH08TM06	1.73	2.63E-10	7.81E-03	6.20E-01
KH08TM20	0.37	9.05E-10	7.73E-03	1.40E-01

[4] The order of N was similar to that from Wesson and Gregg (1994). The order of ε was smaller than their values.

4.3.2. The relationship between R_{OT} and R_{eb}

R_{OT} is necessary for estimating eddy diffusivities [e.g. Clayson and Kantha 2008]. This coefficient is however obtained by only microstructure observations. Is it possible to obtain R_{OT} from hydrographic data?

As mentioned above, Mater *et al*. [2013] used DNS to simulate the relationship between R_{OT} focused on R_{eb} and turbulent time scale N_{TL}. They found that R_{OT} is a function of N_{TL}. Following them, I obtain the relationship between R_{eb} and R_{OT} (Fig. 4.5) from observations:

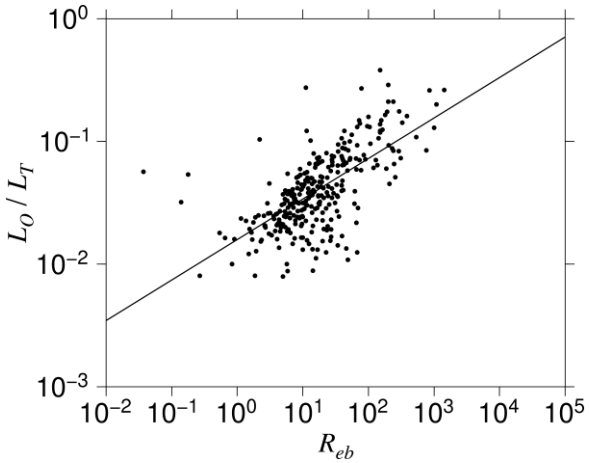

Fig. 4.5 Relationship between R_{eb} and R_{OT}. Black line is a best fitting line.

$$R_{OT} = 1.59 \times 10^{-2} R_{eb}^{\ 0.33}. \qquad (4.7)$$

R_{OT} becomes large when R_{eb} becomes large ($R_{eb} \to \infty$). This equation represents the relationship between the current stage of turbulence and eddy activity. For example, Smyth *et al*. [2001] showed that R_{eb} changed with progress of eddy decay. The value of R_{OT} parameterized in the present study is however smaller than that estimated by Mater *et al*. [2013]. This discrepancy may be caused by difference in resolutions between simulation and observations.

4.3.3. The relationship between R_{eb} and R_i

R_{eb} was estimated by Nakano *et al*. [2014] or chapter 3 in this study using hydrographic data in DDC layers. Lozovatsky and Fernando [2012] estimated it in the atmosphere and proposed a relationship between R_i and R_{eb} in order to reveal the distribution of mixing efficiency with them. These relationships enable us to decide whether the molecular viscosity is important for mixing or not using fine scale data. In this study, R_i was calculated using N and S_h obtained by LADCP observation.

Following Lozovatsky and Fernando [2012], if we assume that R_i and R_{eb} are related to each other in the ocean, then the relationship between R_{eb} and R_i in my observational data is described by

$$R_{eb} = 1.12 \times 10 R_i^{-1.72}. \qquad (4.8)$$

In Figure 4.6, the first EOF mode shows the relationship between the potential of stability and the turbulent activity. The region between 95% confidence intervals shows existence of various eddies and their decay stage.

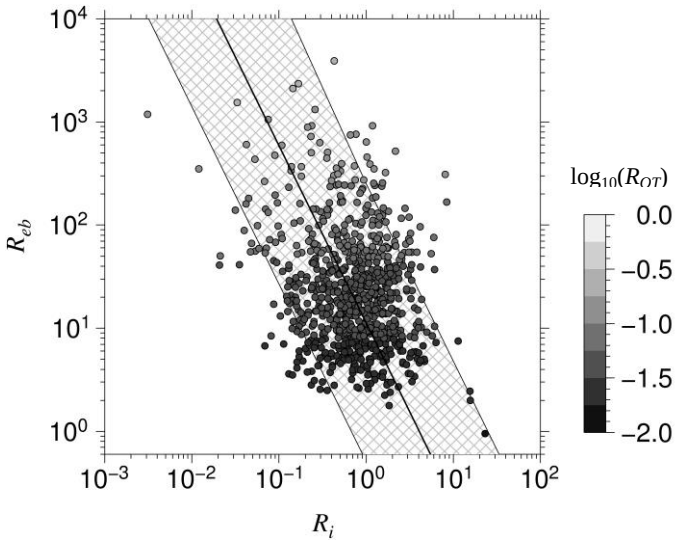

Fig. 4.6 R_{OT} **distribution with** R_i **and** R_{eb}**.**

4.3.4. The relationship between R_{OT} and R_i

Smyth *et al*. [2001] have suggested that the mixing efficiency is a function of R_{OT}.

$$\Gamma = 0.33 R_{OT}^{-0.63}. \qquad (4.9)$$

However, the mixing efficiency is a function of R_i and therefore R_{OT} should become a function of R_i. Eq. (4.9) merely implies that R_{OT} is affected by buoyancy and shear.

Unfortunately, we cannot obtain the relationship between R_{OT} and R_i directly, because of lower resolution of LADCP. Maximum resolution is 4m for LADCP; in contrast, eddy scales are ~O (10^0). However, when I substitute Eq. (4.7) into Eq. (4.8), R_{OT} is obtained as a function of R_i:

$$R_{OT} = 3.50 \times 10^{-2} R_i^{-0.57}. \qquad (4.10)$$

For small values of R_i ($<10^{-3}$), R_{OT} is large (~ 0.8), which is consistent with the idea that strong shear promotes instability. In the previous studies [*e.g.*, Dillon, 1982; Wesson and Gregg, 1994], ε is so high being due to high shear ($R_i << 1$) and their estimated R_{OT} had a large value. This suggests that their parameterization is useful only in high shear regions. The average value of R_i is 0.74 and R_{OT} is estimated to be considerably smaller at 0.04. Eq. (4.10) agrees fairly well with observation results. Thus, we can estimate eddy diffusivity from fine scale observational data in the upper ocean.

The dependence of R_{OT} on R_i (Fig. 4.6) means that the stage of eddy decay

depends on the stability of the water column. If the column is stable (unstable), the range of R_{OT} is in lower value (higher value). In other words, the buoyancy effects can suppress motion of eddies.

4.3.5. Test for the relationship

Anyway, I need to test these relationships, and hence, the data in the offshore of Miyake Island were used. The relationship between L_O and L_T was

$$L_O = 0.15 L_T . \qquad (4.11)$$

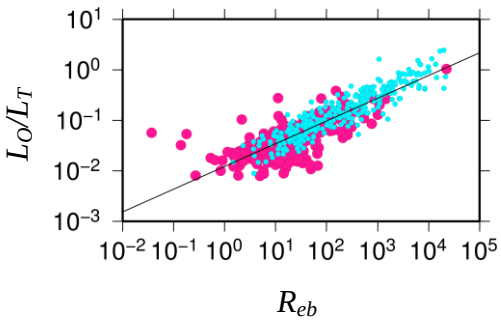

Fig. 4.7 the Relationship between R_{eb} and R_{OT} (KH cruise (pink circles), SY cruise (light blue)). Black line shows Eq. (4.12).

R_{eb} and R_{OT} in the offshore of Miyake Island (Fig. 4.7 light blue dots) are clearly large compared with NPO (Fig. 4.7 pink circles). The relationship between R_{eb} and R_{OT} was wrote as Eq. (4.12) and described as

$$R_{OT} = 1.22 \times 10^{-2} R_{eb}^{\ 0.45} . \qquad (4.12)$$

By the simulation, Mater *et al*. [2013] found the two functional forms between R_{eb} and the turbulent timescale N_{TL} (Fig. 4.8). If N_{TL} becomes larger than unity, the function $R_{OT}^{-1} = (N_{TL})^{3/2}$ changed to $R_{OT}^{-1} = (N_{TL})^{1/2}$. Also, the scatter plot on $L_O - L_T$ plane changed the function when L_O is 2×10^{-1} (in their DNS, the grid is no dimension thus the range is different from observational results in this thesis).

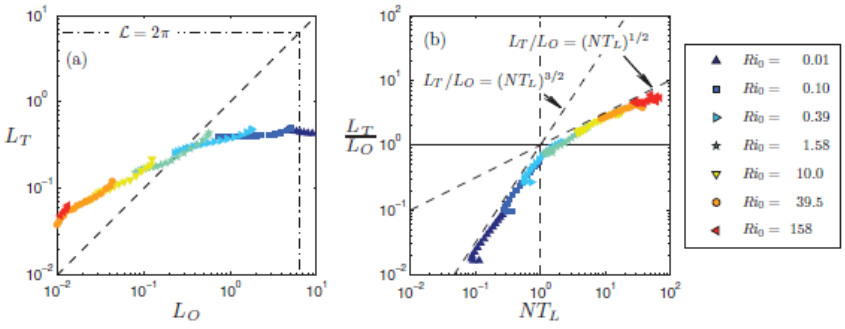

Fig. 4.8 Relationship between R_{eb} and R_{OT} proposed by Mater et al. [2013].

Thus, I focused on functions distinguished the range of R_{eb}: (1) $R_{eb} < 100$ molecular viscosity is important for mixing, (2) $R_{eb} \geq 100$ turbulence is only important for mixing following Shih *et al*. [2005] and Nakano *et al*. [2014, Chapter 3] (Fig. 4.9).

(1) $R_{OT} = 1.61 \times 10^{-2} R_{eb}^{1/3}$ (Dashed and dotted line), (4.13a)

(2) $R_{OT} = 1.07 \times 10^{-2} R_{eb}^{1/2}$ (Broken lien). (4.13 b)

I found the one by three power low and the one by two power low in the progress stages of eddies.

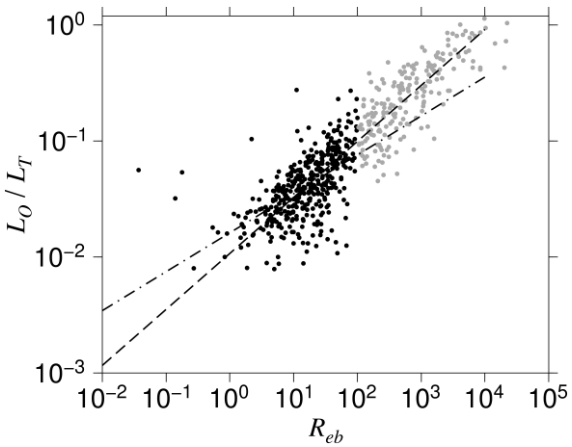

Fig. 4.9 Relationship between R_{OT} and R_{eb}.
(Black points, and dashed and dotted line: $R_{eb} < 100$, gray points and dashed line $R_{eb} \geq 100$**)**

If I use Eq. (4.8) and Eq. (4.13), I could get table 4.2. These values are fairly well coincided with direct estimation values (Table 4.2).

Table 4.2 Comparison of results.

Place	Observed R_{OT}	Observed R_i	Calculated R_{OT}
North Pacific Ocean	0.04	0.72	0.04
Offshore of Miyake island	0.15	0.13	0.18

4.4. Summary and conclusion

The proportionality coefficient R_{OT} in the relationship between L_O and L_T was estimated from microstructure data in the western North Pacific Ocean and the offshore of Miyake island. Its value differs from previous studies [e.g. Dillon 1982]. R_{OT} is found to vary from place to place. It was highly correlated with R_{eb} (Eq. 4.7 and Eq. 4.13), which implies that it depends on the decay stage of eddies. If we use the relationship among Eq. (4.9), Eq. (4.8), and Eq. (4.13), R_{OT} is also a function of R_i. This relationship means that R_{OT} obtained by Eq. (4.13) is affected by buoyancy.

Chapter 5 Mixing efficiency in the western North Pacific Ocean

Abstract

A better parameterization of turbulent mixing in the ocean and the atmosphere requires a better understanding of how turbulence behaves in a stably stratified flow. In this chapter, I estimate the turbulence mixing efficiency Γ (and its equivalent dissipation ratio in regions of DDC) in the western North Pacific Ocean using the dissipation rate of turbulence kinetic energy ε and the dissipation rate of temperature variance χ_θ measured by a microstructure profiler. While the measurements show that the mean geometric mean value of Γ is 0.18, the value of Γ is widely distributed between values of O (10^{-3}) and O (10^{3}). Measurements in DDC layers show that Γ is large for DC, but becomes small compared to values under fully turbulent conditions when SF occurs. This suggests that Γ depends on prevailing hydrographic conditions. Furthermore, Γ appears to be a function of the buoyancy Reynolds number R_{eb}. It becomes large in layers where viscosity dominates and R_{eb} falls below 100. The study also indicates that oceanic eddy diffusivities of momentum and temperature differ from each other.

5.1 Introduction

Except for turbulent mixed layers immediately adjacent to the air-sea interface and the bottom, global oceans (and also the atmosphere) are for the most part stably stratified. For a better understanding and parameterization of turbulent mixing [e.g. Kantha 2003; Kantha and Carniel 2009], it is essential to understand how turbulence behaves in the presence of stable stratification. It is often assumed that the mixing efficiency Γ of turbulence in the ocean, defined as

$$\Gamma = \frac{R_f}{1-R_f}, \tag{5.1}$$

where R_f is the flux Richardson number, having a constant value of somewhere between 0.2 and 0.33. This is equivalent to assuming that R_f has a value between 0.17 and 0.25, which means that only 17 to 25% of turbulent energy gets converted into the potential energy to mix water masses, and the remainder is dissipated. However, it is easy to show that Γ is not a constant and is actually a function of parameters such as $R_i = N^2/S_h^{\,2}$. For example, the second moment closure model of mixing in stably stratified fluids of Kantha and Carniel [2009] demonstrates that for the best agreement with available data over a wide range of R_i values, $\Gamma = \Gamma_\infty\left(1-e^{-cRi}\right)$, where $\Gamma_\infty = 1/3$, corresponding to R_f value of 0.25 and $c = \left(R_{f\infty}\,\mathrm{Pr}_0\right)^{-1} = 5$, Pr_0 being the Prandtl number, the ratio of momentum diffusivity to heat diffusivity. It was Munk and Wunsch [1998],

who first cast some doubt on the constancy of Γ by considering various types of energy sources for mixing in the ocean. Many investigations have been conducted on Γ since then (see the list of references). This study makes use of microstructure observations made recently in the western North Pacific Ocean to shed some more light on this topic. In this region of the ocean, turbulent layers created by both conventional shear turbulence and DDC occur, and therefore the data provide an opportunity to investigate and contrast the behavior of turbulence in the two situations. Note that Γ can be written as

$$\Gamma = \frac{\chi_\theta N^2}{2\varepsilon \bar{T}_z^2}, \tag{5.2}$$

where $\chi_\theta = 6\kappa_T \overline{\left(\partial T'/\partial z\right)^2}$ (where κ_T is the molecular thermal diffusivity, $\partial T'/\partial z$ is the vertical gradient of temperature fluctuation) is the dissipation rate of temperature variance, and $\bar{T}_z$ is the vertical gradient of mean temperature. Microstructure profilers deployed from oceanographic vessels are capable of measuring all the quantities on the right hand side of Eq. (5.2) and hence able to provide values for Γ. In this context, it is important to point out that strictly speaking, Γ can be regarded as mixing efficiency only for conventional shear turbulence. For turbulence generated by DDC, Γ is more correctly called the dissipation ratio, since the actual mixing efficiency, which is equal to the ratio of buoyancy flux to the dissipation rate, is identically equal to 1.0 [Kantha 2016 (personal communication), St. Laurent and Schmitt 1998]. This distinction is important to

remember.

Osborn [1980] was the first to propose the value for Γ of 0.2. Oakey [1982] found Γ to be 0.259 ± 0.214 during the JASIN experiment northwest of Scotland. Oakey [1985] suggested an improved value for Γ of 0.265 (0.066~0.436). Oakey [1988b] also discovered that Γ becomes large compared to the value under turbulent conditions when DC occurs. St. Laurent and Schmitt [1998] also surveyed Γ in fingering layers, and obtained a large value for Γ (~0.6) compared to the value in turbulent layers (~0.2). There has been a surge of interest in Γ in recent years. Lozovatsky *et al*. [2006] studied the relationship between Γ and R_i in the mixed layer. Lozovatsky and Fernando [2012] concluded that Γ is a function of R_i or a pseudo-Reynolds number $R_{eb} = \varepsilon / \nu N^2$, also known as buoyancy Reynolds number. They suggest that Γ can be represented by

$$\Gamma_{R_{eb}}^{\mathrm{Lo13}} = 50 R_{eb}^{-1/2}; \qquad \Gamma_{R_i}^{\mathrm{Lo13}} = 0.005 + 1.7 R_i - 1.1 R_i^2 \quad . \qquad (5.3)$$

However, the utility of the buoyancy Reynolds number R_{eb} is not the same as that of the Reynolds number $\mathrm{Re} = \frac{q\ell}{\nu}$ defined using appropriate velocity and length scales q and ℓ, and regarded traditionally in turbulent flows as a true measure of the relative importance of inertial and viscous terms. As pointed out by Mater *et al*. [2013], $R_{eb} = \mathrm{Re}\left(Nt\right)^{-2}$, where $t = \ell / q$ is the turbulence time scale associated with energy containing eddies. Since R_{eb} depends on the ratio of turbulence time scale to the

buoyancy time scale, it is not a true measure of the relative importance of viscosity. It is traditional to consider the asymptotic state of fully developed turbulence in parameterizing mixing, which requires Re being sufficiently large to drop out of the picture. However, large values for Re does not necessarily imply large values of R_{eb}. As *N* goes to zero and the flow becomes more neutrally stratified, R_{eb} becomes very large even when Re is not necessarily large enough to assure asymptotic state [Kantha 2016 (personal communication)]. This must be kept in mind in evaluating parameterizations based on R_{eb} suggested by various studies. Also, these apply only to conventional shear-generated turbulence and do not hold for turbulence generated by DDC. This distinction is also important to remember.

Laboratory experiments have also been done to determine the value of Γ. Linden [1979] conducted laboratory experiments on the deepening of the mixed layer by the grid generated turbulence, and examined the change in R_f as mixed layer deepened. He found that R_f is related to the overall Richardson number $R_{io} = g\Delta\rho D / \rho_{mean}(\Delta U)^2$, where $\Delta\rho$ is the density difference between the two layers, D is the vertical distance from the bottom of the tank, ρ_{mean} is the mean density of two layers, and ΔU is the velocity difference between the two layers. Fernando [1991] also experimented with turbulence in stratified fluids, and also showed that R_f changes with R_{io}. Monti *et al.* [2008] conducted experiments in stably stratified shear flows and measured density and

velocity structures in order to investigate the temporal evolution of Γ. Prastowo *et al.* [2008, 2009] performed laboratory experiments on gravity currents in narrow straits with various types of sill on the bottom, and considered the relationship among the initial potential energy P_i, the final potential energy P_f, and the potential energy of a hypothetical state without mixing P_h. They suggest that Γ is a function of the energy differences:

$$\Gamma = \frac{P_f - P_h}{P_i - P_h} \quad . \tag{5.4}$$

Other researchers have focused on the relationship between fluxes and Γ. Moum [1996] suggested that Γ is a ratio of fluxes:

$$\Gamma_d^{\mathrm{Mo96}} = F_\chi / F_\varepsilon \, , \tag{5.5}$$

where F_χ is the flux of the heat estimated by χ_θ, and F_ε is that estimated by ε. Gargett and Moum [1995] obtained Γ by direct and indirect measurements of the density flux and indicated that the geometric mean value of Γ is 0.73. The range of $\log_{10}\Gamma$ was however very broad, between -2 and +2.

Additionally, Γ is thought to be related to turbulent eddy activity. Rohr and Vanatta [1987] conducted laboratory experiments on stratified turbulent flows and considered that R_f changed with $R_{OT} = L_O / L_T$, here L_T is the Thorpe scale and L_O is the Ozmidov scale, respectively. Wijesekera and Dillon [1997] investigated the relationship between

R_{OT} and Γ by DNS and found that Γ changes with R_{OT}:

R_{OT}	Γ
< 0.125	0.56
0.125-0.50	0.47
0.5-2.0	0.23
2.0-8.0	0.22
> 8.0	0.33

Smyth *et al*. [2001] parameterized Γ using R_{OT} in their DNS. Considering the decay of turbulent eddies, they found that Γ changes with mixing condition and described it as $\Gamma_{R_{ot}}^{Sm00} = 0.33\left(R_{OT}\right)^{-0.63}$. When they applied this equation to observational data, the eddy diffusivities changed slightly compared with those obtained using the constant value of 0.2 for Γ. Using DNS to study the change of R_f during decay of eddies, Mater and Venayagamoorthy [2014] obtained Γ as a function of R_i and R_{eb}.

de Lavergne *et al*. [2015] studied the effect of variable Γ on diapycnal mixing in the abyssal overturning by numerical simulation. They suggest that the dia-neutral density flux changes when variable value of Γ is used.

It is clear from studies cited above, Γ is not a constant even for conventional shear-driven turbulence in stably stratified flows. Also distinction must be made between conventional turbulence and turbulence induced by DDC in the ocean. However there are

still very few estimates of Γ from observations and not enough in the ocean. In this chapter, I deal with Γ in the upper layers of the western North Pacific Ocean, where both DC and turbulence coexist.

5.2. Data processing

5.2.1. The temperature dissipation rate χ_θ and the Maximum Likelihood Estimation

After obtaining ε (Eq. 3.3), I calculated the temperature dissipation rate χ_θ the temperature fluctuation data $T' = T - \bar{T}$, where $\bar{T}$ is the back ground average temperature measured by FPO-7. T' is passed through the FFT (2048 points) and converted into χ_θ using Maximum Likelihood Estimation (MLE). Ruddick *et al*. [2000] evaluated the average value of vertical temperature fluctuation with the probability density function as

$$C11 = -\sum_{i}^{N}\left(\frac{S_{obs} - S_B + S_n}{S_B + S_n}\right)^2 - \ln(S_B + S_n) + N_{MLE}\left(\frac{1}{4} + \sqrt{\frac{d_{MLE}}{4\pi}}\right), \qquad (5.6)$$

where $S_B = \sqrt{q_B / 2}\, f(\alpha_B)\kappa_T k_B^{-1}\chi_\theta$ is the Batchelor spectrum (κ_T is 1.39×10^{-7} m^2/s, q is 3.2 in this study), S_{obs} is the observed spectral value of temperature fluctuations, and S_n is the instrumental noise spectral value ($=3\times10^{-7}$ (degree/m)^2/cpm). k_B is the Batchelor frequency defined as

$$k_B = \left(\frac{\varepsilon}{\nu\kappa_T{}^2}\right)^{1/4} . \qquad (5.7)$$

d_{MLE} is the degree of freedom and N_{MLE} is the number of observational spectrum in each 10m. I used the average value of ε obtained from the two shear probes. Here, $f(\alpha)$ is written as

$$f(\alpha_B) = \alpha_B \left(e^{-\alpha^2/2} - \alpha_B \int_{\alpha}^{\infty} e^{-x^2/2} \right), \tag{5.8}$$

where α is $\kappa_T k_B^{-1} \sqrt{2q_B}$. Considering the MLE and looking at the functional form of S_B on χ_θ, I set $S_B = A\chi_\theta$. Then, Eq. (5.6) becomes

$$C11 = -\sum_{i=1}^{N} \left(\frac{S_{obs} - (A\chi_\theta + S_n)}{A\chi_\theta + S_n} \right)^2 - \ln(A\chi_\theta + S_n) + N\left(\frac{1}{4} + \sqrt{\frac{d}{4\pi}} \right). \tag{5.9}$$

I differentiate Eq. (5.9) with χ_θ, and considered that the differential Equation should have extreme values, and obtained χ_θ as

$$\chi_\theta = \frac{(\sqrt{3}-1)S_{obs} - S_n}{A}. \tag{5.10}$$

After that, I confirmed the each spectrum visually (Fig. 5.1). Then, the vertical gradients of the temperature $\frac{\partial \bar{T}}{\partial z}$ and the buoyancy frequency N were calculated every 10 m, and used to calculate Γ in each 10 m layer.

$$\Gamma = \frac{\chi_\theta N^2}{2\varepsilon \bar{T}_z^2}, \tag{5.11}$$

Note that, the data obtained while KH07 cruise were ignored in this paper because of strong noise in T' data.

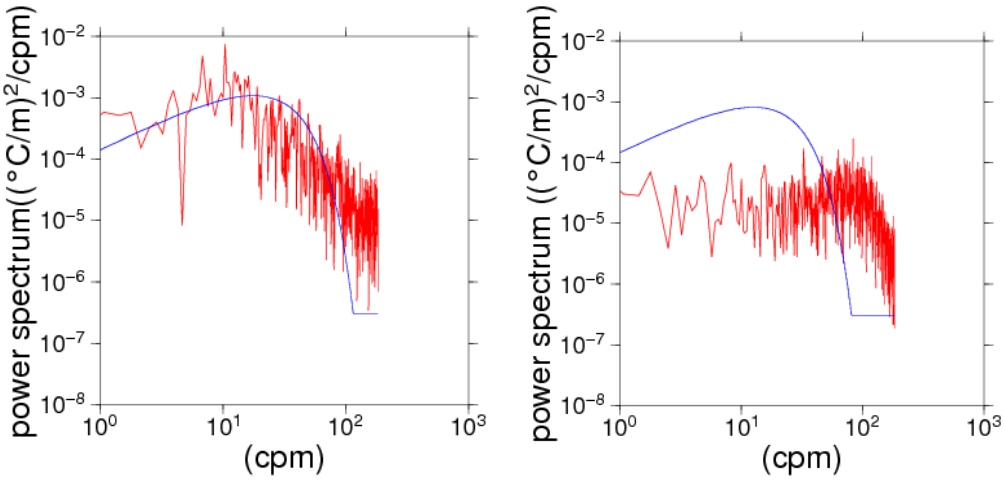

Fig. 5.1 Fitted spectrum (blue) and observed spectrum (red). Spectrum in left panel could pass, in contrast, that in right panel could not pass.

5.3. Results and Discussion

5.3.1. Statically analysis on Mixing Parameters

The estimated geometrical mean value of Γ is 0.18, and the mode is about 0.1 (Fig. 5.2). The mean value is slightly less than the values obtained by Osborn [1980] and Oakey [1982, 1985]. Γ is widely distributed (between $O(10^{-3}) \sim O(10^{3})$), hence cannot be constant. I consider the functional dependence of Γ on R_{eb}, the density ratio R_{ρ}, the gradient Richardson number R_i in the following sections.

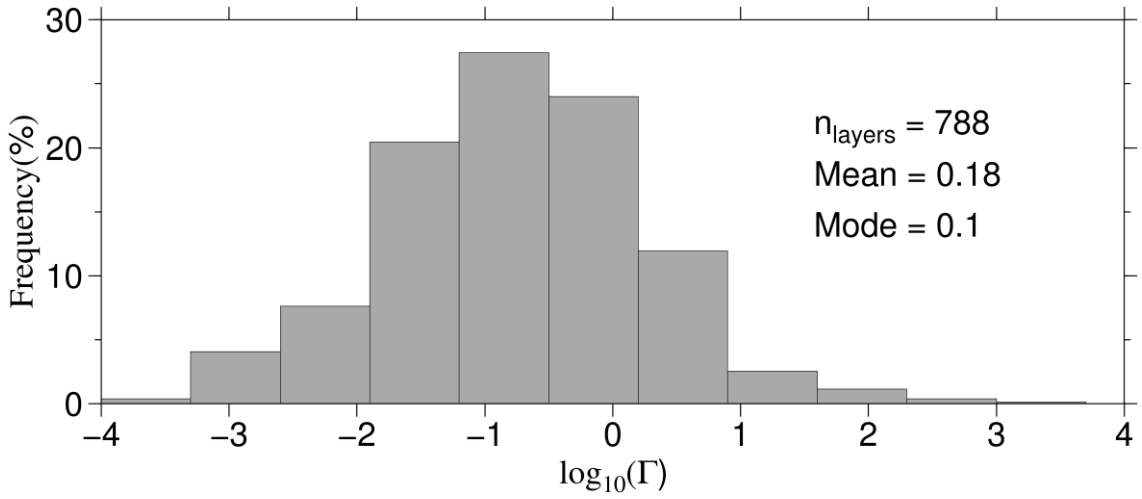

Fig. 5.2 Histogram of $\log_{10}\Gamma$.

5.3.2. Effects of the double diffusive convection and the viscosity

DDC is one of the mixing mechanisms in the western North Pacific Ocean, [e.g. Talley and Yun 2001; Inoue *et al*. 2007; Shimada *et al*. 2007]. Therefore, I focused on the relationship between the dissipation ratio Γ and the density ratio R_ρ (Eq. 3.1). Conditions are conducive to SF when $1 < R_\rho$ (particularly active SF occurs when $1 < R_\rho < 2$) and DC when $0 < R_\rho < 1$ (particularly active DC occurs when $0.5 < R_\rho < 1$).

To understand the relationship between Γ and stratification, following St Laurent and Schmitt [1998], I plotted distributions of Γ with the value of R_ρ and R_i (Figs. 5.3 and 5.4). R_i was calculated using N and the vertical shear of horizontal velocity S_h obtained by LADCP observations (see Eq. 1.14 and Eq. 1.15).

Focusing on the value of Γ for values of R_ρ becoming small (Fig. 5.3), Γ is large, O ($10^0 \sim 10^2$), when weak DC occurs ($0 < R_\rho < 0.5$). The reason might be that during DC the temperature distribution is unstable (the upper layer is cool/fresh and the bottom layer is warm/salty). The temperature variance becomes large, and so do χ_θ and Γ (Eq. 5.11). In contrast, when SF occurs (for $1 < R_\rho$, particularly $2 < R_\rho$), Γ is not so large, O ($10^{-2} \sim 10^0$), because the temperature distribution is stable. The number of DC layers are a fewer (50) than the number of SF layers (502) in my observational data. However the effect of DC layers on Γ cannot be ignored.

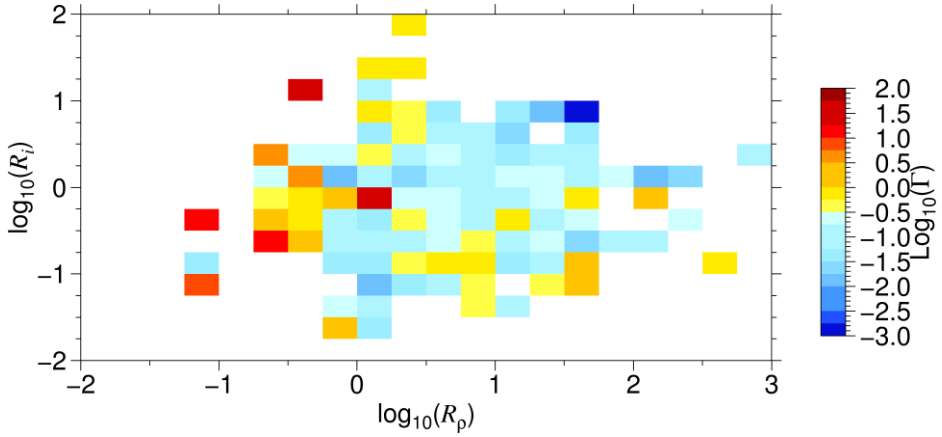

Fig. 5.3 Distribution of the mixing efficiency focusing on R_ρ is positive (in DDC layers).

The value of Γ is broadly distributed and is O (10^{-2}~10^{0}), in the statically stable (SS) layers, characterized by negative values of R_ρ (Fig. 5.4), in which both salinity and temperature are stably stratified. The reason might be due to the damping effect of viscosity. Therefore I will focus on the effect of viscosity on Γ. How does the viscosity affect Γ?

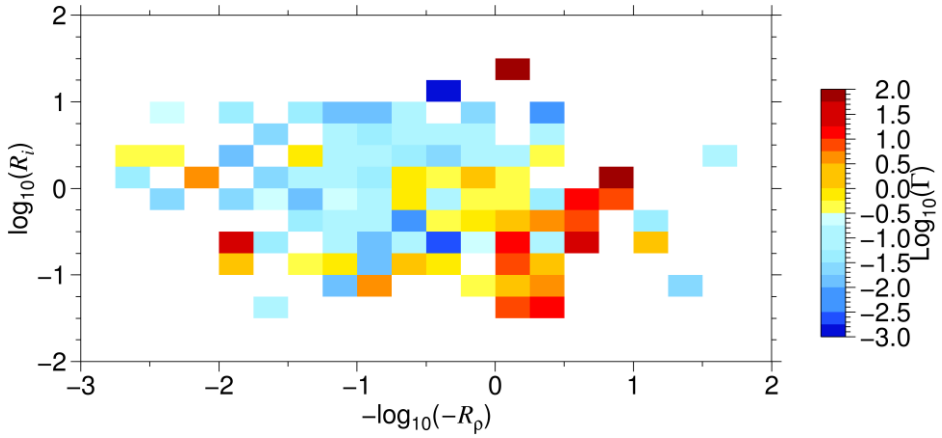

Fig. 5.4 Distribution of the mixing efficiency focusing on R_ρ is negative (in statically stable layers).

The distribution of Γ with R_i, and the buoyancy Reynolds number R_{eb} ($=\varepsilon/\nu N^2$) is different among the DC, SF and SS layers (Fig. 5.5). However, large values of Γ is almost distributed with the smaller values of R_i (<10 in DDC layers, <1 in doubly stable layers), and R_{eb} (<100). Shih *et al*. [2005] found that viscosity is effective when R_{eb} is below 100 and obtained diffusivities by different equations with the value of R_{eb}. They categorized the behavior of mixing ($R_{eb}<7$: diffusive regime, $7<R_{eb}<100$: intermediate regime, $100<R_{eb}$: energetic regime). In the present analysis, large Γ is distributed when R_{eb} is between 1 and 100. Thus, the large value of Γ was caused by turbulence damped by viscosity.

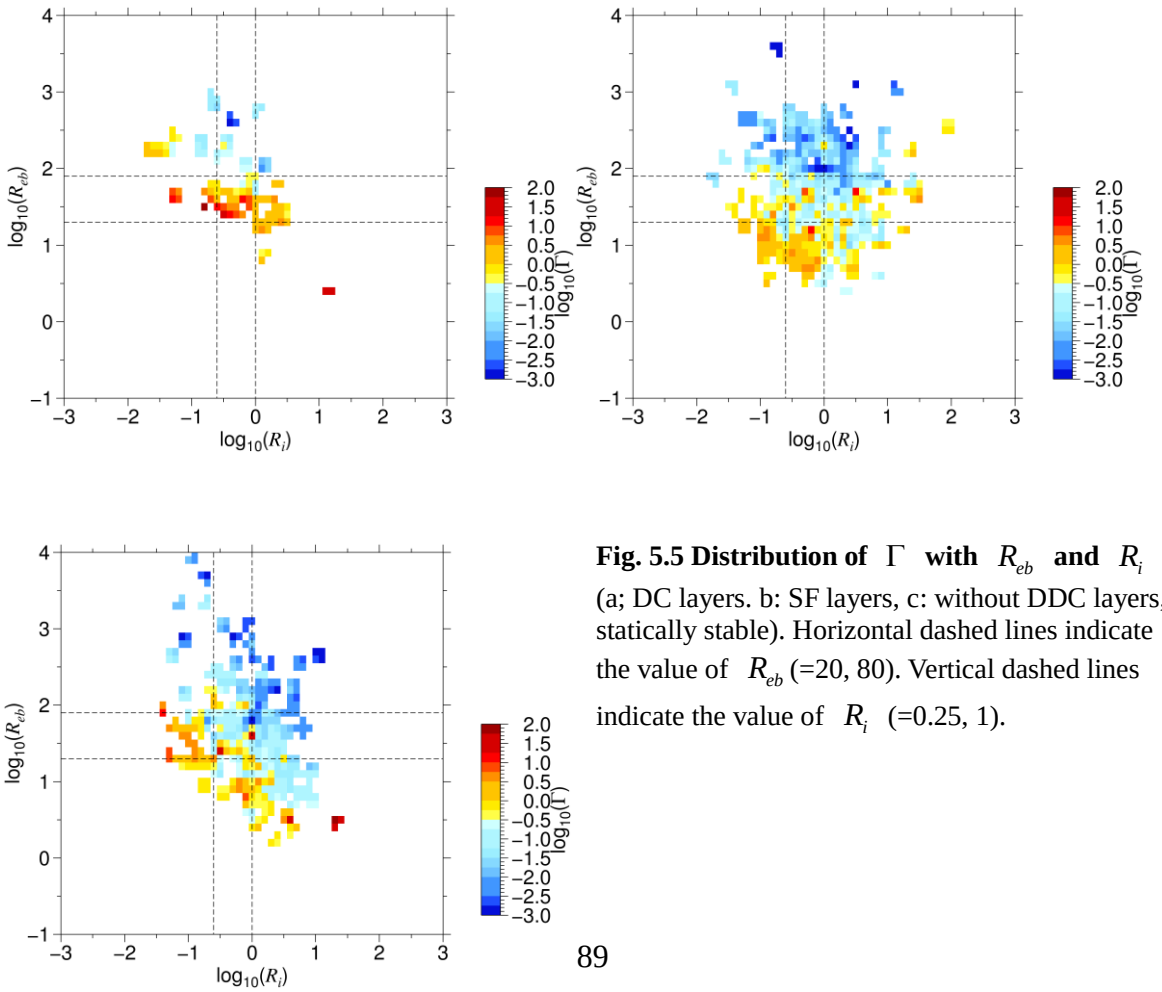

Fig. 5.5 Distribution of Γ with R_{eb} and R_i (a; DC layers. b: SF layers, c: without DDC layers, statically stable). Horizontal dashed lines indicate the value of R_{eb} (=20, 80). Vertical dashed lines indicate the value of R_i (=0.25, 1).

In oceanic flows containing the effect of viscosity, the average value of Γ is clearly determined by R_ρ (Fig. 5.6). In active SF layers, it is 0.10, smaller than that obtained by Oakey [1988b] and St. Laurent and Schmitt [1998], because of the unstable conditions of layers (in this paper: $\log_{10}(R_i) < 1$, St. Laurent and Schmitt [1998]: $2 < \log_{10}(R_i)$).

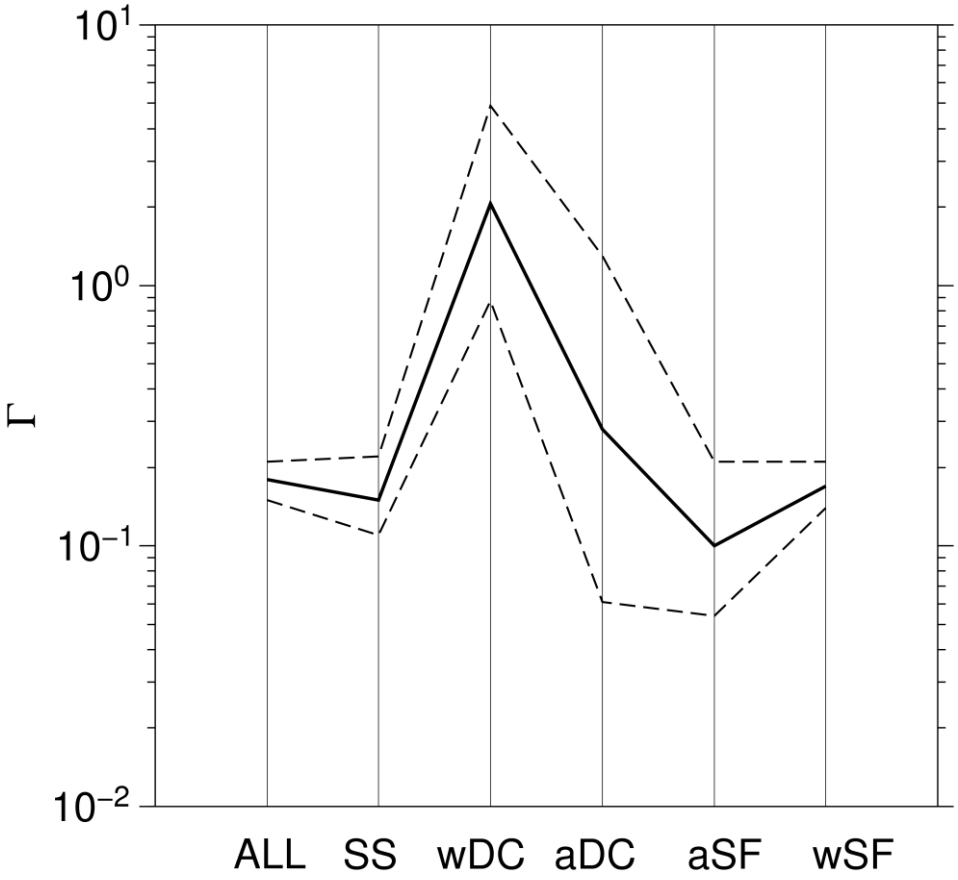

Fig. 5.6 The mixing efficiency distinguished by the density ratio. Dashed lines show the 95% confidential area, and thin line shows geometric mean value. The geometric value s are 0.21 in all layers, 0.22 in only turbulent (statically stable) layers, 2.0 in weak DC layers, 0.28 in active DC layers, 0.10 in active SF layers, and 0.17 in weak SF layers.

5.3.3. Buoyancy Reynolds number

The relationship between Γ and R_{eb} is considered next. Using DNS simulations, Shih *et al*. [2005] suggest

$$\Gamma_{R_{eb}}^{\mathrm{Sh05}} \approx R_f^{\mathrm{Sh05}} \approx 1.5 R_{eb}^{-1/2}, \tag{5.12}$$

whereas Mater and Venayagamoorthy [2014] suggest

$$\Gamma_{R_{eb}}^{\mathrm{MV14}} \approx \Gamma_f^{\mathrm{MV14}} \approx R_f^{\infty} \left\{ 1 - \exp\left(-7.5 R_{eL} S T_L^{-2} R_{eb}^{-1} \right) \right\}, \tag{5.13}$$

where R_f^{∞} is taken as 0.25. ST_L is the shear strength parameter indicative of the stability of flow (the value is 5 in their paper). The turbulent Reynolds number $R_{eL} = T_L / T_\eta$, where T_L is the time scale of the inertial motions and T_η is the Kolmogorov time scale, is 160. The expression is derived by substituting for R_i using the identity $R_i = R_{eL} S T_L^{-2} R_{eb}^{-1}$.

In this study, I found that the relationship between Γ and R_{eb} in the SS layers (Fig.5.7) is best represented by

$$\Gamma_{R_{eb}} = 1.4 R_{eb}^{-2/3}. \tag{5.14}$$

This equation agrees fairly well with those proposed by previous studies (Eqs. 5.12 and 5.13). The geometric mean value of Γ has a similar distribution compared with that obtained by DNS simulations (Shih *et al*., 2005; Mater and Venayagamoorthy 2014).

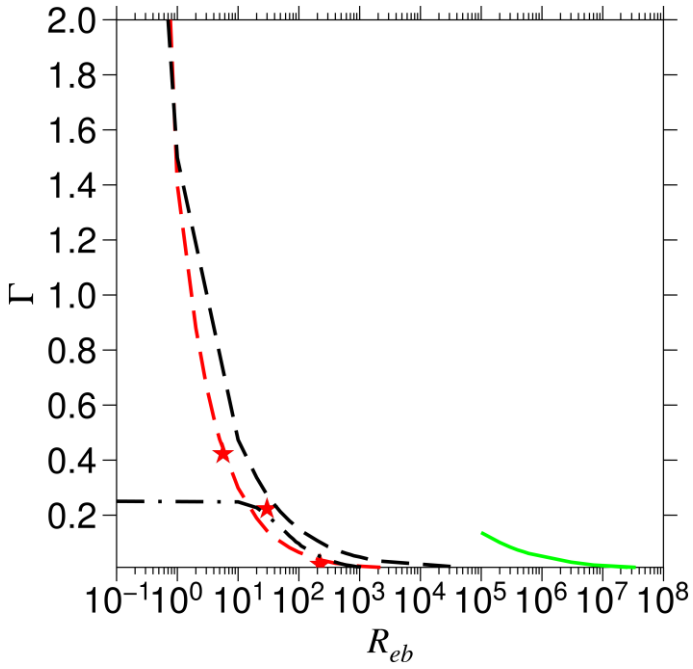

Fig. 5.7 Relationship between Γ and R_{eb} in SS layers. Star is the average values of observational data. Red line is fitted line of observational data. Dashed line is proposed by Shih *et al.* [2005]. Black dashed and dotted line is proposed by Mater and Venayagamoorthy [2014].Green line is proposed by Lozovatsky and Fernando [2012].

If we multiply ν to Eq. 5.11, and we have

$$\nu\Gamma = \frac{\chi_\theta N^2 \nu}{\varepsilon \overline{T}_z^2}. \tag{5.15}$$

From the definition of turbulent diffusivity of heat defined from the ratio of thermal variance to mean temperature gradient, and that of R_{eb}, we have

$$\nu\Gamma = \frac{K_T}{R_{eb}} \rightarrow \Gamma = \frac{K_T}{\nu}\frac{1}{R_{eb}}. \tag{5.16}$$

$\frac{K_T}{\nu}$ is the ratio between thermal diffusivity to molecular momentum diffusivity, and should be call as inverse laminar Prandtl number PrL. Eq. 5.18 means that Γ should be a function of both R_{eb} and PrL (Fig. 5.8). Note that, Γ increases as R_{eb} become small but not shows substantial difference on PrL.

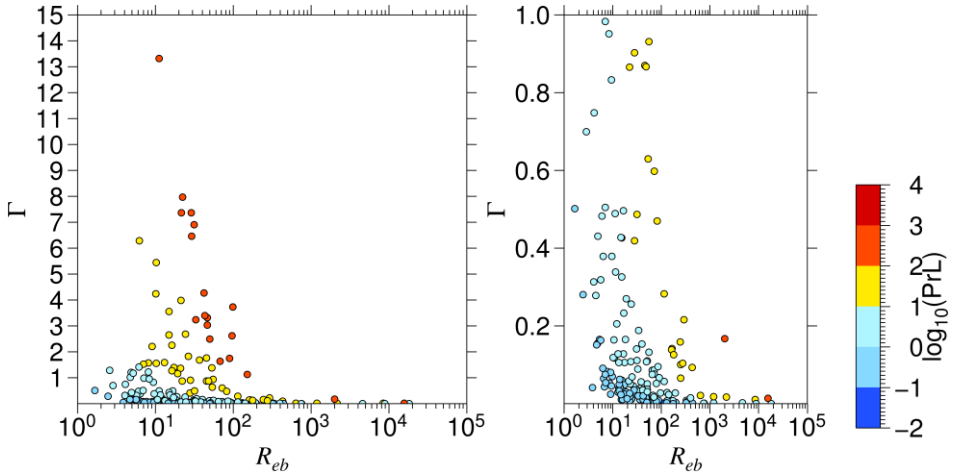

Fig. 5.8 Relationship between Γ and R_{eb} in SS layers. Color shows the order of PrL .

In the DD layers, Γ also becomes large when R_{eb} toward 0. The relationships between Γ and R_{eb} are (Fig.5.9)

SF layers: $\Gamma_{R_{eb}}^{\mathrm{SF}} = 6.6R_{eb}^{-1}$. (5.17a)

DC layers: $\Gamma_{R_{eb}}^{\mathrm{DC}} = 173.5R_{eb}^{-1.3}$. (5.17b)

Γ decreases as R_{eb} increases which means that mixing due to DDC is trivial in fully turbulent condition.

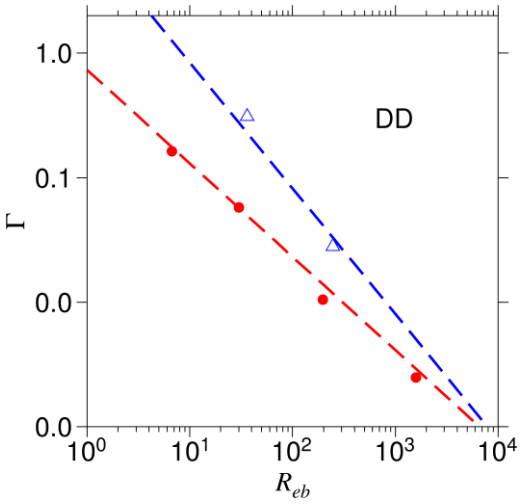

Fig. 5.9 Relationship between Γ and R_{eb} in DDC layers. Blue: DC, Red: SF, circles and triangles: mean values of data.

5.4. Summary and Conclusion

In this chapter, mixing efficiency (for conventional turbulence) and dissipation ratio (for DDC) Γ was estimated using the maximum likelihood estimation with the data of temperature fluctuation obtained by TurboMAP in the North Pacific Ocean. The geometric mean value of Γ is 0.18 and this value is slightly smaller than the value proposed by Oakey [1982, 1985]. The range of Γ distributed widely between O (10^{-3}) and O (10^{3}).

I studied the effect of the DDC on Γ. If it is DC, when the temperature distribution is unstable, Γ becomes large. This means that the temperature is transported more effectively compared with momentum. When the SF convection occurs for which temperature distribution is stable, Γ is smaller than that in DC layers. In contrast, in the doubly stable layers, Γ is in-between 0.11 ~ 0.22

To understand the cause of large Γ in the doubly stable layers, the distributions of Γ with R_{eb} and R_i were considered. I found that Γ was large in the layers where viscosity dominates ($R_{eb} < 100$).

Next, I parameterized Γ using observational data, and compared the results of DNS by previous studies. Γ was parameterized using R_{eb}. This result agrees fairly well with DNS results and, means that Γ becomes large when ocean fields are stable. This fact implies that the heat transports is sometimes efficient compared with

mechanical mixing such as breaking of internal waves.

Eddy diffusivities of heat K_T and momentum K_ρ were calculated, and compared each other (Fig. 5.10). Indeed, the relation between K_T and K_ρ differed due to the ratio of dissipation rate χ_θ and ε.

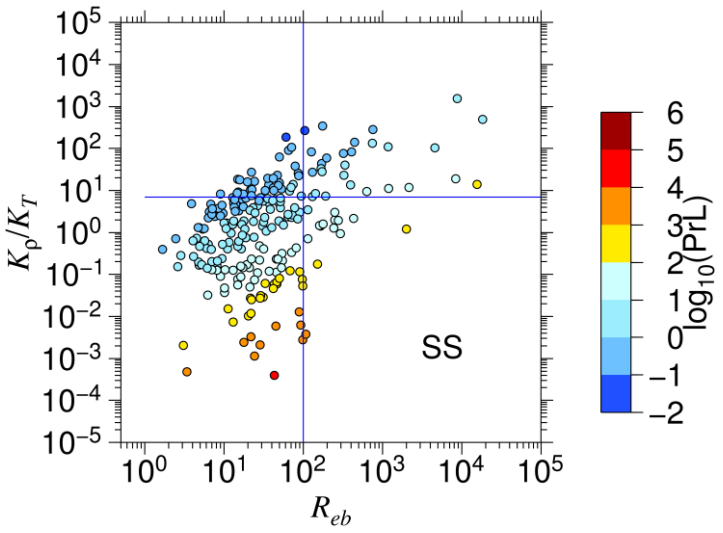

Fig. 5.10 Relationship between the ratio of eddy diffusivities and R_{eb}.

Chapter 6 Summary and conclusion

6.1. Summary

The purpose of this Ph.D. thesis was obtaining suitable parameterizations for estimating eddy diffusivities in the upper ocean and near shore region because observations with high resolution both temporal and space are prevented by few observation due to activities of fisheries and/or limited ship-time.

In chapter 3, a new indicator for DDC was proposed instead of R_{eb}. If R_i is larger than 0.25, we need to estimate eddy diffusivities due to the DDC with the range of R_ρ between 0.5 and 2. Also, refined functions of K_S or K_T focusing on R_ρ and R_i were obtained by observational data by improving the DNS parameterization proposed by Kimura *et al*. [2011].

In chapter 4, the proportionality coefficient of R_{OT} in the relationship between L_O and L_T was estimated from microstructure data in the western NPO and the offshore of Miyake island. R_{OT} is found to vary from place to place. It was highly correlated with R_{eb} (Eq. 4.7 and Eq. 4.13), which implies that it depends on the decay stage of eddies. R_{OT} is also a function of R_i.

In chapter 5, mixing efficiency (for conventional turbulence) and dissipation ratio (for DDC) Γ was estimated using the MLE with the data of temperature

fluctuation. The geometric mean value $\Gamma = 0.18$ is slightly smaller than the value proposed by Oakey [1982, 1985]. The range of Γ distributed widely between O (10^{-3}) and O (10^{3}). The relationship between Γ and R_{eb} was distinguished by the order of $\mathrm{Pr}\,\mathrm{L}$.

As for DDC, Γ was large in DC layers, in contrast, that in the SF layers was small. To understand the cause of large Γ in the doubly stable layers, the distributions of Γ with R_{eb} and R_i were considered. I found that Γ was large in the layers where viscosity dominates ($R_{eb} < 80$).

6.2. Conclusion

In this thesis, I proposed improved threshold R_{eb} is below 80 or R_i is over 0.25 as for DDC. Also, eddy scale parameterization was established by considering shear effects. Taken together, we can estimate eddy diffusivities categorized by R_i and R_ρ following steps (Fig. 6.1).

① Whether the DD dominates or not.

Please use the threshold proposed in Chapter 3 and Chapter 5. If R_{eb} is below 80 or R_i is over 0.25, consider effects of the DDC.

② The activity of DDC is checked.

When the range of R_ρ is between 0.5 and unity, effects of DC are considered.

➔ We can use previous parameterizations (this point will be discussed).

When the range of R_ρ is between unity and two, effects of SF are considered.

➔ We can use improved parameterization in Chapter 3.

③ We can ignore the effects of DDC.

➔Eddy scale parameterization assessed in Chapter 4 is useful for estimating of eddy diffusivities. The decay stage of eddy is described by R_{eb} and R_i.

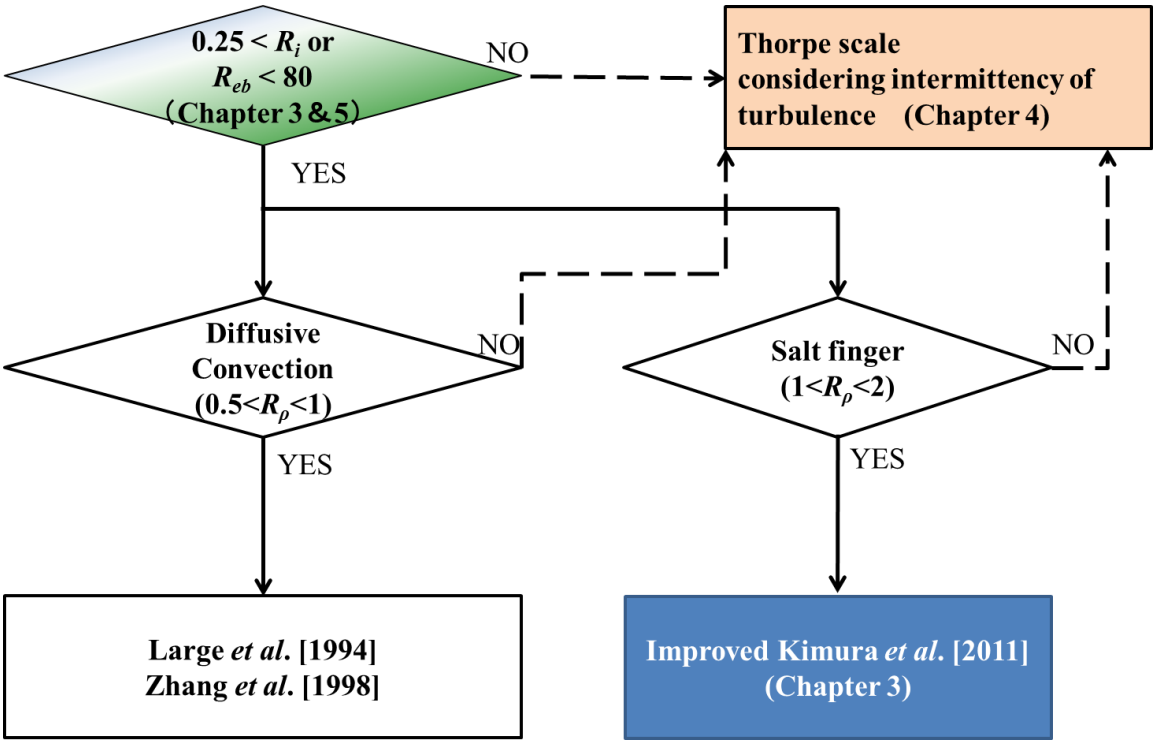

Fig. 6.1 Schematic of this Ph.D. thesis.

Chapter 7 Future work

In this chapter, some parts of future works were shown. Future works were found during analysis and discussion with other researchers. Following homework is needed to solve. I have been tackling tasks from mixing.

7.1. Refining the GK filter

Some improvements for GK filter have been conducted. Stansfield *et al*. [2001] pointed out that the regions having weak mixing and weak density gradients are limited by slow sensor response time. A relative importance of depth and density resolution for a CTD is obtained by $R(=\frac{d\rho}{dz}\frac{z_{res}}{\rho_{res}})$, where $\frac{d\rho}{dz}$ is the back ground density gradient, ρ_{res} is the density resolution of CTD, and z_{res} is the vertical resolution of CTD. If $R>1$, vertical resolution of depth is a limitation factor for calculating L_T. In contrast, If $R<1$, density resolution limits for calculating L_T. After that, Johnson and Garrett [2004] considered the effect of noise on the run length and L_T. First, Q $(=\frac{\Delta\rho_N}{(d\rho/dz)H})$ was calculated by an amplitude of noise $\Delta\rho_N$, $\frac{d\rho}{dz}$ and depth H_{dep}. Next, the number of data n_{section} in a certain section is calculated by the ratio between H_{dep} and sampling interval h. Finally, B_{JG} $(=\frac{\Delta\rho_N}{(d\rho/dz)h})$ is calculated. A critical value of run length is changed with Q.

In these days, Gargett and Garner [2008] proposed a new method for determination of overturning. The method is a combination of an overturn ratio R_O $(=\min(L^+/L, L^-/L))$, where L^+ and L^- are maximum and minimum values of the vertical distance of the Thorpe displacements and the buoyancy frequency N. If the inversion is a perfect single overturn, L^+/L equals to L^-/L. Thus, the value of R_O is 0.5, and the critical value is 0.2. Inversions were discriminated from noise by this method,

however, 13% signals were misunderstanding in their analysis.

Incidentally, there is an odd relationship between T and S due to DDC [*e.g.* Turner 1974]. DDC strengthens stratification nevertheless the unstable states of temperature or salinity. In the perturbed region off *Sanriku* coast, Japan, it is effective for the modification water mass, and generates intrusion and wiggles [Nagata *et al*., 1970; Nagasaka *et al*., 1999; Talley and Yun 2003; Inoue *et al*., 2007; Shimada *et al*., 2008]. This characteristic also appears in $T-S$ diagram as loops, and is similar to overturning [figures in Galbraith and Kelley 1996].

Therefore, the contamination of DDC in overturning has been considered, however, an appropriate evaluation of the effects of DDC has not been done. Density inversions continuously observed while intrusions appeared by DDC's effect. Hence, Galbraith and Kelley [1996] did not consider the active intrusion layers, also excluded layers affected by DDC. Thompson *et al*. [2007] only considered L_T in regions where DDC affects. Also, the effect of DDC on R_O has not been investigated.

In addition, the GK filter and one methods shown in chapter 5 were used simultaneously [Jing and Wu 2010; Frants *et al*. 2013]. Passing the GK filter, inversions need to pass the overturn ratio filter in order to determine as overturning; however, interaction of the filters have not been investigated.

Thus, I will compare filters as was mentioned above and make a filter to avoid

contaminations of DDC.

7.2. Turbulence due to creatures

How is the contribution by creatures to ocean mixing? Is it important? Kunze *et al*. [2006b] found the mixing hot spot in the below layers of school of zooplankton. Visser [2006] proposed Γ as a function of L_a / L_O, where L_a is the size of creature. If L_a was larger than L_O, Γ was 0.2. Katija and Dabiri [2009] found that jellyfish could make turbulence. Can we ignore motions of creatures? How are effects of turbulence due to creatures? If we applied the method with closure model, perhaps, we could obtain the answer.

Acknowledgements

I would like to express my gratitude to Prof. Jiro Yoshida for his great advices on whole research of mine. I exhausted by quarrels to him every time, but he also did. I need to follow his kindness and patience.

Prof. Yujiro Kitade gave me opportunities facing to research. His comments were also invaluable. So, I appreciate him for his great help.

I owe a very important debt to Associate Prof. Masao Nemoto. He arbitrated Prof. Yoshida and me. He encouraged me every time.

I am particularly grateful for the assistance given associate Prof. Masashi Ohnawa. His comments were so beneficial. Welcome to TUMSAT!!! I'm glad to meet you.

I appreciate Dr. Hideki Nagashima. My research history on physical oceanography starts with his good class. His class of physics is very interesting for me. Also, he always gave me good comments and advice for paper.

Prof. Toshiyuki Hibiya is a very good adviser for me. In Brisbane, Australia, Prof. Hibiya gave me the chance to talk with Dr. Robin Robertson. In Japan, I could meet Prof. Lakshmi Kantha by a corporation with Prof. Hibiya. He gave me good chances to discuss with researchers all over the world.

I am glad to meet Prof. Lakshmi Kantha. He gave me valuable comments and

advice for my studies. Also he encouraged me every time. Thanks to his comments for my English, my writing skill is improved (…however more improvements are needed). Discussions with him have been insightful.

Associate Prof. Robin Robertson is the first person of my foreign friend. Meeting her in Brisbane, Australia is exciting event in my life. So, I would like to express my deepest appreciation to her.

I could have the great journey with members of R/V Hakuho-maru (JAMSTEC) in North Pacific Ocean. KH11-8 cruise and KH12-5 are so interesting for me. Associate Profs. Toshio Suga, Shinzo Fujio and Daigo Yanagimoto encouraged me during cruises. In my doctoral thesis, most of the data were obtained by KH05-4, KH07-1, and KH08-3 cruises. I appreciated the members R/V Hakuho-maru (JAMSTEC). Particularly, corporation of late Prof. Kawabe was needed for conducting the cruises. I appreciate for his corporation.

Also the data in this paper were collected by Members of R/V Soyo-maru (FRA). Particularly, Dr. Shimizu Yugo gave me chances for conducting microstructure observations.

Members of R/V Seiyomaru (TUMUSAT, especially B/S Hideyoshi Jumonji) taught me how was the research vessels. Due to their thorough training, I could conduct observation safely in other R/Vs.

Societe franco-japonaise d'oceanographie, Tokyo gave me the great prize for paper my titled "Eddy diffusivities due to the DDC". This award encouraged me but I thought better research is needed for me.

The foundation from the Oceanographic Society of Japan enabled me to join the Asia Oceania Geoscience Society 2013 in Brisbane, Australia. The meeting which I first joined meeting abroad was exciting for me. Talking with foreign researchers was a good experience.

The Marine Science Foundation gave me the chance to join the ocean science meeting 2014 in Hawaii, USA. I presented my research there. I also could discuss HF radar in Sagami bay with Dr. Igeta in Hawaii.

I deeply appreciate to the Sasakawa Scientific Research Grant from The Japan Science Society. I could join the AGU Fall Meeting in San Francisco, America. The meeting is the event which changed my life. Also, the paper was published with the supports from this grant.

My observation was conducted with the TurboMAP every time. It measured all microstructure data which contributed to whole research in the present doctor thesis.

I appreciate mom, dad, and younger sister. Warm soup, cheering words and big smile encouraged me. Also, my grandpa and late grandma were encouraged me. Particularly, I believe that my grandma was glad because of my carrier to choose.

Finally, I express my great thanks to my colleagues in my laboratory. Especially, Mr. Kou Shiozaki taught me how to use the FORTRAN and the GMT and so on. His knowledge is contributed for analyzing parts in my research and our researches on my laboratory. I appreciate his good skills for using PC.

Reference

Akimoto S. and N. Takahashi. (2008). The influence of the oceanic condition and bottom topography to the formation of fish school in the fishing ground where alfosino Beryx splendens inhabit. *Kanagawa Prefectural Government*, 3: 25-33.

Bryan F. O. (1987). Parameter sensitivity of primitive equation ocean general circulation models. *J. Phys. Oceanogr.,* 17: 970-985.

Caldwell D. R., T. M. Dillon and J. N. Moum. (1985). The rapid-sampling vertical profiler. *J. Atomos. Oceanic Tech.,* 2: 615-625.

Cheng L. and Y. Kitade. (2014). Quantitative evaluation of turbulent mixing in the Central Equatorial Pacific. *J. Oceanogr.,* 70: 63-79.

Clayson C. A. and L. Kantha. (2008). On turbulence and mixing in the free atmosphere inferred from high-resolution soundings. *J. Atomos. Ocean. Tech.,* 25(6): 833-852.

Crawford W. R. (1986). A comparison of length scales and decay times of turbulence in stably stratified flows. *J. Phys. Oceanogr.,* 16: 1847–1854.

de Lavergne C., G. Madec, J. Le Sommer, A. J. G. Nurser and A. C. N. Garabato. (2015). The impacts of variable mixing efficiency on the abyssal overturning. *J. Phys. Oceangr.,* doi:10.1175/JPO-D-14-0259.1.

Dewey R. K., W. R. Crawford, A. E. Gargett and N. S. Oakey. (1987). A microstructure instrument for profiling oceanic turbulence in coastl bottom boundary layers. *J. Atmos. Oceanic. Technol.,* 4: 288-297.

Dillon T. M. (1982). Vertical overturns: A comparison of Thorpe and Ozmidov length scales. *J. Geophys. Res,* 87: 9601-9613.

Fernando H. J. S. (1991). Turbulent mixing in stratified fluids. *Annu. Rev. Fluid Mech.,* 23: 455-493.

Ferron B., H. Mercier, K. Speer, A. Gargett and K. Polzin. (1998). Mixing in the Romanche Fracture Zone. *J. Phys. Oceanogr.,* 28: 1929–1945.

Frants M., G. M. Damerell, A. T. Gill, K. J. Heywood, J. MacKinnon and J. Sprintall. (2013). An assesment of density-vbased fine-scale methods for estimating

diapycnal diffusivity in the Southern Ocean. *J. Atmos. Oceanic Tech.*, doi: 10.1175/JTECH-D-12-00241.1.

Galbraith P. and D. Kelley. (1996). Identifying overturns in CTD profiles. *J. Atmos. Oceanic Technol.*, 13: 688-702.

Gargett A. E. and G. Holloway. (1984). Dissipation and diffusion by internal wave breaking. *J. Mar. Res.*, 42: 15-27.

Gargett A. E. and G. Holloway. (1992). Sensitivity of the GFD model to different diffusivities for heat and salt. *J. Phys. Oceanogr.*, 22:1158-1177.

Gargett A. E. and J. N. Moum. (1995). Mixing efficiencies in turbulent tidal fronts: results from direct and indirect measurements of density flux. *J. Phys. Oceanogr.*, 25: 2583-2608.

Gargett A. and T. Garner. (2008). Determing Thorpe scales from ship-lowered CTD density profiles. *J. Atoms. Oceaninc Tech.*, 25: 1657-1670.

Garrett C. (2003). Mixing with latitude. *Nature*, 422: 477-488.

Garret C. and W. Munk. (1972). Oceanic mixing by breaking internal waves. *Deep-Sea Res.*, 19: 823-832.

Garrett C. and W. Munk. (1975). Space-time scales of internal waves: a progress report. *J. Geophy. Res.*, 80(3): 291-297.

Grant H. L., R. W. Stewart and A. Moilliet. (1962). Turbulence spectra from a tidal channel. *J. Fluid Mech.*, 12(2): 241-268.

Gregg M. C. (1976a). Finestructure and microstructure observations during the passage of a mild storm. *J. physi. oceanogr.*, 6: 528-555.

Gregg M. C. (1976b). Temperature and salinity microstructure in the Pacifc equotrial undercurrent. *J. Geophys. Res.*, 81(6): 1180-1196.

Gregg M. C. (1989). Scaling turbulent dissipation in the thermocline. *J. Phys. Oceanogr.*, 94: NO. C7, 9686-9698.

Gregg M. C. and C. S. Cox. (1971). Measurements of the oceanic microstructure of temperature and electrical conductivity. *Deep-Sea Res.*, 18: 925-934.

Gregg M. C. and Sanford T. B. (1988). The dependence of turbulent dissipation on stratification in a diffusively stable thermocline. *J. Geophys. Res.*, doi: 10.1029/JC093iC10p12381.

Gregg M. C., C. S. Cox and P. W. Hacker. (1973). Vertical microstructure measurements in the central North Pacifc. *J. Physi. Oceanogr.*, 3: 458-469.

Gregg M, W. Nodland, E. Aagaard and D. Hirt. (1982). Use of a fiber-optic cable with a free-fall microstructure profiler. *IEEE, Oceans*, 14: 260-266.

Hebert D. (1988). Estimates of salt - finger fluxes. *Deep Sea Res.*, 35(12); 1887-1901 .

Hebert D., Oakey, N. and Ruddick, B. (1990). Evolution of a Mediterranean salt lens: scalar properties. . *J. Phys. Oceanogr.*, 20: 1468-1483.

Henyey F., J. Wright, and S. M. Flatte. (1986). Energy and action flow throgh the internal wave field: an eikonal approach. *J. Gepphys. Res.*, 91: NO. C7, 8487-8495.

Hibiya T. and M. Nagasawa. (2004). Latitudinal dependence of diapycnal diffusivity in the thermocline estimateing using a finescale parameterization. *Geophys. Res. Lett.*, 31: LO1201, doi:10.1029/2003GL017998.

Ijichi T. (2013). Assessment of fine-scale parameterizations of turbulent dissipation rates using a multi-scale profiler. *MC thesis, The University of Tokyo, Tokyo, Japan* . pp 54.

Inoue R., M. C. Gregg. and R. R. Harcourt. (2010a). Mixing rates across the Gulf stream, Part 1: On the formation of Eighteen Degree Water. *J. Mar. Res.*, 68: 643–671.

Inoue R., R. R. Harcourt and M. C. Gregg. (2010b). Mixing rates across the Gulf Stream, Part 2: Implications for nonlocal parameterization of vertical fluxes in the surface boundary layers. *J. Mar. Res.*, 68: 673-698.

Inoue R., R. -C. Lien and J. N. Moum. (2012). Modulation of equatorial turbulence by a tropical instability wave. *J. Geophys. Res.*, 117, C10009 doi:10.1029/2011JC007767, 2012.

Inoue R., H. Yamazaki, F. Wolk, T. Kohno and J. Yoshida. (2007). An estimation of buoyancy flux for a mixture of turbulence and double diffusion. *J. Phys. Oceanogr*, 37: 611-624.

Itsweire E. C. (1986). Measurements of vertical overturns in a stably stratified turbulent flow. *Phys. Fluids*, 27: 764-766.

Ivey G. N. and J. Imeberger. (1991). On the nature of turbulence in astratified fluid. part 1: the energetics of mixing. *J. Physi. Oceanogr.*, 21: 650-658.

Jing Z. and L. Wu. (2010). Seasonal variation of turbulent diapycnal mixing in the north western Pacific stirred by wind stress. *Geophys. Res. Lett.*, 37; L23640, doi:10.1029/2010GL045418,2010.

Johnson H. L. and C. Garrett. (2004). Effects of Noise on Thorpe scales and run lenghs. *J. Phys. Oceanogr.*, 34: 2359-2372.

Joyce T. M. W. Zenk and J. M. Toole. (1978). An anatomy of the antarctic polar front in the Drake Passage. *J. Geophys. Res.*, 83: 6093-6113.

Kantha L. (2003). On an improved model of for the turbulent PBL. *J. Atmos. Sci*, 60: 2239-2246.

Kantha L. (2016). A Note on the significance of buoyancy Reynolds number in stable stratified flows and double diffusive convection(to be submitted for publication).

Kantha L. and A. Carniel. (2009). A note on modeling mixing in stably stratified flows. *J. Atmos. Sci.*, 66: 2501-2505.

Kantha L, S. Carniel, M. Sclavo and A. Bergamasco. (2013). On identifying double diffusive mixing in the ocean. (Unpublished manuscript).

Karl D. M. (1999). A sea of change: biogeochemical variability in the North Pacific Subtropical Gyre. *Ecosystems*, 2: 181-214.

Katija K. and J. O. Dabiri. (2009). A viscosity-enhanced mechanism for biogenic ocean mixing. *Nature*, 460: 624-627.

Kelley D. (1984). Effective diffusivities within oceanic theirmohaline staircase. *J. Geophys. Res.*, 89: 10484-10488.

Kelley D. (1986). Oceanic thermocline staircase. *Ph.D. Thesis, Dalhousie University, Halifax, NS, Canada*, pp 333.

Kelley D. (1990). Fluxes through diffusive staircases: a new formulation. *J. Geophys. Res.*, 95(C3): 3365-3371.

Kimura S., W. Smyth and E. Kunze. (2011). Turbulence in a sheared, salt-fingering-favorable environment: an isotropy and effective diffusivities. *J. Phys. Oceanogr.*, 41: 1144-1159.

Kitade Y., T. Kusaka, Y. Kawamura, Y. Niwa, A. Noda, T. Hayashi, H. Hamada, S. Yamasaki, Y. Koike and M. Matsuyama. (2003a). Latitudinal variation of vertical eddy diffusivity estimated from the distribution of overturns in the western part of south Pacific Ocean. *J.Tokyo University of Fisheries*, 90: 13-21.

Kitade Y., M. Matsytama and J. Yoshida. (2003b). Distribution of overturning induced by internal tides and Thorope scale in Uchiura Bay. *J. Oceanogr.*, 59; 845-850.

Kunze E. (1987). Limits on growing, finite-length salt fingers: a Richardson number consistent. *J. Mar. Res.*, 45: 533-556.

Kunze E. (1990). Observations of shear and vertical stability from a neutrally buoyant float. *J. Geophys. Res.*, 95(18): 127-142,.

Kunze E. and T. B. Sanford. (1996). Abbyssal mixing; where it isn't. *J. Phys. Oceanogr.*, 26: 2663- 2693.

Kunze E. and S. G. L. Smith. (2004). The role of small-scale topography in turbulent mixing of the global ocean. *Oceanography*, 17(1): 55-56.

Kunze E., E. Fining, J. Hummon, T. K. Chereskin and A. M. Thurnherr. (2006a). Global Abyssal mixing inferred from lowered ADCP shear and CTD strain profiles. *J. Phys. Oceanogr.*, 36; 1553-1576.

Kunze E., J. F. Dower, L. Beveridge, R. Dewey and K. P. Bartlett. (2006b). Observations of biologically generated turbulence in a coastal lnlet. *Science*, 313: 1768-1770.

Large W. G., J. C. McWilliams and S. C. Doney. (1994). Oceanic vertical mixing: a review and a model with a nonlocal boundery layer parameterization. *Rev. Geophysics*, 32（4）: 363-403.

Ledwell J. R., A. J. Watson and C. S. Law. (1991). Evidence of slow mixing across the pycnoline from an open-ocean tracer release experiment. *Nature*, 364: 701-703.

Linden P. F. (1979). Mixing in stratified fluids. *Geophys. Astrophys. Fluid Dynamics*, 13: 3-23.

Lozovatsky I. D. and H. J. S. Fernando. (2012). Mixing efficiency in natural flows. *Phill Trans. R. Soc A 371,* http://doi.org/10.1098/rsta.2012.0213.

Lozovatsky I. D., E. Roget., H. J. S. Fernando, M. Figueroa and S. Shapovalov. (2006). Sheared turbulence in aweakly stratified upper ocean. *Deep-Sea Res. Ⅰ*, 53: 387-407.

Marmorino G. O. and D. R. Caldwell. (1976). Heat and salt transport through a diffusive thermohaline interface. *Deep Sea Res.*, 23: 59-67.

Mater B. D. and S. K. Venayagamoorthy. (2014). The quest for an unambiguous parameterization of mixing efficiency in stably stratified geophysical flows. *Geophys. Res. Lett.*, doi:10.1002/2014GL060571.

Mater B. D., S.M. Scaad and S.K. Vebayagamoorthy. (2013). Relevance of the Thorpe length scale in stably stratified turbulence. *Phys. Fluids*, 25: 076604(2013); doi: 10.1063/1.4813809.

McComas C. H. and P. Muller. (1981). The dynamic balance of internal waves. *J. phys. Oceanogr*., 11: 970-986.

Merryfield W., G. Holloway and A. E. Gargett. (1999). A global ocean model with double - diffusive mixing. *J. Phys. Oceangr.*, 29: 1124-1142.

Monti P., G. Querzoli, A. Cenedese and S. Piccinini . (2007). Mixing properties of stably stratified parallel shear layer. *Phys. Fluids*, 19: 085104.

Mori K., K. Uehara, T. Kameda and S. Kakei. (2008). Direct measurements of dissipation rate of turbulent kinetic energy of North Pacific subtropical mode water. *Geophy. Res. Lett*, Vol.35, L05601、doi:10.1029/2007/GL032867,2008.

Moum J. N. (1996). Efficiency of mixing in the main thermocline. *J. Geophys. Res.*, 101: 12057-12069.

Munk W. H. (1966). Abbyssal recipes. *Deep-Sea res.*, 13: 707-730.

Munk W. and C. Wunsch. (1998). Abyssal recipes Ⅱ: energetics of tidal and wind mixing. *Deep-Sea Res. 1*, 45: 1977-2010.

Nagasaka M., J. Yoshida, H. Nagashima, M. Matsuyama, K. Kawasaki and K. Yokouchi. (1999). On the double diffusive intrusion obserbed in the Oyashio Frontal region.

Theoretical and Applied Mech., 48: 385-392.

Nagasawa M., T. Hibiya, K. Yokota and T. Niwa. (2007). Microstructure measurements in the mid-depth waters of the North Pacific. *Geophy. Res. Lett.*, 34: L05608, doi: 10.1029/2006GL028695, 2007.

Nagata Y. (1970). Detailed tempreture cross section of the coled-water belt along the nothern edge of the Kuroshio. *J. Mar. Res.*, 28: 1-14.

Nakano H., K. Shimada, M. Nemoto and J. Yoshida. (2014). Parameterization of the eddy diffusivity due to double diffusive convection. *La mer*, 52: 91-98.

Oakey N. S. (1982). Determination of the rate of dissipation of turbulent energy from simultaneous temperature and velocity shear microstructure measurements. *J. Physi. Oceanogr.*, 12: 256-271.

Oakey N. S. (1985). Statistics of mixing parameters in the upper ocean during JASIN Phase 2. *J. Phys. Oceanogr.*, 15: 1662-1675.

Oakey N. S. (1988a). :EPSONDE: an instrument to measure turbulence in the deep ocean. *IEEE J. Oceanic Eng.*, 13(3): 124-128.

Oakey N. S. (1988b). Estimating of mixing infereed from temperature and velocity microstructure. *Small-Scale Turbulence and Mixing in the Ocean*, Elesvier Oceanography Series, 46: 239-247.

Osborn T. R. (1974). Vertical profiling of velocity microstructure. *J. Physi. Oceanogr.*, 4: 109-115.

Osborn T. R. (1980). Estimates of the local rate of vertical diffusion from dissipation measurements. *J. Phys. Oceanogr.*, 10: 83-89.

Ozmidov R. V. (1965). On the turbulent exchange in a stably stratified ocean. *Izv. Acad. Sci, USSR, Atmos. Oceanic Phys.*, 853-860.

Pacanowski R. C. and S. G. H. Philander. (1981). Parameterization of vertical minxing in numerical motdels of tropical oceans. *J. Phys. Oceangr.*, 11: 1443-1451.

Padman L. and T. M. Dillon. (1987). Vertical heat fluxes through the Beaufort Sea thermohaline staircase. *J. Geophys. Res*, 92: doi: 10.1029/JC092iC10p10799.

Peters H., M. C. Gregg and J. H. Toole. (1988). On the parameterization of equatorial

turbulence. *J. Geophys,. Res.*, 93(C2): 1199-1228.

Polzin K. L., J. M. Toole and R. W. Schmitt. (1995). Finescale parameterizations of turbulent dissipation. *J. Phys. Oceangr.*, 25: 306-328.

Polzin K. L., J. M. Toole, J. R. Ledwell and R. W. Schmitt. (1997). Spatial Variability of Turbulent Mixing in the Abyssal Ocean. *Science*, 276(4): 93-96.

Prastowo T., R. W. Griffiths, G. O. Huges. and A. M. Hogg. (2008). Mixing efficiency in controlled exchange flows. *J. Fluid Mech.*, 600; 235-244.

Prastowo T., R. W. Griffiths, G. O. Hughes and A. M. Hogg. (2009). Effects of topography on the cumulative mixing efficiency in exchange flows. *J. Geophys. Res.*, 114: C08008, doi:10.1029/2008JC005152.

Rehmann C. R. and T. F. Duda. (2000). Diapycnal Diffusivity inferred from Scalar microstructure measurements near the New England shelf/slope front. *J. Physi. Oceanogr.*, 30: 1354-1371.

Richards K. and H. Banks. (2002). Characteristics of inter leaving in the western equatorial Pacific. *J. Geophys. Res.*,107: 3231 doi: 10.1029/2001JC000971.

Robertson R. and L. Padman and M. D. Levine. (1995). Fine structure, microstructure, and vertical mixing processes in the upper ocean in the western Weddel Sea. *J. Geophys. Res.*, 100: 18517-18535 .

Rohr J. and C. Vanatta. (1987). Mixing efficiency in stably stratified growing turbulence. *J. Geophys. Res.*, 92: 5481-5488.

Ruddick B. R. and Turner J. S. (1979). The vertical length scale of double-diffusive intrusions. *Deep-Sea Res.*, 26A: 903-913.

Ruddick B. R. and A. E. Gargett (2003). Oceanic double - diffusion: introduction . *Prog. Oceanogr.*, 56(3): 381-393.

Ruddick B. R., A. Anis, and K. Thompson. (2000). Maximum likelihood spectral fitting: the batchelor spectrum. *J. Atoms. Ocean. Thechnol.*, 17(11), 1541-1555.

Schmitt R. W. (1981). Form of temperature - salinity relationship in the central water: evidence of double - diffusive mixing. *J. Phys. Oceanogr*, 11: 1051-1026.

Schmitt R. W. (1987). The Caribbean Sheets and Layers Transects (C-SALT) program. *Eos*,

Transactions of the American Geophysical Union,, 68(5): 57–60.

Schmitt R. W. (1998). Double-diffusive convection: Its role in ocean mixing and parameterization schemes for large scale modeling. *Ocean Modeling and Parameterization, Edited by E. Chassignet and J. Verron, Kluwer Academic Publishers*, 215-234.

Schmitt R. W., E. T. Montgomery and J. M. Toole. (1995). A free-vehicle explores deep-sea mixing. *Oceanus*, 38 (1): 21-25.

Schmitt R. W., J. R. Ledwell, E. T. Montogomery, K. L. Polzin and J. M. Toole. (2005). Enhanced diapycnal mixing by salt fingers in the thermocline of the tropical Atlantic. *Science*, 308: 685-688.

Shih L. H., J. R. Koseff, G. N. Ivey and J. H. Ferziger. (2005). Paremeterization of turbulent fluxes and scale using homogeneous sheared stably stratified turbulence simulations. *J. Fluid Mech.*, 525; 193-214.

Shimada K., Nemoto. M. and Yoshida, J. (2007). Distribution of the density ratio in the North Pacific. *La mer*, 45(3):149-158.

Smyth W. D., J. N. Moum and D. R. Caldwell. (2001). The efficiency of mixing in turbulent patches: Inferences from direct simulations and microstructure observations. *J, Phys. Oceanogr.*, 31: 1969-1992.

Smyth W. D., J. D. Nash and J. N. Moum. (2005). Differential diffusion in breaking Kelvin–Helmholtz billows. *J. Phys. Oceanogr.*, 35: 1004-1022.

St. Laurent L. and R. W. Schmitt. (1999). The contribution of salt fingers to vertical mixing in the North Atlantic tracer release experiment. *J. Phys. Oceangr.*, 29: 1404-1424.

Stansfield K., C. Garrett and R. Dewey. (2007). The probability distribution of the Thorpe displacement with overturns in Juan de Fuca Strait. *J. Phys. Oceanogr.*, 31; 3421-3434.

Stern M. E. (1960). The ”salt-fountain” and thermohaline convection. *Tellus*, 12: 172-175.

Stommel H., A. B. Arons and Blanchard, D. (1956). An oceanographic curiosity: the perpetual salt fountain. *Deep-Sea Res.*, 3: 152-153.

Talley L. D. and Y. Yun. (2001). The role of cabbeling and double diffusion in setting the

density of the North Pacific intermediate water salinity minimum. *J. Phys. Oceanogr.*, 31: 1538-1549.

Taylor G. I. (1938). The spectrum of turbulence. *Proc. R. Soc. London A*, 164:476.

Taylor J. (1991). Laboratory experiments on the formation of salt fingers after the decay of turbulence. *J. Geophys. Res.*, 96: 12497-12510.

Thompson A. F., J. A. MacKinnon and J. Sprintall. (2007). Spatial and temporal patterns of small-scale mixing in Drake Passage. *J. Phys. Oceanogr.*, 37: 572-592.

Thorpe S. A. (1977). Turbulence and mixing in a Scottish Loch. *Philos. Trans. Roy. Soc. London*, A286: 125-181.

Thorpe S. A. (2005). Recent developments in the study of ocean turbulence. *Annual. Rev. Earth Planet. Sci.*, 32: 91–109.

Timmermans M. L., C. Garrett and E. Carmack. (2003). The thermohaline structure and evolution of the deep waters in the Canada Basin. *Deep-Sea Res. I*, 50: 1305-1321.

Toole J. M. and D. T.Georgi. (1981). On the dynamics and effects of double-diffusively driven intrusions. *Prog. Oceanogr.*, 10: 123-145.

Toyama K. and T. Suga. (2012). Roles of mode waters in the formation and maintenance of central water in the North Pacific. *J. Oceanogr*, 68: 79-92.

Turner J. S. (1974). Double-diffusive phenomena. *Annual Review of Fluid Mechanics*, 6: 37-54 doi: 10.1146/annurev.fl.06.010174.000345.

Turner J. S. (1978). The vertical lengt,h scale of double-diffusive intrusions. *J. Geophys. Res.*, doi: 10.1029/JC083iC06p02887.

Turner J. S. and Stommel H. (1964). A new case of convection in the presence of combined vertical salinity and temperature gradients. . *Proc. Nut. Acad. Sci. U.S.A.*, 52; 49-53.

Visser A. W. (2007). Biomixing of the Oceans? *Science*, 316: 838-839.

Waterhouse A., J. MacKinnon, J. Nash, M. Alford, E. Kunze, H. Simmons, K. Polzin, L. St. Laurent, O. Sun, R. Pinkel, L. D. Talley, C. Whalen, T. Huussen, G. Cater, I. Fer, S. Waterman, A. Naveira-Garabato, T. Sanford and C. Lee. (2014). Diapycnal mixing from measurements of the turbulent dissipation rate. *J. Phys. Oceanogr.*,

doi:10.1175/JPO-D-13-0104.1.

Wesson J. C. and M. C. Gregg. (1988). Turbulent dissipation on the Strait of Gibraltar and associated mixing. *In* J. N. Jamart, *Small-Scale Turbulence and Mixing in the Ocean* (pp. 201-212). Amsterdam: Elsevier Oceanography Series, Elsevier.

Whalen C. B., L. D. Tally and J. A. Mackinnon . (2012). Spatial and temporal variability of global ocean mixing inferred from Argo Profiles. *Geophys. Res. Lett.*, 39: L18612, doi:10.1029/2012GL053196.

Wijesekera H. W. and T. M. Dillon. (1997). Shannon entropy as an indicator of age for turbulent overturns in the oceanic thermocline. *J. Geophys. Res.*, 102: 3279-3291.

Zhang J., R. W. Schmitt and R. X. Huang. (1998). The sensitivity of the GFDL modular ocean model to parameterization of double -diffusive processes. *J. Phys. Oceanogr.*, 28: 589-605.

Appendix A Energy equation of turbulence

In this appendix, the energy Equation of turbulence is explained. Eq. (A.1) is Naiver-Stokes Equation.

$$\rho\frac{\partial u_i}{\partial t}+\rho u_j\frac{\partial u_i}{\partial x_j}=-\frac{\partial p}{\partial x_i}-\rho g\delta_{i3}+\rho\nu\frac{\partial^2 u_i}{\partial x_j\partial x_j},$$

$$(i=1,2,3\ \ j=1,2,3). \qquad \text{(A.1)}$$

$u_i\,(i=1,2,3)$ is velocity components in x, y and z directions, respectively. p is the pressure. Now, we use the Einstein summation convention. δ_{ij} is the Kronecker delta defined as follows: when $i=j$, $\delta_{ij}=1$, otherwise, $\delta_{ij}=0$.

$$\frac{\partial u_i}{\partial x_i}=0 \qquad \text{(A.2)}$$

Now, Reynolds procedure is applied to Eq. (A.1) by dividing each quantity into both its mean and its fluctuating part

$$u_i=\bar{u}_i+u_i',\ p=\bar{p}+p',\ \rho=\bar{\rho}+\rho',\ T=\bar{T}+T'\ . \qquad \text{(A.3)}$$

Eq. (A.3) is also applied to Eq. (A.2), and consider that the mean velocity field is non divergent $\frac{\partial\bar{u}_i}{\partial x_i}=0$, then the fluctuation velocity field is also non-divergent $\frac{\partial\overline{u'}_i}{\partial x_i}=0$, Eq. (A.3) is applied to the first term of the left member of Eq. (A.2) is

$$\overline{\bar{\rho}\frac{\partial u_i}{\partial t}}=\overline{\bar{\rho}\frac{\partial}{\partial t}\left(\bar{u}_i+u_i'\right)}=\bar{\rho}\frac{\partial\bar{\bar{u}}_i}{\partial t}+\bar{\rho}\left(\frac{\partial\overline{u_i'}}{\partial t}{}_{(=0)}\right)=\bar{\rho}\frac{\partial\bar{u}_i}{\partial t}, \qquad \text{(A.4)}$$

The second term of the left member of Eq. (A.1) is

$$\overline{\bar{\rho}u_j\frac{\partial u_i}{\partial x_j}}=\overline{\bar{\rho}\left(\bar{u}_j+u_j'\right)\frac{\partial}{\partial x_j}\left(\bar{u}_i+u_i'\right)}=\overline{\bar{\rho}\bar{u}_j\frac{\partial \bar{u}_i}{\partial x_j}}+\overline{\bar{\rho}\bar{u}_j\frac{\partial u_i'}{\partial x_j}}+\overline{\bar{\rho}u_j'\frac{\partial \bar{u}_i}{\partial x_j}}+\overline{\bar{\rho}u_j'\frac{\partial u_i'}{\partial x_j}}$$

$$=\bar{\rho}\bar{u}_j\frac{\partial \bar{u}_i}{\partial x_j}+\bar{\rho}\frac{\partial}{\partial x_j}\left(\overline{u_j'u_i'}\right). \qquad \text{(A.5)}$$

The first and second terms of the right member of Eq. (A.1) is

$$\overline{-\frac{\partial p}{\partial x_i}-\rho g\delta_{i3}}=-\frac{\partial}{\partial x_i}\left(\overline{\bar{p}+p'}\right)-\left(\overline{\bar{\rho}+\rho'}\right)g\delta_{i3}$$

$$=-\frac{\partial \bar{p}}{\partial x_i}-\bar{\rho}g\delta_{i3}. \qquad \text{(A.6)}$$

The third term of the right member of Eq. (A.1) is

$$\overline{\bar{\rho}\nu\frac{\partial^2 u_i}{\partial x_j\partial x_j}}=\bar{\rho}\nu\frac{\partial^2}{\partial x_j\partial x_j}\left(\overline{\bar{u}_i+u_i'}\right)=\bar{\rho}\nu\frac{\partial^2 \bar{u}_i}{\partial x_j\partial x_j}. \qquad \text{(A.7)}$$

Taken together, Eq. (A.1) is described as

$$\bar{\rho}\frac{\partial \bar{u}_i}{\partial t}+\bar{\rho}\bar{u}_j\frac{\partial \bar{u}_i}{\partial x_j}=-\frac{\partial \bar{p}}{\partial x_i}-\bar{\rho}g\delta_{i3}+\frac{\partial}{\partial x_j}\left(\bar{\rho}\nu\frac{\partial \bar{u}_i}{\partial x_j}-\bar{\rho}\overline{u_j'u_i'}\right). \qquad \text{(A.8)}$$

Here, we multiply Eq. (A.8) by u' to obtain the energy Equation, and then we have

$$\bar{\rho}\frac{\partial}{\partial t}\left(\frac{1}{2}\overline{u_i'u_i'}\right)+\bar{\rho}\bar{u}_j\frac{\partial}{\partial x_j}\left(\frac{1}{2}\overline{u_i'u_i'}\right)$$

$$=-\frac{\partial}{\partial x_j}\left(\overline{p'u_j'}+\frac{1}{2}\bar{\rho}\overline{u_i'u_i'u_j'}-\bar{\rho}\nu\frac{\partial}{\partial x_j}\left(\overline{u_i'\left(\frac{\partial u_i'}{\partial x_j}+\frac{\partial u_j'}{\partial x_i}\right)}\right)\right)$$

$$-\frac{1}{2}\bar{\rho}\overline{u_i'u_j'}\left(\frac{\partial \bar{u}_i}{\partial x_j}+\frac{\partial \bar{u}_j}{\partial x_i}\right)-\overline{u_i'\rho' g\delta_{i3}}-\frac{\bar{\rho}\nu}{2}\overline{\left(\frac{\partial u_i'}{\partial x_j}+\frac{\partial u_j'}{\partial x_i}\right)^2}. \qquad \text{(A.9)}$$

So, triple correlation term is neglected and after some manipulation of Eq. (A.9), we

finally obtain

$$\frac{d}{dt}\left(\frac{1}{2}q^2\right) = -\overline{u'w'}\frac{\partial \bar{u}}{\partial z} - \frac{\overline{\rho'w'}}{\bar{\rho}}g - \varepsilon\left[= \frac{15}{2}\overline{\left(\frac{\partial u'}{\partial z}\right)^2}\right], \qquad \text{(A.10)}$$

where q is the turbulent velocity scale ($q^2 = \overline{u'^2} + \overline{v'^2} + \overline{w'^2}$). The first term of Eq. (A.10) in right hand means the kinematic energy source for turbulence. The second term of Eq. (A.10) in right hand means buoyancy effects on turbulence motion. The third term is the energy dissipation rate. When the second term of the right member of (Eq. A.11) (without density stratification) is zero,

$$\varepsilon = \frac{15}{2}\overline{\left(\frac{\partial u'}{\partial z}\right)^2} = -\overline{u'w'}\frac{\partial \bar{u}}{\partial z}\,. \qquad \text{(A.11)}$$

We call ε as the energy dissipation rate.

Appendix B The beginning of studies on double diffusive convection

B.1. Evidence of the double diffusive convection.

Stommel *et al*. [1956] assumed a perpetual motion in the ocean (Fig. B.1, this paper has only two pages!). They considered a case when we put a long pipe in the ocean, and pump up the water and then, even when we stop the pump, water should have been upwelling; because water in the pipe becomes lighter losing its heat through the wall of the pipe nevertheless its salinity is conserved. This is a thought experiment. After that, Stern [1960] focused the difference of the molecular diffusivities between heat and salt, and proposed that if there is no pipe; water should continue to up well.

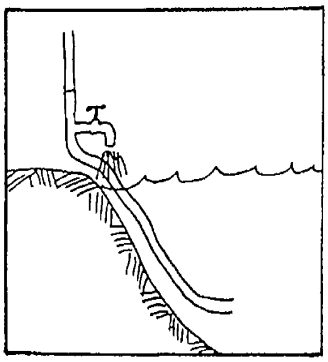

Arnold sketches a faucet in the tube at about a half meter above sea-level because he sees that it can run forever.

Fig. B.1 Schematic figure of pump in the ocean interior from Ruddick and Gargett (2003).

In order to investigate mechanisms of this physical process, some scientists have been conducted laboratory experiments. Turner and Stommel [1964] first succeeded in this experiment, and they found the peculiar type of convection now called as the Salt Finger. Turner [1978] and Ruddick and Turner [1979] also investigated the interleaving caused by the DDC. As a result, they found that warmer and salinity water interleave toward upper layer, and cold and fresh water interleave toward bottom layer (Fig. B.2).

Fig. B.2 Horizontal interleaving experimented by Ruddick and Turner (1999)
Blue water is cold/fresh, Yellow is warm/salty.

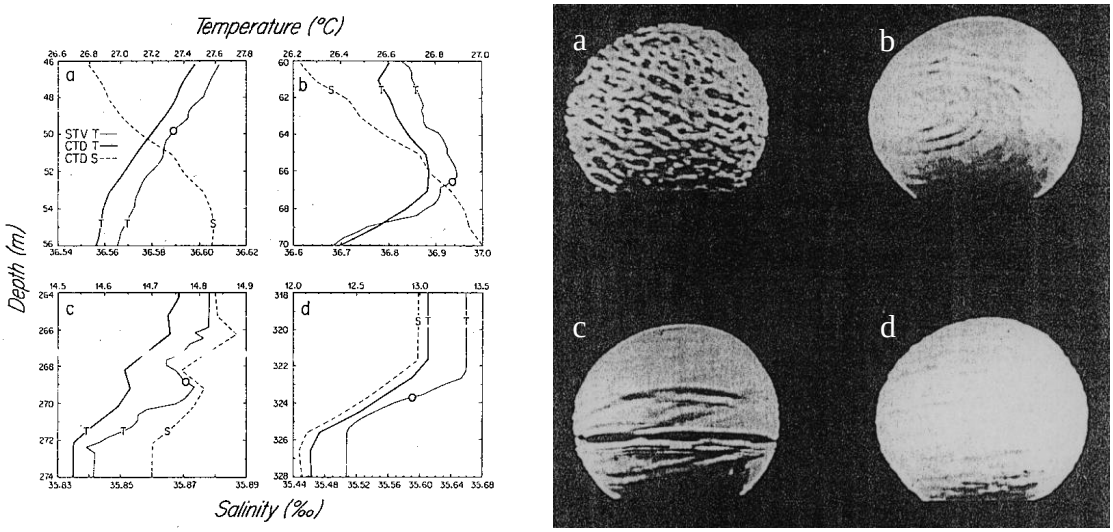

Fig. B.3. (Left) Vertical profiles of a temperature (thick line), and salinity (dashed line) in the Caribbean Sea. (Right) Shadow graph images of (a) stratified turbulence, (b) shear instability, (c) diffusive interface, and (d) Salt finger tilted by shear, obtained at the depth showed by circles in the corresponding profile on the left from Schmitt [1987]

Does DDC occur in the ocean? In the Caribbean Sea, Schmitt [1987] took the photo using the shadow graph method (Fig. B.3). Thus, the DDC is confirmed as one of the physical processes in the ocean.

B.2. Fine Structure due to the double diffusive convection

From the laboratory experiments, DDC might be generating the interleaving. Before this experiment, Nagata [1970] had already conducted detailed Mechanical BathyThermograph (MBT) observation in the perturbed region off *Sanriku* coast, and found the successive temperature inversion layers (Fig. B.4). Also Nagasaka *et al*. [1999] indicated that the interlacing was caused by DDC. Joyce *et al*. [1978] focused on the interleaving in the Drake Passage, and suggested that the interleaving is caused by the DDC. Richards and Banks [2002] investigated the interleaving in the Equator in the South Pacific Ocean and found the large scale intrusions crossing the Equator.

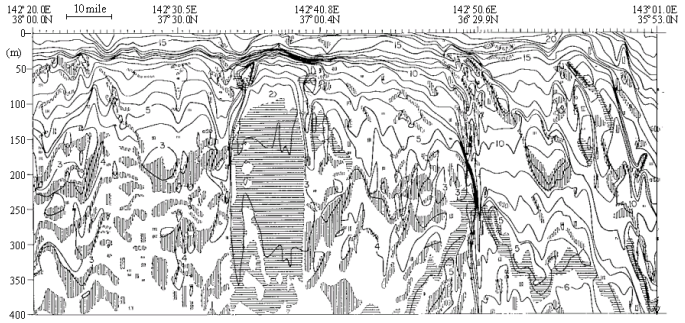

Fig. B.4. Vertical cross section of temperature off *Sanriku* coast (Nagata 1970). Hatched area shows temperature inversion layers.

Additionally, Herbert *et al*. [1990] focused on the Meddy and showed that the Meddy lost its salinity by the effect of DDC (Fig. B.5).

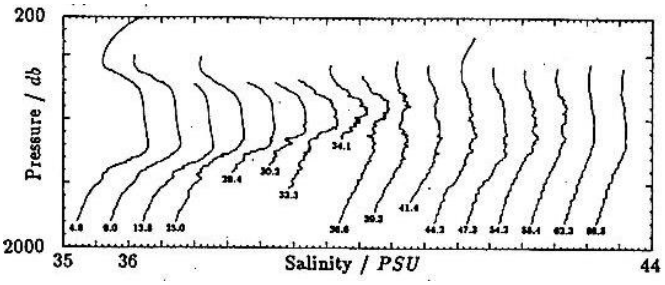

Fig. B.5 Variation of salinity profiles in the Meddy from Herbert [1990].

Taken together, DDC concerns with sub mesoscale processes such as interleaving and eddies.

B.3. Turbulent parameters due to the salt finger

Assuming the SF in the energy equation (Eq. A.11) in the absence of velocity shear, we get the balance equation between ε and the energy production by buoyancy.

$$0 = \varepsilon + g\frac{\overline{\rho' w'}}{\rho}. \tag{B.1}$$

Vertical fluxes of salt F_S and heat F_T are negative for the SF. So, the total flux of density $F_\rho = -\rho\alpha F_T + \rho\beta F_S$ is negative (density is transported to the lower layer). The second term of Eq. (B.1) is written as

$$g\frac{\overline{\rho' w'}}{\rho} = g\frac{F_\rho}{\rho} = g(\beta F_s - \alpha F_T) = g\beta F_s\left(1 - \frac{\alpha F_T}{\beta F_S}\right). \tag{B.2}$$

$\frac{\alpha F_T}{\beta F_S}$ is the density flux ratio γ. Thus, Eq. (B.1) is re-written as

$$\varepsilon = -g\beta F_s(1-\gamma). \tag{B.3}$$

In contrast, from the equation of state

$$\rho = \rho_0\left\{1 - \alpha(T - T_0) + \beta(S - S_0)\right\}, \tag{B.4}$$

buoyancy frequency N is described as a function of gradients of temperature and salinity, as

$$-N^2 = \frac{g}{\rho_0}\frac{\partial\rho}{\partial z} = -g\alpha\frac{\partial T}{\partial z} + g\beta\frac{\partial S}{\partial z}. \tag{B.5}$$

Thus, N is a function of R_ρ

$$-N^2 = g\beta\frac{\partial S}{\partial z}(1 - R_\rho). \tag{B.6}$$

Also, $F_\rho = -\rho\alpha F_T + \rho\beta F_S$ is rewritten by K_ρ, K_S and K_T, as follows

$$-K_\rho \frac{g}{\rho_0}\frac{\partial \rho}{\partial z} = \alpha K_T \frac{\partial T}{\partial z} - \beta K_S \frac{\partial S}{\partial z}. \tag{B.7}$$

Thus, the eddy diffusivity of density K_ρ due to the DDC is

$$K_\rho = \frac{K_T R_\rho - K_S}{R_\rho - 1}. \tag{B.8}$$

In order to obtain K_ρ by ε, I multiply $\frac{g}{\rho}$ to $F_\rho = -K_\rho \frac{\partial \rho}{\partial z}$.

$$g\frac{F_\rho}{\rho} = -K_\rho \frac{g}{\rho}\frac{\partial \rho}{\partial z} \Rightarrow K_\rho N^2 = g\frac{\overline{\rho' w'}}{\rho}. \tag{B.9}$$

Using the Eq. (B.1) and, K_ρ is obtained from Eq. (B.10),

$$K_\rho = -\frac{\varepsilon}{N^2} < 0. \tag{B.10}$$

Next, we consider F_S, using the equation of diffusion $\beta F_S (<0) = -K_S \beta \frac{\partial \bar{S}}{\partial z} (>0)$ and

Eq. (B.6),

$$g\beta F_S = -K_S \frac{N^2}{R_\rho - 1}. \tag{B.11}$$

$\varepsilon = -g\beta F_s (1-\gamma)$ is obtained by Eq. (B.2), thus

$$K_S = \frac{R_\rho - 1}{1-\gamma}\frac{\varepsilon}{N^2} \quad . \tag{B.12}$$

Additionally,

$$R_\rho = \frac{\alpha \frac{\partial \bar{T}}{\partial z}}{\beta \frac{\partial \bar{S}}{\partial z}} = \frac{-\frac{\alpha F_T}{K_T}}{-\frac{\beta F_S}{K_S}} = \frac{K_S}{K_T}\gamma. \tag{B.13}$$

So, we can easily obtained the K_T as

$$K_T = \frac{\gamma}{R_\rho} K_S \,. \tag{B.14}$$

If we can obtain K_T from observational data, K_S is a function of the dissipation ratio Γ^{DDC}.

$$K_S = \frac{R_\rho}{\gamma} \cdot \frac{\chi_T}{2\left(\frac{\partial \bar{T}}{\partial z}\right)^2} = \frac{R_\rho}{\gamma} \cdot \frac{\varepsilon}{N^2} \cdot \Gamma^{\mathrm{DDC}} . \tag{B.15}$$

Γ^{DDC} depends on the density ratio, as

$$\Gamma^{\mathrm{DDC}} = \left(\frac{R_\rho - 1}{R_\rho}\right) \cdot \left(\frac{\gamma}{1-\gamma}\right).$$

In the laboratory experiments, $\Gamma^{\mathrm{DDC}} = 0.88$ with $R_\rho = 1.6$ and $\gamma = 0.7$.

B.4. Turbulent parameters due to the diffusive convection

Fluxes of salt F_S and heat F_T are positive for the DC, but the total flux of density $F_\rho = -\rho\alpha F_T + \rho\beta F_S$ is negative (density is transported to the lower layer). The second term of Eq. (B.1) is written as

$$g\frac{\overline{\rho' w'}}{\rho} = g\frac{F_\rho}{\rho} = g(\beta F_s - \alpha F_T) = g\beta F_T\left(\gamma - 1\right). \tag{B.16}$$

We consider F_S, using the equation of diffusion $\beta F_S(>0) = -K_S\beta\frac{\partial \bar{S}}{\partial z}(<0)$ and Eq. (B.6),

$$g\beta F_S = K_S\frac{N^2}{1-R_\rho}. \tag{B.17}$$

Using $\varepsilon = g\alpha F_T\left(1-\gamma\right)$ obtained by Eq. (B.2) and Eq. (B.16), ε is

$$\varepsilon = g\alpha F_T\left(1-\gamma\right) = \frac{1-\gamma}{\gamma}K_S\frac{N^2}{1-R_\rho}. \tag{B.18}$$

Thus, K_S is

$$K_S = \frac{\gamma\left(1-R_\rho\right)}{1-\gamma}\frac{\varepsilon}{N^2}. \tag{B.19}$$

Also, using Eq. (B.13), K_T is

$$K_T = \frac{\gamma}{R_\rho}K_S. \tag{B.20}$$

If we input Eq. (B.19) and (B.20) into Eq. (B.8), we can obtain K_ρ due to the DC,

$$K_\rho = -\frac{1-\gamma}{R_\rho - 1}K_S = -\frac{\varepsilon}{N^2} < 0. \tag{B.21}$$

Appendix C Latitudinal dependence of mixing due to internal waves

Henyey *et al*. [1986] described the dependence of ε on the angular frequency of internal waves ω. $d\varepsilon/d\omega$ is

$$\frac{d\varepsilon}{d\omega} =$$

$$(3\pi R_{ic}^{1/2}/4f)[a\pi^{-1}j_*BNE_{GM}f]^2\left(\frac{k_c}{k_v}\right)\left[\frac{1+\ln k_v/k_c}{2}\right]\frac{1-r}{1+r}\frac{N}{\omega\sqrt{N^2-\omega^2}}. \quad \text{(C.1)}$$

In this equation, in order to obtain latitudinal variation of ε, we integrate the term $\frac{N}{\omega\sqrt{N^2-\omega^2}}$ with the existence range of internal wave ($f<\omega<N$) as follows;

$$\int_f^N \frac{N}{\omega\sqrt{(N^2-\omega^2)}}d\omega$$

$$=\frac{1}{N}\int_f^N \frac{1}{\frac{\omega}{N}\sqrt{(1-\frac{\omega^2}{N})}}d\omega. \quad \text{(C.2)}$$

By the definition ($\int_a^b \frac{1}{\frac{x}{b}\sqrt{(1-\frac{x^2}{b})}}dx = \ln\left(\frac{1+\sqrt{1-\left(\frac{x}{b}\right)^2}}{\frac{x}{b}}\right)_a^b$)

$$=\ln\left(\frac{1+\sqrt{1-\left(\frac{\omega}{N}\right)^2}}{\frac{\omega}{N}}\right)_f^N$$

$$=\ln\frac{1+\sqrt{1-\left(\frac{f}{N}\right)^2}}{\frac{f}{N}}$$

$$= \ln\left(\frac{N}{f} + \sqrt{\left(\frac{N}{f}\right)^2 - 1}\right). \quad \text{(C.3)}$$

By the formulation of hyperbolic function ($\ln(z + \sqrt{z^2 - 1}) = \cosh^{-1}(z)$), Eq. (C.3) is described as

$$= \cosh^{-1}\left(\frac{N}{f}\right). \quad \text{(C.4)}$$

Thus,

$$\varepsilon \propto fN^2 \cos^{-1}\left(N/f\right) \times E_{GM}^2 . \quad \text{(C.5)}$$

Appendix D The GM spectrum

The GM spectrum is the universal spectrum of internal waves. Munk (1986) described the energy spectrum as

$$\text{Strain: } F_{\xi}(\omega, j) = b^2 N_0 N^{-1}\left(\omega^2 - f^2\right)\omega^{-2} E(\omega, j), \quad \text{(D.1)}$$

$$\text{Shear: } F_u(\omega, j) = F_{u1} + F_{u2} = b^2 N_0 N\left(\omega^2 + f^2\right)\omega^{-2} E(\omega, j), \quad \text{(D.2)}$$

$$\text{Total: } F_e(\omega, j) = \frac{1}{2}\left(F_u + N^2 F_{\xi}\right) = b^2 N_0 N E(\omega, j). \quad \text{(D.3)}$$

Here, in the limit when $\omega >> f$ (non-rotating case), F_e is equally provided to potential and kinematic energy as

$$\frac{1}{2}F_u = \frac{1}{2}N^2 F_{\xi}. \quad \text{(D.4)}$$

$E(\omega, j)$ is non-dimensional energy density described as

$$E(\omega, j) = B(\omega)\cdot H(j)\cdot E, \quad \text{(D.5)}$$

$$B(\omega) = 2\pi^{-1} f \omega^{-1}\left(\omega^2 - f^2\right)^{-\frac{1}{2}}, \int_f^{N(z)} B(\omega)\, d\omega = 1, \quad \text{(D.6)}$$

$$H(j) = \frac{\left(j^2 + j_*^2\right)^{-1}}{\sum_1^{\infty}\left(j^2 + j_*^2\right)^{-1}}, \sum_{j-1}^{\infty} H(j) = 1. \quad \text{(D.7)}$$

Here, j_* is the mode number (=3) , and $E = 6.3\times10^{-5}$.

Consider the potential energy associated with the internal wave displacement as

$$\left\langle \xi^2 \right\rangle = \int b^2 N_0 N^{-1}\left(\omega^2 - f^2\right)\omega^{-2} E(\omega, j)\, d\omega$$

$$= \int_f^N \left(\omega^2 - f^2\right)\omega^{-2} B(\omega) d\omega \cdot H(j) b^2 N_0 N^{-1} E . \quad \text{(D.8)}$$

We put $B(\omega)$ to Eq. (D.8), and then we have

$$= 2\pi^{-1} \int_f^N f\left(\omega^2 - f^2\right)^{\frac{1}{2}} \omega^{-3} d\omega \cdot H(j) b^2 N_0 N^{-1} E . \quad \text{(D.9)}$$

Integration term is shown as

$$\int_f^N f\left(\omega^2 - f^2\right)^{\frac{1}{2}} \omega^{-3} d\omega = \int_f^N \frac{f\sqrt{\omega^2 - f^2}}{\omega^3} d\omega . \quad \text{(D.10)}$$

Here, we put $\frac{\omega}{f} = x$ and $d\omega = f dx$, then we have

$$\int_1^{\frac{N}{f}} \frac{f^2\sqrt{x^2 - 1}}{x\omega^2} dx \Rightarrow \int_1^{\frac{N}{f}} \frac{\sqrt{x^2 - 1}}{x^3} dx . \quad \text{(D.11)}$$

From rules of integration: $\int \frac{\sqrt{x^2 - a^2}}{x^3} dx = -\frac{\sqrt{x^2 - a^2}}{2x^2} + \frac{1}{2a}\sec^{-1}\left|\frac{x}{a}\right| + C$

$$= \left[-\frac{\sqrt{x^2 - 1}}{2x^2} + \frac{1}{2}\sec^{-1}|x| \right]_1^{\frac{N}{f}} = -\frac{\sqrt{(N/f)^2 - 1}}{2(N/f)^2} + \frac{1}{2}\sec^{-1}\left|\frac{N}{f}\right| . \quad \text{(D.12)}$$

If $N >> f$, then

$$-\frac{\sqrt{(N/f)^2 - 1}}{2(N/f)^2} = 0 , \text{ and } \frac{1}{2}\sec^{-1}\left|\frac{N}{f}\right| = \frac{1}{2}\frac{\pi}{2} = \frac{\pi}{4} . \quad \text{(D.13)}$$

So,

$$\int_f^N f\left(\omega^2 - f^2\right)^{\frac{1}{2}} \omega^{-3} d\omega = \frac{\pi}{4} . \quad \text{(D.14)}$$

Consequently,

$$\left\langle \xi^2 \right\rangle = \frac{1}{2} H(j) b^2 N_0 N^{-1} E \Rightarrow \frac{1}{2} b^2 N_0 N^{-1} E . \quad \text{(D.15)}$$

In contrast, momentum energy of horizontal shear is described as

$$\left\langle u^2 \right\rangle = \int_f^N b^2 N_0 N \left(\omega^2 + f^2\right)\omega^{-2} B(\omega) H(j) E d\omega$$

$$= \int_f^N \left(\omega^2 + f^2\right)\omega^{-2} B(\omega) d\omega \cdot b^2 N_0 N H(j) E \,. \tag{D.16}$$

We put $B(\omega)$ into Eq. (D.16), so the integration term is described as

$$2\pi^{-1}\int_f^N \left(\omega^2 + f^2\right)\omega^{-3} f\omega^{-1}\left(\omega^2 - f^2\right)^{-\frac{1}{2}} d\omega$$

$$=2\pi^{-1}\int_f^N \frac{f\left(\omega^2 + f^2\right)}{\omega^3\sqrt{\omega^2 - f^2}} d\omega \Rightarrow 2\pi^{-1}\int_f^N \frac{\left\{\left(\omega/f\right)^2 + 1\right\}}{\left(\omega/f\right)^3 f\sqrt{\left(\omega/f\right)^2 - 1}} d\omega \,. \tag{D.17}$$

Same procedures conducted for Eq. (D.11) is applied to Eq. (D.17), and we have

$$2\pi^{-1}\int_1^{\frac{N}{f}} \frac{\left(x^2+1\right)}{x^3\sqrt{x^2-1}} dx \tag{D.18}$$

$$= \int_1^{\frac{N}{f}} \frac{\left(x^2+1\right)}{x^3\sqrt{x^2-1}} dx = \int_1^{\frac{N}{f}} \left(\frac{1}{x\sqrt{x^2-1}} + \frac{1}{x^3\sqrt{x^2-1}}\right) dx \,. \tag{D.19}$$

From rules of integration:

$$\int \frac{1}{x^3\sqrt{x^2-a^2}} dx = \frac{\sqrt{x^2-a^2}}{2a^2x^2} + \frac{1}{2a^2}\sec^{-1}\left|\frac{x}{a}\right| + C \,, \tag{D.20}$$

$$\int \frac{1}{x\sqrt{x^2-a^2}} dx = \frac{1}{a}\sec^{-1}\left|\frac{x}{a}\right| + C$$

$$= \left[\frac{\sqrt{x^2-1}}{2x^2} + \frac{1}{2}\sec^{-1}|x|\right]_1^{\frac{N}{f}} + \left[\sec^{-1}|x|\right]_1^{\frac{N}{f}}$$

$$= \frac{\sqrt{\left(N/f\right)^2 - 1}}{2\left(N/f\right)^2} + \frac{1}{2}\sec^{-1}\left(\frac{N}{f}\right) + \sec^{-1}\left(\frac{N}{f}\right). \tag{D.21}$$

If N is sufficiently larger than *f*, then

$$\frac{\sqrt{\left(N/f\right)^2 - 1}}{2\left(N/f\right)^2} \Rightarrow 0, \sec^{-1}\left(\frac{N}{f}\right) \Rightarrow \frac{\pi}{2} \,,$$

$$2\pi^{-1}\int_1^{\frac{N}{f}} \frac{\left(x^2+1\right)}{x^3\sqrt{x^2-1}}dx = 2\pi^{-1}\left(\frac{3}{4}\pi\right) = \frac{3}{2}. \tag{D.22}$$

So,

$$\therefore \left\langle u_1^2 + u_2^2 \right\rangle = \int b^2 N_0 N\left(\omega^2 + f^2\right)\omega^{-2}B(\omega)H(j)Ed\omega$$

$$= \frac{3}{2}b^2 N_0 NH(j)E = \frac{3}{2}b^2 N_0 NE. \tag{D.23}$$

Thus, the total energy is obtained by the sum of Eq. (D.15) and Eq. (D.23) as

$$E = \frac{1}{2}\left(\left\langle u_1^2 + u_2^2 \right\rangle + N^2\left\langle \xi^2 \right\rangle\right) = b^2 N_0 NE. \tag{D.24}$$

The ratio of kinematic energy to potential energy R_ω (shear-strain ration) as (Appendix E)

$$R_\omega = \frac{\frac{1}{2}\left\langle u_1^2 + u_2^2 \right\rangle}{\frac{1}{2}N^2\left\langle \xi^2 \right\rangle} = \frac{\omega^2 + f^2}{\omega^2 - f^2} = \frac{\frac{3}{4}b^2 N_0 NE}{\frac{1}{4}b^2 N_0 NE} = 3. \tag{D.25}$$

Thus, in the range of GM spectrum

$$R_\omega = 3 \Rightarrow \omega^2 = 2f^2 \Rightarrow \omega = \sqrt{2}f. \tag{D.26}$$

Appendix E The shear and the strain ratio

Polzin *et al*. [1995] defined the shear - strain ratio R_ω which indicates the variance caused by internal waves. It is described as follows:

$$R_\omega = \frac{\left\langle S_h{}^2 \right\rangle}{N^2 \left\langle \xi_z{}^2 \right\rangle}, \tag{E.1}$$

$$R_\omega = \frac{\left\langle S_h{}^2 \right\rangle}{N^2 \left\langle \xi_z{}^2 \right\rangle} = \frac{\left\langle \left(\frac{\partial u}{\partial z}\right)^2 + \left(\frac{\partial v}{\partial z}\right)^2 \right\rangle}{N^2 \left\langle \left(\frac{\partial \eta}{\partial z}\right)^2 \right\rangle} \approx \frac{\left\langle u^2 + v^2 \right\rangle}{N^2 \left\langle (\eta)^2 \right\rangle}, \tag{E.2}$$

where ξ_z is the strain, and S_h is the shear, and η is the vertical displacement, u and v is horizontal velosity. To obtain Eq.(E.1) and Eq.(E.2), I first consider the two dimensonal internal wave. ξ_z is obtained by theses equations are as follows

$$\frac{\partial u}{\partial t} = -\frac{1}{\rho_0}\frac{\partial p'}{\partial x}, \tag{E.3}$$

$$\frac{\partial w}{\partial t} = -\frac{\rho'}{\rho_0} g - \frac{1}{\rho_0}\frac{\partial p'}{\partial z}, \tag{E.4}$$

$$\frac{\partial \rho'}{\partial t} + w\frac{\partial \rho_0}{\partial z} = 0 \ , \tag{E.5}$$

$$\frac{\partial u}{\partial x} + \frac{\partial w}{\partial z} = 0, \tag{E.6}$$

$$\frac{\partial \eta}{\partial t} = w, \tag{E.7}$$

where ρ_0 is the average of density, u is horizontal velosity, w is vertical velosity, p' is presser and ρ' density perturbations, respectively. We multyply Eq.(E.3) by u

$$u\frac{\partial u}{\partial t} = -\frac{1}{\overline{\rho_0}}u\frac{\partial p'}{\partial x},$$

$$\frac{\partial}{\partial t}\left(\frac{1}{2}\overline{\rho_0}u^2\right) = -u\frac{\partial p'}{\partial x},$$

$$\frac{\partial}{\partial t}\left(\frac{1}{2}\overline{\rho_0}u^2\right) = -\frac{\partial\left(p'u\right)}{\partial x} + p'\frac{\partial u}{\partial x}. \tag{E.8}$$

We multiply Eq. (E.4) by *w*,

$$w\frac{\partial w}{\partial t} = -\frac{\rho' w}{\overline{\rho_0}}g - \frac{1}{\overline{\rho_0}}w\frac{\partial p'}{\partial z},$$

$$\frac{\partial}{\partial t}\left(\frac{1}{2}\overline{\rho_0}w^2\right) = -\rho' wg - w\frac{\partial p'}{\partial z},$$

$$\frac{\partial}{\partial t}\left(\frac{1}{2}\overline{\rho_0}w^2\right) = -\rho' wg - \frac{\partial\left(p'w\right)}{\partial z} + p'\frac{\partial w}{\partial z}. \tag{E.9}$$

Then we sum up Eq. (E.8) and Eq. (E.9),

$$\frac{\partial}{\partial t}\left(\frac{1}{2}\overline{\rho_0}u^2 + \frac{1}{2}\overline{\rho_0}w^2\right)$$

$$= -\rho' wg - \left\{\frac{\partial\left(p'u\right)}{\partial x} + \frac{\partial\left(p'w\right)}{\partial z}\right\} + p'\left(\frac{\partial u}{\partial x} + \frac{\partial w}{\partial z}\right). \tag{E.10}$$

Using the continuity equation,

$$\frac{\partial}{\partial t}\left(\frac{1}{2}\overline{\rho_0}u^2 + \frac{1}{2}\overline{\rho_0}w^2\right) = -\rho' wg - \left\{\frac{\partial\left(p'u\right)}{\partial x} + \frac{\partial\left(p'w\right)}{\partial z}\right\}. \tag{E.11}$$

From Eqs. (E.5), (E.6) and (E.7), we have

$$\frac{\partial \rho'}{\partial t} + \frac{\partial \eta}{\partial t}\frac{\partial \rho_0}{\partial z} = 0, \tag{E.12}$$

$$\frac{\partial}{\partial t}\left(\rho' + \eta\frac{\partial \rho_0}{\partial z}\right) = 0,$$

Then, the term in the bracket is constant and is taken to be zero, we have

$$\rho' = -\eta \frac{\partial \rho_0}{\partial z}. \tag{E.13}$$

If we put Eq. (E.13) into Eq. (E.11), we have

$$\frac{\partial}{\partial t}\left(\frac{1}{2}\overline{\rho_0 u^2} + \frac{1}{2}\overline{\rho_0 w^2} \right)$$

$$= \eta \frac{\partial \overline{\rho_0}}{\partial z} wg - \left(\frac{\partial \rho' u}{\partial x} + \frac{\partial \rho' w}{\partial z} \right)$$

$$= \frac{g}{\rho_0} \frac{\partial \overline{\rho_0}}{\partial z} \rho_0 w\eta - \left(\frac{\partial \rho' u}{\partial x} + \frac{\partial \rho' w}{\partial z} \right). \tag{E.14}$$

We use Eq. (E.7) into the equation above

$$\frac{\partial}{\partial t}\left(\frac{1}{2}\overline{\rho_0 u^2} + \frac{1}{2}\overline{\rho_0 w^2} \right)$$

$$= -\left(-\frac{g}{\rho_0} \frac{\partial \overline{\rho_0}}{\partial z} \right) \rho_0 \eta \frac{\partial \eta}{\partial t} - \left(\frac{\partial \rho' u}{\partial x} + \frac{\partial \rho' w}{\partial z} \right)$$

$$= -\frac{\partial}{\partial t}\left(\frac{1}{2} N^2 \rho_0 \eta \right) - \left(\frac{\partial \rho' u}{\partial x} + \frac{\partial \rho' w}{\partial z} \right). \tag{E.15}$$

So,

$$\frac{\partial}{\partial t}\left(\frac{1}{2}\overline{\rho_0 u^2} + \frac{1}{2}\overline{\rho_0 w^2} + \frac{1}{2} N^2 \rho_0 \eta \right) = -\left(\frac{\partial \rho' u}{\partial x} + \frac{\partial \rho' w}{\partial z} \right). \tag{E.16}$$

This is the energy conservation equation for two dimensional internal waves. We can have some form of energy equation for three dimensional internal waves. Thus we have the expression of strain as

$$\eta(z,t) = -\frac{\rho'(z,t)}{\frac{\partial \rho_0}{\partial z}} = \frac{\frac{\overline{\overline{g}}}{\rho_0}\rho'(z,t)}{-\frac{\overline{\overline{g}}}{\rho_0}\frac{\partial \rho_0}{\partial z}} = \frac{\frac{\overline{\overline{g}}}{\rho_0}\rho'(z,t)}{N_0^2}. \tag{E.17}$$

Here, consider $\rho(z,t) = \rho'(z,t) + \rho_0(z)$, and deviate with z

$$\xi_z = \frac{\partial \eta}{\partial z} = \frac{\frac{g}{\rho_0}\frac{\partial \rho'}{\partial z}}{N_0^2} = \frac{N'^2}{N_0^2} = \frac{N^2 - N_0^2}{N_0^2} = \frac{N^2}{N_0^2} - 1 = \frac{N^2(z,t)}{N_0^2(z)} - 1. \quad \text{(E.18)}$$

R_ω is the ratio between the horizontal kinetic energy and the potential energy. As for single internal wave propagating at an angle φ to the vertical, φ is described as

$$\tan^2 \varphi = \frac{m^2}{k^2 + l^2} = \frac{N^2 - \omega^2}{\omega^2 - f^2}. \quad \text{(E.19)}$$

Here, (k, l, m) are the horizontal and vertical wave numbers, respectively. In this case, horizontal kinematic energy and potential energy are

$$u^2 + v^2 \approx \left(1 + \frac{f^2}{\omega^2}\right)\tan^2 \varphi, N^2 \eta^2 \approx \frac{N^2}{\omega^2}. \quad \text{(E.20)}$$

From this, shear-strain ratio is described as

$$R_\omega = \frac{\left(1 + \frac{f^2}{\omega^2}\right)\tan^2 \varphi}{\frac{N^2}{\omega^2}} = \frac{\omega^2 + f^2}{N^2}\tan^2 \varphi = \frac{\omega^2 + f^2}{N^2}\frac{N^2 - \omega^2}{\omega^2 - f^2}. \quad \text{(E.21)}$$

If $N >> f$, Eq. (E.18) is reduced to Eq. (D.25).

Appendix F Maximum likelihood estimation

Ruddick *et al*. [2000] evaluated the average value of vertical temperature fluctuation with the provability density function as

$$C11 = -\sum_{i}^{N}\left(\frac{S_{obs} - S_B + S_n}{S_B + S_n}\right)^2 - \ln(S_B + S_n) + N_{MLE}\left(\frac{1}{4} + \sqrt{\frac{d_{MLE}}{4\pi}}\right), \qquad \text{(F.1)}$$

where S_B is the Bachelor spectrum ($=\sqrt{q/2}\,f(\alpha)\kappa_T k_B^{-1}\chi_\theta$), S_{obs} is the observed spectrum of temperature fluctuation (2048 points FFT), $q = 3.2$, κ_T is molecular diffusivity of heat ($=1.39\times10^{-7}$), S_n is the instrumental noise spectrum ($=3\times10^{-7}$). k_B is the Bachelor frequency and is described as

$$k_B = \left(\frac{\varepsilon}{\nu\kappa_T{}^2}\right)^{1/4}. \qquad \text{(F.2)}$$

Here, $f(\alpha)$ is written as

$$f(\alpha) = \alpha\left(e^{-\alpha^2/2} - \alpha\int_{\alpha}^{\infty} e^{-x^2/2}\right), \qquad \text{(F.3)}$$

Where α is $\kappa_T k_B^{-1}\sqrt{2q}$. If we consider maximum likelihood estimation, looking at the functional form of S_B on χ_θ, we must seek the value of χ_θ which maximize the probability function C11. We set $S_B = A\chi_\theta$, Eq. (F.1) becomes

$$C11 = -\sum_{i}^{N}\underbrace{\left(\frac{S_{obs} - (A\chi_\theta + S_n)}{A\chi_\theta + S_n}\right)^2}_{①} \underbrace{-\ln(A\chi_\theta + S_n) + N\left(\frac{1}{4} + \sqrt{\frac{d}{4\pi}}\right)}_{②}. \qquad \text{(F.4)}$$

Then, the derivative of ① of Eq. (F.1) with respect to χ_θ is

$$\frac{\partial ①}{\partial \chi_\theta}:\sum_i^N 2\left(\frac{S_{obs}-(A\chi_\theta+S_n)}{A\chi_\theta+S_n}\right)\times\left(\frac{-A(A\chi_\theta+S_n)-A(S_{obs}-A\chi_\theta-S_n)}{(A\chi_\theta+S_n)^2}\right)$$

$$=\sum_i^N 2\left(\frac{S_{obs}-A\chi_\theta-S_n}{A\chi_\theta+S_n}\right)\times\left(\frac{-A(A\chi_\theta+S_n+S_{obs}-A\chi_\theta-S_n)}{(A\chi_\theta+S_n)^2}\right)$$

$$=\sum_i^N 2\left(\frac{S_{obs}-A\chi_\theta-S_n}{A\chi_\theta+S_n}\right)\times\left(\frac{-A(S_{obs})}{(A\chi_\theta+S_n)^2}\right)$$

$$=\sum_i^N \frac{-2AS_{obs}(S_{obs}-A\chi_\theta-S_n)}{(A\chi_\theta+S_n)^3}. \qquad \text{(F.5)}$$

Next, the derivative of ② of Eq. (F.1) is

$$\frac{\partial ②}{\partial \chi_\theta}:\frac{A}{A\chi_\theta+S_n} \qquad \text{(F.6)}$$

Taken together,

$$\frac{\partial C11}{\partial \chi_\theta}=\sum_i^N \frac{2AS_{obs}(S_{obs}-A\chi_\theta-S_n)}{(A\chi_\theta+S_n)^3}-\frac{A}{A\chi_\theta+S_n}=0$$

$$=\sum_i^N \frac{2AS_{obs}(S_{obs}-A\chi_\theta-S_n)-A(A\chi_\theta+S_n)^2}{(A\chi_\theta+S_n)^3}=0. \qquad \text{(F.7)}$$

Therefore, $\sum_i^N 2S_{obs}(S_{obs}-A\chi_\theta-S_n)-(A\chi_\theta+S_n)^2=0$ is necessary for using MLE, so that

$$\sum_i^N\left(2S_{obs}(S_{obs}-A\chi_\theta-S_n)-(A\chi_\theta+S_n)^2\right)=0. \qquad \text{(F.8)}$$

$$\sum_i^N\left((A\chi_\theta+S_n)^2+2S_{obs}(A\chi_\theta+S_n)-2{S_{obs}}^2\right)=0. \qquad \text{(F.9)}$$

So, $A\chi_\theta+S_n$ is

$$A\chi_\theta+S_n=-S_{obs}\pm\sqrt{{S_{obs}}^2+2{S_{obs}}^2}$$

$$=-S_{obs}\pm\sqrt{3}S_{obs}\ . \qquad \text{(F.10)}$$

χ_θ should be larger than 0, then we have

$$\chi_\theta = \frac{(\sqrt{3}-1)S_{obs} - S_n}{A} . \qquad \text{(F.11)}$$

This χ_θ maximize the probability function of C11.

Appendix G Abbreviation and symbols

G.1. Abbreviation

ADCP: Acoustic Doppler Current Profiler

AMP: Advanced Micro structure Profiler

CMW: Central Mode Water

CTD (O): Conductivity Temperature Depth (Oxygen) profiler

DC: Diffusive Convection

DNS: Direct Numerical Simulation

DDC: Double Diffusive Convection

EDW: Eighteen Degree Water

EPSONDE: Epsilon Sonde

FLY2: The Fast Light Yo-yo

FRA: Fisheries Research Agency of Japan

FSP: Fine Scale Parameterization

GM: Garret and Munk

HRP: High Resolution Profiler

Imp: Improve (subscript)

JAMSTEC: Japan Agency for Marine-Earth Science and Technology

LADCP: Lowered Acoustic Doppler Current Profiler

MOC: Meridional Overturning Circulation

MSR: Micro Structure Recorder

MLE: Maximum Likelihood Estimation

NATRE: North Atlantic Tracer Release Experiment

NPIW: North Pacific Intermediate Water

NPO: North Pacific Ocean

Obs: Observational data (subscript)

PSI: Parametric Sub-harmonic Instability

RMS: Root Mean Square

RSVP: Rapid Sampling Vertical Profiler

SF: Salt finger convection

STMW: SubTropical Mode Water

STPG: SubTropical Pacific Gyre

TKE: Turbulent Kinematic Energy

TM: TurboMAP

TUMSAT: Tokyo University of Marine Science and Technology

Turb: Turbulence (subscript)

XCTD: eXpendable Conductivity Temperature Depth profiler

XCP: eXpendable Current Profiler

G.2. Symbols

A, B: The averages value of C^S, C^T in chapter 3

A_B: Coefficient for the calculation of MLE ($=\kappa_T k_B^{-1}\sqrt{q_B/2}\,f\left(\alpha_B\right)$)

B_{JG}: The parameter used in Johnson and Garrett [2004] ($=\frac{\Delta\rho_N}{(d\rho/dz)h}$)

C^S, C^T: The coefficients of each layers for improving Kimura *et al*. [2011] formulation

*C*11: Equation proposed by Ruddick *et al*. [2000], Eq. (5.6) in this thesis

d : The Thorpe displacement scale $d = Dep - Dep'$

d_{MLE}: The degree of freedom

D: The ratio between K_S and K_T

Dep: Real depth

Dep': Reordered depth

D_v: The vertical distance from bottom of tank of experiment by Linden [1979]

E_{GM}: The energy spectrum of internal waves considering GM spectrum.

F_S: The vertical flux of salinity

F_T: The vertical flux of heat

f: The Coriolis parameter ($f = 2\Omega\sin\varphi$. $f_{30} = f\left(30^\circ\right)$)

$f1$: The root mean square (rms) of density fluctuations between observed density ρ and liner fit density ρ_S.

$f2$: The root mean square (rms) of density fluctuations between observed density ρ

and liner fit density ρ_θ.

$f3$: The root mean square (rms) of density fluctuations between observed density ρ and density fluctuation ρ'.

GK96 filter: The filters proposed by Galbraith and Kelley [1996]

g: Gravitational acceleration

H: The typical thermocline vertical scale ($=[\partial\rho/\partial z]/[\partial^2\rho/\partial z^2]$)

H_{dep} : The depth for Johnson and Garrett [2004]

h: The sampling interval

i: Unit vector of x - direction

j: Unit vector of y - direction

k: Unit vector of z - direction

k_B: The Batchelor frequency

K_ρ: Vertical eddy diffusivity of density

K_ρ^{DDC}: for DDC, K_ρ^{Turb}: for conventional turbulence

K_ρ^{GH84}: K_ρ proposed by Garget and Holloway [1984]

K_v: Vertical eddy diffusivity of momentum

K_v^{P81}: K_v proposed by Pacanowski and Philander [1981]

K_v^{P88}: K_v proposed by Peters *et al*. [1988]

$K_v^{\mathrm{K06}\xi}$ $K_v^{\mathrm{K06}V}$: K_v proposed by Kunze *et al*. [2006a]

K_{v_0} : Parameter proposed by is Pacanowski and Philander [1981] .

$O(0.005\sim0.015\text{cm}^2/\text{s})$.

K_{v_b} : Parameter proposed by is Pacanowski and Philander [1981]. $0.001\text{m}^2/\text{s}$

K_S : Vertical eddy diffusivity of salinity

K_S^{SF} : for SF, K_S^{DC} : for DC, K_S^{Turb} : for conventional turbulence

$K_S^{\text{Large,SF}}$, $K_S^{\text{Large,DC}}$: K_S proposed by Large *et al*. [1984]

$K_S^{\text{Zhang,SF}}$, $K_S^{\text{Zhang,DC}}$: K_S proposed by Zhang *et al*. [1998]

$K_S^{\text{SF,DNS}}$: K_S proposed by Kimura *et al*. [1998]

K_S^{Obs}: K_S obtained by observational data

K_T : Vertical eddy diffusivity of heat

K_T^{SF} : for SF, K_T^{DC} : for DC, K_T^{Turb} : for conventional turbulence

K_T^{P81}: K_T proposed by Pacanowski and Philander [1981]

K_T^{P88}: K_v proposed by Peters *et al*. [1988]

$K_T^{\text{Large,SF}}$, $K_T^{\text{Large,DC}}$: K_T proposed by Large *et al*. [1984]

$K_T^{\text{Zhang,SF}}$, $K_T^{\text{Zhang,DC}}$: K_T proposed by Zhang *et al*. [1998]

$K_T^{\text{SF,DNS}}$: K_T proposed by Kimura *et al*. [1998]

K_T^{Obs}: K_T obtained by observational data

K_{T_b} : Parameter proposed by is Pacanowski and Philander [1981]. $0.0001\text{m}^2/\text{s}$.

K_0 : $0.05\times10^{-4}\mathrm{m}^2/\mathrm{s}$

L_a : The length of animals

L_O : The Ozmidov scale

L_T : The Thorpe scale

L^+, L^- : The maximum and minimum values of the vertical distance of the Thorpe displacements

l : Turbulent length scale

N : The buoyancy frequency

N_0 : The mean buoyancy frequency 5.2×10^{-3}rad/s

N_{MLE} : The number of observational spectrum in each 10m

n : The number of data points in each overturn

PrL : The inverse laminar Prandtl number ($=K_T/\nu$)

p : The pressure

Q : The parameter used in Johnson and Garrett [2004] ($=\frac{\Delta\rho_N}{(d\rho/dz)H_{dep}}$)

q : Turbulent velocity scale ($q^2=\overline{u'^2}+\overline{v'^2}+\overline{w'^2}$)

q_B : The constant used for MLE (=3.2)

R : The ratio indicating limitation of depth or density resolution ($=\frac{d\rho}{dz}\frac{z_{res}}{\rho_{res}}$)

R_O : The overturn ratio ($=\min(L^+/L, L^-/L)$)

R_{OT} : The ration between the Thorpe scale and the Ozmidov scale ($=L_T/L_O$)

Re : The turbulent Reynolds number ($=ql/\nu$)

R_{eL} : The turbulent Reynolds number ($=T_L/T_\eta$)

R_{eb} : The buoyancy Reynolds Number ($=\varepsilon/\nu N^2$)

R_f : The flux Richardson number ($=g\overline{\rho' w'}\Big/-\rho\overline{u'w'}\left(\frac{\partial\overline{U}}{\partial z}\right)$)

R_i : The gradient Richardson number ($=N^2/S_h{}^2$)

R_{io} : The overall Richardson number ($=g\Delta\rho D/\rho_{mean}(\Delta U)^2$)

R_ρ : The density ratio ($=\alpha\frac{\partial\theta}{\partial z}\Big/\beta\frac{\partial S}{\partial z}$)

R_ω : The shear - strain ratio

S : Salinity

S_z $\left(\partial S/\partial z\right)$: The vertical gradient of salinity

S_n : Noise spectrum defined for MLE

S_{obs} : The spectrum detected by observation for MLE

S_B : The Batchelor spectrum for MLE

$S_h{}^2$:The squared vertical gradients of horizontal velocity ($=\left(\partial u/\partial z\right)^2+\left(\partial v/\partial z\right)^2$)

S_{TL} : The shear strength parameter

T_z $\left(\partial\theta/\partial z\right)$: The vertical gradient of temperature

T_u : The Turner angle($=\tan^{-1}\left[(R_\rho+1)/(R_\rho-1)\right]$)

T' : Temperature fluctuation

$\bar{T}$: The back ground average temperature

T_L : The Kolmogorov time scale

T_η : The time scale of inertial motion

t : Turbulent time scale $t = l/q$

ΔU : The velocity difference between two layers of experiment by Linden [1979]

u_i : The velocity components in x, y and z directions

u : The horizontal velocity (x - direction)

u' : The fluctuation velocity(x - direction)

$\bar{u}$: The mean velocity (x - direction)

v : The horizontal velocity (y - direction)

v' : The fluctuation velocity (y - direction)

W : Falling speed of TurboMAP or other microstructure profilers

w : The vertical velocity (upwelling velocity), about 1cm/day (～1.15×10^{-7}m/s),

Munk [1966]

$\bar{w}$: The mean velocity of z - direction

x : the horizontal coordinate positive eastwards

y : The horizontal coordinate positive northwards

z : The vertical coordinate positive upwards

z_{res} : The vertical resolution of instruments

α_{GH84} : Proportional coefficients of buoyancy frequency proposed by Gargett and Holloway [1984]

α_B : $\kappa_T k_B^{-1}\sqrt{q_B}$

α : The thermal expansion coefficient

β_{GH84} : power of N proposed by Gargett and Holloway [1984]

β : The haline contraction coefficients

γ^{SF} : the density flux ratio of Salt Finger convection $\gamma^{SF} = \sqrt{R_\rho}\left(\sqrt{R_\rho} - \sqrt{R_\rho - 1}\right)$

γ^{DC} : the density flux ratio of diffusive convection $\gamma^{DC} = \dfrac{1/R_\rho + 1.4\left(1/R_\rho - 1\right)^{3/2}}{1 + 14\left(1/R_\rho - 1\right)^{3/2}}$

Γ : The mixing efficiency $(= Rf/(1-Rf))$ or dissipation ratio

ε : The kinematic energy dissipation rates $= \dfrac{15}{2}\nu\overline{\left(\partial u'/\partial z\right)^2}$

χ_θ : The dissipation rate of temperature variance $\chi_\theta = 6\kappa_T\overline{\left(\partial T'/\partial z\right)^2}$

ζ_{GK} : ζ_T or ζ_S

ζ_T : $f1/f3$

ζ_S : $f2/f3$

ξ_z : strain

η : The vertical displacement

θ : Potential temperature

κ_S : The molecular diffusivities for salt

κ_T : The molecular diffusivities for heat

λ : Wave length of waves

ν : The kinematic viscosity

π : 3.14

ρ : Density

ρ_o : The reference density

ρ' : The density fluctuation

$\Delta\rho$: The density difference between two layers by experimented by Linden [1979]

$\Delta\rho_N$: The amplitude of noise

ρ_{mean} : The mean density of two layers by experimented by Linden [1979]

ρ_θ : Liner relationship between temperature and density $\rho_\theta = a_\theta + b_\theta\theta$,

ρ_S : Liner relationship between salinity and density $\rho_S = a_S + b_S\theta$,

ρ_{res} : The density resolution of instruments

τ : The turbulent time scale

φ : Latitude

ω : The frequency of internal waves

Ω : Angular speed of the Earth

$\partial U/\partial z$: The vertical gradient of velocity

$\partial u'/\partial t$: The time derivation of the fluctuation of velocity

$\partial u'/\partial z$: The vertical gradient of the fluctuation of velocity

$\partial u'/\partial z$: The second derivative of the velocity fluctuation

$\partial u/\partial z$, $\partial v/\partial z$: The vertical gradient of horizontal velocity

$\partial \rho/\partial z$: The vertical density gradient

$\partial^2 \rho/\partial z^2$: The second derivative of density gradient